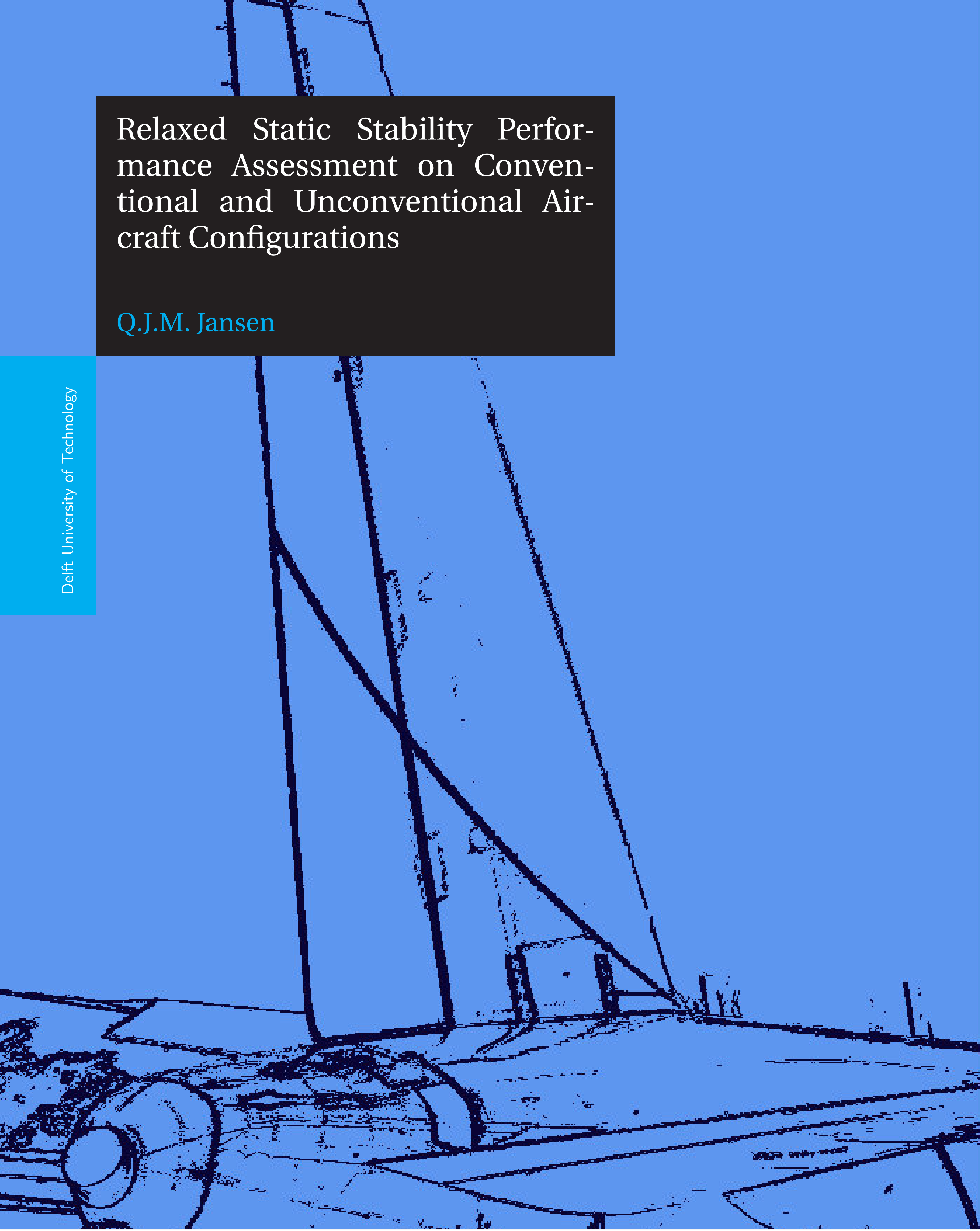

Relaxed Static Stability Performance Assessment on Conventional and Unconventional Aircraft Configurations

Q.J.M. Jansen

Delft University of Technology

Delft University of Technology

Challenge the future

RELAXED STATIC STABILITY PERFORMANCE ASSESSMENT ON CONVENTIONAL AND UNCONVENTIONAL AIRCRAFT CONFIGURATIONS

by

Q.J.M. Jansen

in partial fulfillment of the requirements for the degree of

Master of Science
in Aerospace Engineering

at the Delft University of Technology,
to be defended publicly on Friday January 16, 2015 at 9:00 AM.

Student number:	4017579
Thesis registration:	019#15#MT#FPP
Word count:	29803

An electronic version of this thesis is available at http://repository.tudelft.nl/.

Faculty of Aerospace Engineering · Delft University of Technology

DELFT UNIVERSITY OF TECHNOLOGY
DEPARTMENT OF
FLIGHT PERFORMANCE AND PROPULSION

The undersigned hereby certify that they have read and recommend to the Faculty of Aerospace Engineering for acceptance a thesis entitled **"Relaxed Static Stability Performance Assessment on Conventional and Unconventional Aircraft Configurations"** by **Quinten Jansen** in partial fulfilment of the requirements for the degree of **Master of Science.**

Dated: January 16th, 2015

Head of department: ______________________

Prof. dr. ing. G. Eitelberg

Supervisor: ______________________

Dr. ir. R. Vos

First reader: ______________________

Dr. ir. G. La Rocca

Second reader: ______________________

Dr. ir. C.C. de Visser

I think you have to try and fail, because failure gets you closer to what you’re good at.

Louis C.K.

ABSTRACT

During the last fifty years large efforts are made, in the commercial aviation industry, to find methods to reduce aircraft weight, with the purpose of increasing aircraft performance and reducing fuel consumption. The design of statically unstable modern fighter aircraft, operating with relaxed static stability, introduces interesting possible performance advantages for commercial applications. Where relaxed static stability increases supersonic maneuverability for fighter aircraft, it could potentially decrease the maximum take-off mass and cruise drag for transport aircraft.

This thesis assignment focuses on the influence of a reduced static stability margin on the performance of conventional and unconventional aircraft configurations. Unconventional aircraft configurations are defined as a canard two-surface aircraft and a three-aircraft. For the longitudinal stability and control analysis of a reduced static stability margin on the aircraft performance, a stabilizing surface sizing methodology is developed and implemented in a conceptual aircraft sizing tool, the Initiator.

The Initiator is a preliminary sizing tool for conventional and unconventional aircraft configurations, developed at the Delft University of technology (TU Delft). The developed stabilizing surface sizing methodology is implemented in the Initiator as a design module. An integral part of the stabilizing surface sizing module is a methodology to predict the average downwash angle at an arbitrary point in the flow field behind a wing with high-lift devices and the prediction of the average upwash angle at an arbitrary point in the flow field in front of a wing with high-lift devices, both in- and outside the ground effect region.

The downwash prediction methodology is validated in- and outside the ground effect region for a T-tail aircraft and fuselage mounted stabilizer aircraft within an accuracy $\pm 1^{o}$. The stabilizing surface sizing methodology is validated for four aircraft within an accuracy of ±5%. It is found that when the stability margin is decreased from +10% to -8%, the maximum take-off mass is reduced by 1.73% and 3.08% for an equal payload, respectively for a typical sing-aisle mid-range aircraft and a typical two-aisle long-range aircraft. For an equal stability margin reduction as on the conventional aircraft, the maximum take-off mass is reduced by 0.15% for an equal payload in case of a single-aisle mid-range canard aircraft, whereas the reduction of the maximum take-off mass for a single-aisle mid-range three-surface aircraft is 0.94%.

ACKNOWLEDGEMENTS

During the last project, as a master student at the Delft University of Technology, I was able to fully utilize the skills I obtained during my education at the Aerospace Engineering faculty. However, without the guidance and help of others, the work presented in this report would not have been made possible.

First, I would like to thank my supervisor Roelof Vos, who has guided and advised me on very interesting ideas throughout my final thesis work. I also really enjoyed the periodic feedback discussions, which I always left full of motivation to improve the methods I developed.

Secondly, I would like to thank the members of the committee: Georg Eitelberg, Gianfranco La Rocca and Coen de Visser who took the time to asses my work and share their expert insights.

During my years as a student at the TU Delft, I appreciated the attainment of a very useful set of skills, by studying on numerous interesting subjects, which allows me to pursue a successful career in various engineering fields.

Finally, I would like to thank my parents for their never ending support throughout my studies. Without their encouragement, the writing of this thesis report would not have been possible.

CONTENTS

Abstract iii

List of Figures ix

List of Tables xi

Nomenclature xiii

I Thesis Report 1

1 Introduction 3

2 Background theory 5
- 2.1 Horizontal stabilizer and canard requirements . . . 5
- 2.2 Aircraft configurations . . . 6
  - 2.2.1 Two-surface aircraft . . . 6
  - 2.2.2 Three-surface aircraft . . . 7
- 2.3 Stability and control . . . 8
  - 2.3.1 Static longitudinal stability . . . 9
  - 2.3.2 Dynamic longitudinal stability . . . 11
  - 2.3.3 Longitudinal control . . . 11
- 2.4 Down- and upwash prediction . . . 12
- 2.5 Ground effect aerodynamics . . . 16
  - 2.5.1 Reduction in average downwash angle . . . 17
- 2.6 Stabilizing surface sizing methods . . . 17
  - 2.6.1 Volume coefficients . . . 18
  - 2.6.2 X-plot methodology . . . 18
- 2.7 Relaxed static stability . . . 19
- 2.8 Ice accretion . . . 20
- 2.9 Initiator . . . 21

3 Down- and upwash prediction methodology 23
- 3.1 Vortex Lattice Method (VLM) . . . 23
  - 3.1.1 Out of ground effect . . . 24
  - 3.1.2 In ground effect . . . 24
  - 3.1.3 Simulation of high-lift devices . . . 24
- 3.2 Downwash prediction methodology . . . 26
  - 3.2.1 Accuracy of the methodology . . . 28
- 3.3 Validation of the downwash prediction . . . 28
- 3.4 Comparison between downwash prediction methods . . . 31
- 3.5 Downwash prediction for unconventional configurations . . . 32

4 Stabilizing surface sizing methodolody 33
- 4.1 Stabilizing surface sizing requirements . . . 34
- 4.2 Loading diagram . . . 35
- 4.3 Sizing methodology . . . 36
  - 4.3.1 Dominant forward center of gravity limit . . . 36
  - 4.3.2 Dominant aft center of gravity limit . . . 37
  - 4.3.3 Rotation capacity . . . 38
  - 4.3.4 Stick-fixed maneuver points . . . 39
  - 4.3.5 Satisfactory short period oscillation characteristics . . . 39
  - 4.3.6 Wing optimization methodology . . . 40

4.3.7 Validation of the pitching moment . . . 43
4.3.8 Comparison of the aerodynamic center . . . 43
4.4 Validation of the sizing methodology . . . 44
4.5 Ground effect analysis . . . 46
4.6 Implementation of the sizing methodology . . . 47

5 Results and discussion **49**
5.1 Reduced stability margin on conventional aircraft . . . 50
5.1.1 Discussion of the mass reduction on conventional aircraft. . . . 51
5.2 Reduced stability margin on unconventional aircraft . . . 53
5.2.1 Canard aircraft . . . 53
5.2.2 Three-surface aircraft . . . 55

6 Conclusion and recommendations **57**
6.1 Conclusion . . . 57
6.2 Recommendataions. . . . 58

II Code Documentation **59**

7 Introduction **61**
7.1 Background . . . 61

8 Program structure **63**
8.1 Downwash module . . . 63
8.1.1 AVL input file . . . 64
8.2 Stabilizing surface sizing module . . . 67
8.3 Design convergence. . . . 69

Bibliography **71**

A Appendix A **73**

B Appendix B **79**

LIST OF FIGURES

2.1 Two-surface aircraft, a conventional McDonnell Douglas KC-10 and a canard Beechcraft Starship I [1]. 7
2.2 Three-surface aircraft configuration, Piaggio P180 Avanti[2] 8
2.3 Example of a developed loading diagram within the stabilizing surface sizing methodology. 9
2.4 Terminology of the longitudinal parameters for control and stability analysis 10
2.5 Pitching moment contribution of complete aircraft compared to an aircraft without stabilizing surfaces [2]. 11
2.6 Variation of the pitching moment due to increasing flap and slat deflections [3]. 12
2.7 Downwash at the horizontal stabilizer for a conventional aircraft configuration [4]. . . 13
2.8 Downwash at the wing for a canard aircraft configuration[4]. 13
2.9 ESDU 97021 average downwash angle validation OGE 14
2.10 ESDU 72023 average downwash angle validation IGE 15
2.11 Slingerland average downwash angle validation OGE 15
2.12 Slingerland average downwash angle validation IGE 16
2.13 Reduction of the average downwash angle with altitude for the Airbus A330. 17
2.14 Example of a x-plot developed with the stabilizing surface sizing methodology. 19
2.15 Size comparison between the MD-11 and the DC-10. 20

3.1 Downwash angle of a lifting surface Out of Ground Effect (OGE). 24
3.2 Mirroring technique for a wing and tail in ground effect. 25
3.3 Downwash angle of a lifting surface In of Ground Effect (IGE). 25
3.4 Redrawn figure of the reduction of the effective flap angle for single-slotted flaps and double-slotted flaps with vanes [3]. 26
3.5 Two-dimensional representation of the wing lay-out with high-lift devices [5]. 26
3.6 Two-dimensional wing planform representation. 29
3.7 VLM Validation of the average downwash angle at the horizontal stabilizer of the Airbus A330 Out of Ground Effect (OGE). 30
3.8 VLM Validation of the average downwash angle at the horizontal stabilizer of the Fokker 100 Out of Ground Effect (OGE). 30
3.9 VLM Validation of the average downwash angle at the horizontal stabilizer of the Fokker 100 and the Airbus A330 In Ground Effect (IGE). 31

4.1 Loading diagram for different wing positions for a typical single-aisle transport aircraft. 35
4.2 Center of gravity ranges diagram and x-plot for a conventional aircraft. 41
4.3 Center of gravity ranges diagram and x-plot for a canard aircraft. 41
4.4 Center of gravity ranges diagram and x-plot for a three-surface aircraft. 42
4.5 Validation of the VLM and Torenbeek tail-off pitching moment coefficient calculation. 44
4.6 Comparison of the aerodynamic center calculation between the graphical Torenbeek method and the VLM. 45

5.1 Percentage mass reduction of the components of a typical single-aisle mid-range conventional transport aircraft. 50
5.2 Percentage mass reduction of the components of a typical double-aisle long-range conventional transport aircraft. 52
5.3 Reduced aircraft size with decreasing stability margin on conventional aircraft configurations 53
5.4 Percentage mass reduction of the components of a canard. 54
5.5 Reduced aircraft size with decreasing stability margin on a canard aircraft configuration 55
5.6 Percentage mass reduction of the components of a three-surface aircraft. 56

5.7 Reduced aircraft size with decreasing stability margin on a three-surface aicraft. 56

8.1 Activity diagram of the developed downwash prediction methodology. 64
8.2 Example of an AVL input file of an conventional aircraft. 65
8.3 Example of the chord- and spanwise panel distribution of the lifting surfaces of a conventional aircraft, used in the down- and upwash prediction methodology. 66
8.4 Example of the chord- and spanwise panel distribution of the lifting surfaces of a canard aircraft, used in the down- and upwash prediction methodology. 66
8.5 Example of the chord- and spanwise panel distribution of the lifting surfaces of a three-surface aircraft, used in the down- and upwash prediction methodology. 66
8.6 Activity diagram of the developed stabilizing surface sizing methodology. 68
8.7 Activity diagram of the Initiator design convergence with the implemented *Stabilizing-SurfaceSizing* module. 69

A.1 Actual figure, as presented by Torenbeek, and the digitized figure developed for the stabilizing surface sizing methodology of parameter μ_2[2]. 75
A.2 Actual figure, as presented by Torenbeek, and the digitized figure developed for the stabilizing surface sizing methodology of parameter μ_2[2]. 75
A.3 Actual figure, as presented by Torenbeek, and the digitized figure developed for the stabilizing surface sizing methodology of parameter μ_3[2]. 76
A.4 Actual figure, as presented by Torenbeek, and the digitized figure developed for the stabilizing surface sizing methodology of parameter $\frac{\Delta c}{c_f}$ [2]. 77
A.5 Comparison of the graphical calculation of parameter μ_2 and the ditigized calculation of the latter parameter. 77

B.1 Actual representation of the carpet plots [2]. 80
B.2 Digitization of the carpet plots. 81

LIST OF TABLES

2.1 Pitching moment coefficient for different flap settings 12
2.2 Design differences between the DC-10-30 and the MD-11 20

3.1 Maximum lift force when the lift coefficient is assumed to be zero. 28
3.2 Comparison of the three downwash prediction methods, Out of Ground Effect (OGE). 31
3.3 Comparison of the three downwash prediction methods, In Ground Effect (IGE). 32

4.1 Validation of the stabilizing surface sizing module. 45
4.2 Results of the landing flare trim analysis. 46

5.1 Mass reduction of the components of a typical single-aisle mid-range conventional transport aircraft. 50
5.2 Mass reduction of the components of a typical double-aisle long-range conventional transport aircraft. 51
5.3 L/D ratios during cruise conditions of the single-aisle mid-range aircraft and the double-aisle long-range aircraft. 52
5.4 Mass reduction of the components of a canard aircraft. 54
5.5 Mass reduction of the components of a three-surface aircraft. 55

NOMENCLATURE

LIST OF SYMBOLS

Latin letters

A	Aspect ratio	-
b	Span	m
$\bar{c}$	Mean aerodynamic chord	m
C_d	2D Drag coefficient	-
C_D	3D Drag coefficient	-
C_l	2D Lift coefficient	-
C_L	3D Lift coefficient	-
C_m	2D Pitching moment coefficient	-
C_M	3D Pitching moment coefficient	-
C_{L_α}	Lift slope	1/rad
D	Drag force	N
g	Gravitational acceleration	m/s^2
h	Height	m
H	Altitude	m
i	Incidence angle	deg
I_{yy}	Second moment of inertia about the y-axis	$[m^2]$
l	Moment arm	m
L	Lift force	N
L_α	Factor characterizing the longitudinal manoeuvrability	[-]
K_Y	Non-dimensional radius of inertia in pitch	[-]
M	Mach number	-
q	Dynamic pressure	N/m^2
R_Y	Non-dimensional radii of gyration about the y-axis	[-]
S	Surface area	m^2
T	Thrust force	N
V	Velocity component	m/s,
W	Weight	N
x	Longitudinal coordinate	m
y	Lateral coordinate	m
z	Vertical coordinate	m

Greek letters

α	Angle of Attack	deg
β	Prandtl compressibility factor	[-]
δ	Deflection Angle	deg
ϵ	Downwash Angle	deg
η	Dynamic Pressure Ratio, airfoil efficiency factor	-
$\dot{\theta}$	Take-off rotation rate	[deg/s]
λ	Taper ratio	[-]
Λ	Sweep angle	[deg]
μ	Roll Friction Coefficient	-
μ_1	Factor in Equation A.6	-
μ_2	Factor in Equation A.6	-
μ_3	Factor in Equation A.6	-
ρ	Density	kg/m^3
τ	Taper Ratio	-
ϕ	Velocity Potential	-
ω_n	Undamped natural frequency of an oscillation	-

Subscripts

0	Zero lift condition
2	Take-off safety speed
∞	Free stream condition
ac	Aerodynamic center
AFT	Aft location
b	Basic lift contribution
c	Canard
c/2	Half chord
c/4	Quarter chord
cg	Center of gravity
cruise	Cruise conditions
e	Elevator
eff	Effective deflection angle
eng	Engine
f	Friction component, flap
fn	Fuselage nose
fus	Fuselage
FWD	Forward location
g	Ground effect condition, landing gear
geo	Geometric deflection angle
h	Horizontal stabilizer
i	Induced drag component
jet	Jet exhaust flow
landing	Landing conditions
max	Maximum value
min	Minimum value
mo	Maximum operating speed
mp	Maneuver point
nac	Nacelle
np	Neutral point
o	Ambient condition
R	Take-off rotation
ref	Reference
S	Stall condition
takeoff	Take-off conditions
w	Wing

LIST OF ACRONYMS

AE	Aerospace Engineering
AGARD	Advisory Ground for Aerospace Research and Development
AVL	Athena Vortex Lattice
BWB	Blended-Wing-Body
CG	Center of Gravity
ESDU	Engineering Science Data Unit
EXP	Experimental Data
FPP	Flight Performance and Propulsion
IGE	In Ground Effect
LEMAC	Leading Edge Mean Aerodynamic Chord
MAC	Mean Aerodynamic Chord
MTOM	Maximum Take-Off Mass
OEM	Operational Empty Mass
OGE	Out of Ground Effect
SM	Static Margin
SP	Short Period Oscillation
TSA	Three-Surface Aircraft
TUD	Delft University of Technology
UML	Unified Modelling Language
VLM	Vortex Lattice Method

I

THESIS REPORT

1

INTRODUCTION

The introduction of artificial longitudinal stability on modern fighter aircraft, significantly increases the supersonic manoeuvrability and decreases cruise trim drag. For a conventional, statically stable supersonic fighter aircraft, the centre of gravity is located in front of the neutral point of the aircraft during subsonic cruise. This requires a negative balancing lift force on the horizontal stabilizer. During supersonic cruise, the neutral point of the aircraft moves further aft which increases the longitudinal stability of the aircraft. This results in an increase in trim drag, due to the larger balancing negative lift force required on the horizontal stabilizer. For an aircraft which possesses relaxed static stability, the centre of gravity is located behind the neutral point during subsonic cruise. This results in a negative Stability Margin (SM) and represents an unstable subsonic flight condition. During the supersonic cruise phase the neutral point of the aircraft moves aft to a point at which it is located just behind the centre of gravity, requiring only a small negative balancing lift force on the horizontal stabilizer. This significantly increases the supersonic manoeuvrability and decreases the supersonic trim drag. The increased manoeuvrability during supersonic cruise flight is irrelevant for modern transport aircraft. However, the possibility of a relaxed static stability during the subsonic flight phase shows interesting possible performance advantages for commercial transport aircraft.

When a modern jet transport aircraft possess relaxed static stability, during the subsonic flight phase, the required horizontal stabilizer lift force is greatly reduced. This allows for a lighter horizontal stabilizer design. A well-known phenomena in the aviation industry is the increased mass snowball effect. When the mass of an aircraft component increases, the aircraft becomes heavier, requiring a larger lift force. This in turn increases the wing weight and drag coefficient, requiring more powerful engines and thus more fuel. The opposite is also true, when for example the horizontal stabilizer area decreases (i.e. decreased horizontal stabilizer weight), due to a reduced stability margin, the aircraft is lighter and requires a smaller lift force. In turn this could result in a lighter wing and lighter engines which requires less fuel. A reduced stability margin influences major aircraft components and could potentially increase the overall performance of the aircraft. The latter statement results in the following research question:

"What is the influence of a decreased static longitudinal stability on the overall aircraft performance in terms of maximum take-off mass?"

At the Aerospace Engineering (AE) faculty at the Delft University of Technology (TU Delft) a preliminary aircraft sizing tool, called the Initiator is developed for conventional and unconventional aircraft configurations. The Initiator [6],[7], is a module based software, which allows for the development and implementation of separate modules. An accurate sizing module for the stabilizing surfaces is however not present at the moment of writing. This leads to the research objective of this thesis:

"Develop and implement a stabilizing surface sizing module for conventional and unconventional aircraft configurations in the Initiator."

In order to keep the Initiator generic and give the user the flexibility to opt for conventional and unconventional aircraft configurations, a sizing methodology needs to be developed for two-surface (i.e. conventional and canard) and three-surface aircraft configurations. Other configurations, such as the Prandtl plane and Blended-Wing-Body (BWB) are left out of the framework, because general design rules do not apply to the latter two aircraft configurations.

An integral part of the sizing module is the prediction of the average down- and upwash angle at an arbitrary point in the flow field. When multiple lifting surfaces are present in a single flow field, interference effects are present. Lifting surfaces placed in the wake of an upstream surface, experience a reduced effective angle of attack due to the downwash distribution. Lifting surfaces upstream of another lifting surface experience an increased effective angle of attack due the upwash of the lifting surface further downstream. This influences effective angles of attack of these surfaces and thus the lift coefficients are affected. In the case of a conventional aircraft, where the horizontal stabilizer produces a negative lift force, the downwash distribution of the wing increases the negative effective angle of attack of the horizontal stabilizer. When the altitude of the aircraft decreases, during the landing approach, the aircraft is subjected to the ground effect. Due to the presence of a ground plane the tip vortices of the wing are unable to fully develop. This reduces the average downwash angle at the horizontal stabilizer location, decreasing the negative effective angle of attack. In the latter case, the horizontal stabilizer needs to be able to produce a required negative lift force in order to pitch the aircraft up to the stall angle, with the centre of gravity in the most adverse position (i.e. the most forward located centre of gravity position) and the full flap setting. This produces the largest negative pitching moment of the aircraft less tail configuration. This highlights the importance of the prediction of the downwash distribution In Ground Effect (IGE).

This thesis document consists out of two parts. The first part is the thesis report which contains the theory, methodologies, results, discussion and conclusion the developed sizing methodology module. The second part of the report is the code documentation, which contains the architecture and explanation of the code.

Part I. Thesis Report
Part I of the thesis report contains all the background theory, the methodology of the down- and upwash prediction module and the methodology of the stabilizing surface sizing module. Both tools are validated against experimental data or compared to actual aircraft. The background theory is presented in Chapter 2. The down- and upwash prediction module is discussed and validated in Chapter 3. The stabilizing surface sizing methodology is presented and validated in Chapter 4. The results of a reduced stability margin on the overall aircraft performance for conventional and unconventional aircraft configurations is presented in Chapter 5. The conclusion and recommendations are given in the final chapter of Part I, Chapter 6.

Part II. Code Documentation
Part II of the thesis report contains the documentation of the developed code for this thesis assignment. The introduction on the code documentation is presented in Chapter 7. Chapter 8 contains the methodology and structuring of the code.

2

BACKGROUND THEORY

The Initiator is a preliminary sizing module, initially developed by T.H.M. Langen [6] at the Delft University of Technology in 2010. The Initiator is used for the initial sizing of various aircraft configurations, such as conventional, canard, Three-Surface Aircraft (TSA),Prandtl and Blended-Wing-Body. The Initiator is further developed by R.J.M. Elmendorp [7] and is redesigned as a module based software. This means that various aircraft components, such as the fuselage, wing, landing gear and stabilizing surfaces can be designed as separate modules and can be easily integrated in the Initiator. This thesis assignment focuses on the sizing of the stabilizing surfaces (i.e. horizontal stabilizer and canard) of two-surface and three-surface aircraft configurations. Currently the stabilizing surfaces in the Initiator are sized with the Class I volume coefficient method from Roskam [1]. The size estimation of the horizontal stabilizer and canard area with the use of volume coefficients is an approximation method based on the volume coefficient of previously built comparable aircraft. The limitation of this method is that the sizing is not based on specific design requirements, but on available aircraft data, which in itself is another limitation for unconventional aircraft. In the recent history of aviation the majority of the aircraft which are built are conventional aircraft. This means that there is a significant amount of data available for conventional aircraft, however the availability of unconventional aircraft, such as canard and Three-Surface Aircraft (TSA) configurations is rather limited. This reduces the accuracy of the approximation method using volume coefficients. This makes the Class I volume coefficient method not reliable enough for the sizing of the stabilizing surfaces. This means that for the two-surface and three-surface aircraft configurations a new quick reliable aerodynamic sizing methodology is needed in the Initiator. The goal of the thesis assignment is to develop and implement a suitable sizing method for the stabilizing surfaces of the pre-defined aircraft configurations. Because the downwash and upwash distributions behind and in front of the wing influence the lifting capabilities of the lifting surfaces further down- and upstream a methodology is needed to determine these influences. Therefore, the sub goal of this thesis assignment is to develop an accurate methodology to predict the average downwash angle at an arbitrary point in the flow field behind a wing with high-lift devices and to predict the average upwash angle at an arbitrary point in the flow field in front of a wing with high-lift devices, both in- and our outside the ground effect region.

2.1. HORIZONTAL STABILIZER AND CANARD REQUIREMENTS

The stabilizing surfaces, the horizontal stabilizer and canard, of two-surface and three-surface aircraft configurations play an important role in the overall design of the aircraft. They have to provide longitudinal static and dynamic stability as well as provide control for the pilot. The requirements for a satisfactory design are presented in this section. The requirements are derived from the Certification Specifications for Large Aeroplanes (CS-25)[8]. The following requirements from CS-25 must be kept in mind during the design process in order to arrive at a satisfactory design.

CS 25.145a Longitudinal Control

It must be possible at any point between the trim speed and stall speed to pitch the nose downward and trim the aircraft with the landing gear extended, the wing-flaps retracted and extended and with power off and at maximum continuous power on the engines.

CS 25.161 Stability
The aeroplane must be longitudinally, directionally and laterally stable. Suitable stability and control feel is required in any condition normally encountered in service.

CS 25.161 Trim
The aeroplane must maintain longitudinal trim during:

- A climb with maximum continuous power with landing gear and wing-flaps retracted or in take-off position.
- A glide with power off at a speed not more than 1.3 V_{SR_1} with the landing gear and wing-flaps retracted or extended and the most unfavorable center of gravity position and aircraft weight.
- Level flight at any speed from V_{SR_1} to V_{MO}/M_{MO}

CS 25.181 Dynamic Stability
Any short period oscillation, not including combined lateral-directional oscillations, occurring between 1.13 V_{SR} and maximum allowable speed appropriate to the to the configuration of the aeroplane must be heavily damped with the primary controls.

From the previous requirements, it is concluded that a satisfactory design is determined by a longitudinal stable aircraft which is controllable and can be trimmed at any given point in time. The longitudinal stability and controllability are further explained in 2.3. Another requirements which should be kept in mind during the design process is the pitch rate during the take-off rotation. The stabilizing surface(s) must be able to pitch up the aircraft, within a specified amount of time, by providing a large enough lift force. The aircraft must be able to safely reach the take-off velocity, V_2, on the runway during the take-off procedure. This could be a downward force in case of a horizontal stabilizer or an upward force in case of a canard aircraft. No specifications on the minimum required pitch rate during the take-off rotation are found in the Certification Specifications, however from Torenbeek it follows that for large transport aircraft a minimum pitch rate, $\dot{\theta}$, of 3 deg/s is a good estimate for the take-off rotation in order to safely reach V_2 [2].

2.2. AIRCRAFT CONFIGURATIONS

The vast majority of all operating transport aircraft are conventional shaped aircraft, where in a two lifting surface configuration the horizontal stabilizer is placed behind the wing. There are however reasons to differ from that option. This is discussed in the next two sections about two-surface and three-surface aircraft configurations. In order to make the sizing methodology generic and give the user greater design flexibility, the stabilizing surfaces of these three configurations need to be sized for a given wing-body geometry input. Within the preliminary size estimation software, the Initiator, it is also possible to estimate the size of Blended-Wing-Bodies (BWB) and Prandtl aircraft configurations. However due to the fact that general design rules do not apply to these types of aircraft, they are left out of the framework of this thesis assignment. BWB and Prandtl aircraft designs require an extensive knowledge of exotic aircraft design.

2.2.1. TWO-SURFACE AIRCRAFT

Two-surface aircraft are defined as an aircraft with two lifting surfaces. The possible two-surface aircraft configurations are the conventional and canard aircraft. The canard has a stabilizing surface, called a canard, in front of the wing instead of a horizontal stabilizer behind the wing. There can be design requirements why an aircraft engineer might opt for a canard configuration over a conventional configuration. One advantage of a canard aircraft is, that the aircraft can be trimmed, where both lifting surfaces provide a lift force in the positive direction. In contrast to a conventional aircraft, where the horizontal stabilizer will provide a relatively small down force in order to balance the nose down pitching moment of the wing-fuselage combination. Two examples, one of a conventional and one of a canard configuration are presented in Figure 2.1, where a McDonnell Douglas KC-10 is displayed as the conventional aircraft and a Beechcraft Starship I as the canard aircraft.

The result of a down force on the horizontal stabilizer, is that the wing of the conventional configuration has to compensate for this down force by increasing lift and thus increasing induced drag, D_i. Canard aircraft generally have better stalling characteristics than conventional aircraft, because the stabilizing surface is only slightly influenced by the upwash of the wing, whereas the horizontal stabilizer is in the wake of the wing and experiences a downwash. This is exaggerated with deflections of high-lift devices and flight cases with higher angles of attack. The induced drag of two-surface aircraft configurations is minimized when the lift force of the stabilizing surface equals zero [9].

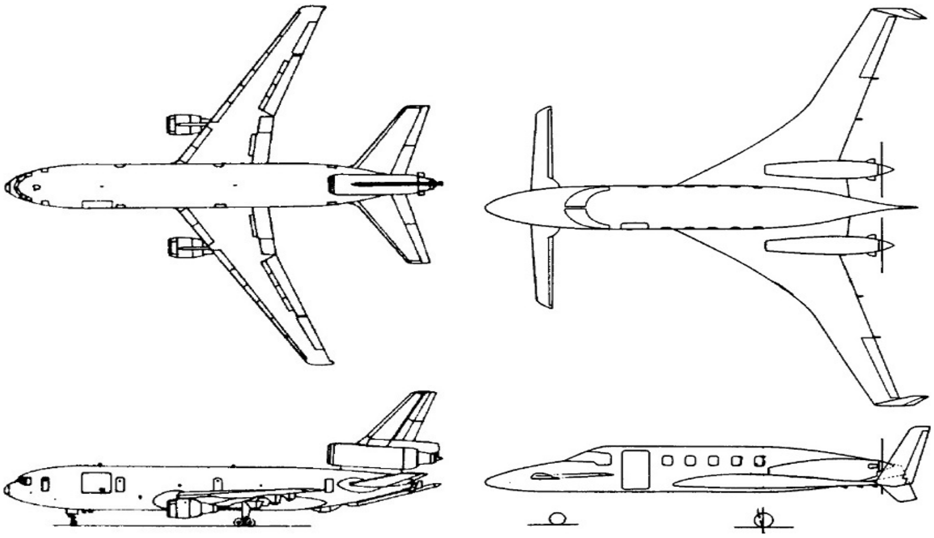

(a) A conventional aircraft

(b) A canard aircraft

Figure 2.1: Two-surface aircraft, a conventional McDonnell Douglas KC-10 and a canard Beechcraft Starship I [1].

2.2.2. THREE-SURFACE AIRCRAFT

Besides the possible advantages of canard aircraft over a conventional aircraft, three-surface aircraft have also shown to have beneficial characteristics. A study by Butler, G.E. has shown that the induced drag of a three-surface aircraft can be potentially lower than the induced drag of either a conventional or a canard configuration in cruise and in high-lift conditions [10]. Another advantage of a three-surface aircraft, is that the allowable center of gravity range is larger compared to two-surface aircraft. The real benefit of this larger allowable center of gravity range lies in the fact that the induced drag of three-surface aircraft can reach a state of minimum induced drag for all allowable center of gravity positions [11]. This is not possible in two-surface configurations, because the conventional and canard aircraft can only achieve minimum induced drag at one center of gravity location, namely the location where the lift force of the stabilizing surface is zero (i.e. either L_h or L_c). As mentioned before, the canard aircraft cannot fly at the trimmed condition for minimum induced drag and be inherently stable. The conventional aircraft requires a small down force during almost all flight conditions. This down force has to be compensated by the wing lift and therefore thus increasing induced drag. An example of a three-surface aircraft is given in Figure 2.2. The Piaggio P180 Avanti is a well known successful three-surface aircraft. From a study by Kendall, E., it follows that the minimum induced drag of a three-surface aircraft can be reached when the lift force of the canard equals the lift force of the horizontal stabilizer in the opposite direction, see equation 2.1 [12].

$$L_c = -L_h \tag{2.1}$$

A three-surface aircraft has two stabilizing surfaces. It has to be mentioned that the findings from Kendall do posses some limitations. Kendall did not account for interference effects between lifting surfaces. The aerodynamic representation of the model is very simplified. Fuselage, nacelle and thrust influences are neglected. These are contributions which can significantly influence the aerodynamic characteristics. A study by Selberg, B.P and Rokhsaz, K shows that the simplified model from Kendall, does over predict the performances of three-surface aircraft [13]. However the Piaggio P180 Avanti proofs that three-surface aircraft can indeed be successful. Therefore in the conceptual design phase, the designer might chose a TSA over other configurations. In order to keep the existing Initiator software generic, the stabilizing surface sizing methodology should be able to handle all two- and three-surface aircraft configurations.

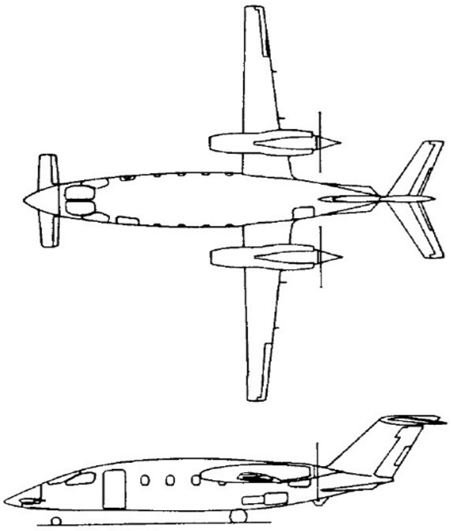

Figure 2.2: Three-surface aircraft configuration, Piaggio P180 Avanti[2]

2.3. STABILITY AND CONTROL

From the functions and requirements in section 2.1, the stabilizing surfaces of two-surface and three-surface aircraft have to provide longitudinal stability and control. This section covers the basic theory related to the longitudinal stability and control of two-surface and three-surface aircraft configurations. The longitudinal stability and controllability of any aircraft is closely related to the position of the center of gravity and the neutral point of the aircraft. In order to design a neutrally longitudinal statically stable aircraft, the neutral point of the aircraft should be located at the same longitudinal position as the center of gravity. When the neutral point moves further aft, the aircraft becomes stable. The further aft the neutral point the more stable the aircraft is. When the neutral point of the aircraft lies in front of the center of gravity, the aircraft is called unstable. A negative consequence of an increasing longitudinal stability is the decrease in controllability. Every aircraft has an allowable range of center of gravity positions, called the operational range. These center of gravity positions are derived from a loading diagram. An example of a developed loading diagram is given in 2.3.

The start of the loading diagram is the Operational Empty Mass (OEM), this is the mass which is independent of loading the aircraft and therefore has a fixed center of gravity position. Many different loading scenarios are possible which results in different allowable center of gravity positions. It is therefore of interest to know at an early stage what the most forward and aft located allowable center of gravity locations are. These minimum and maximum values are derived from the loading diagram.

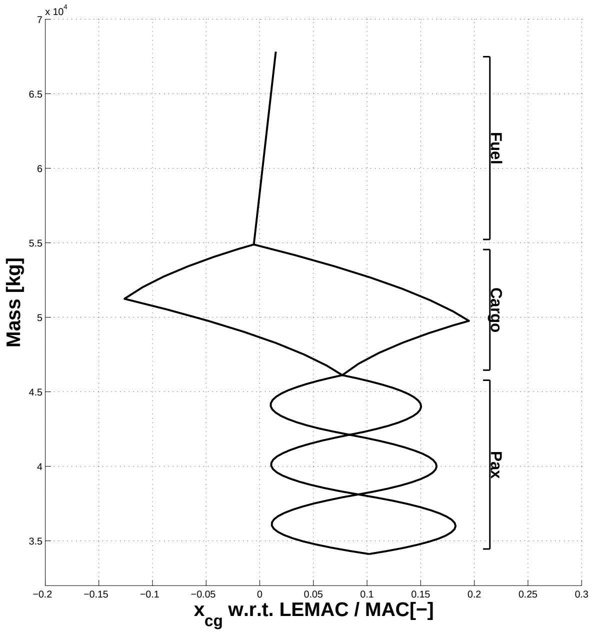

Figure 2.3: Example of a developed loading diagram within the stabilizing surface sizing methodology.

The purpose of the loading diagram is to cover all loading possibilities and therefore derive the minimum and maximum center of gravity locations. From the start point, the OEM, the aircraft is first filled with passengers, followed by the cargo and finally the fuel, this is clearly visible in 4.1. From the latter figure it can also be seen that the passenger and cargo loading diagram covers a certain area, whereas the fuel loading is visualized by two curves. These two areas for the passenger and cargo loading are a result of the different loading scenarios. Two extremes cases are simulated for the cargo and passenger loading. The front-to-back loading and back-to-front loading. In the first case the passengers are loaded, by there respectively traveling class (i.e. economy, business and first class), from the front to the back, this results in the most forward center of gravity position due to passenger loading. The back-to-front loading results in the most aft center of gravity position due to passenger loading. The same loading technique applies to the cargo loading. When the most forward and aft located center of gravity positions are known, the center of gravity range can be determined. This is an important design parameter for the minimum required stabilizing surface area. The importance of this parameter is further elaborated in 2.6. In this thesis assignment only longitudinal stabilizing surfaces are designed with the sizing methodology, therefore only longitudinal stability and control is considered. The longitudinal stability is discussed first, this is followed up with theory on longitudinal control.

2.3.1. STATIC LONGITUDINAL STABILITY

As mentioned in the previous section, the stability of the aircraft is related to the position of the center of gravity and the neutral point. The neutral point is an artificial point on the aircraft at which the total lift force acts. The terminology used in this section is clarified in Figure 2.4. It is common practice to calculate with dimensionless variables. In the case of a stability analysis, the distances are made dimensionless by dividing the longitudinal distance by the Mean Aerodynamic Chord (MAC). The longitudinal distances are measured from the Leading-Edge of the Mean Aerodynamic Chord (LEMAC), as is illustrated in Figure 2.4, where the reference location is the LEMAC. The aerodynamic center in the latter figure denotes the aerodynamic center of the aircraft less tail configuration. It can be seen that the aerodynamic center of the aircraft less tail is located in front of the center of gravity.

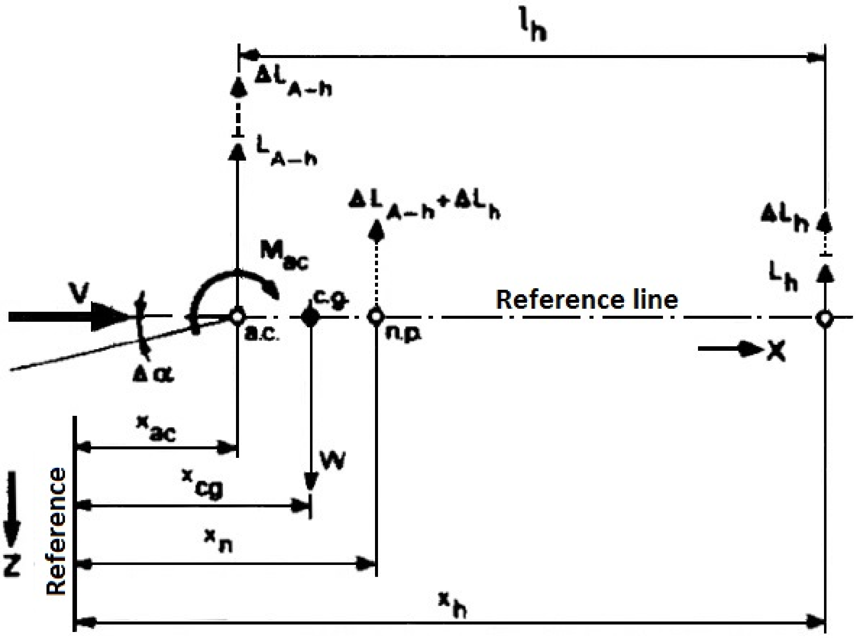

Figure 2.4: Terminology of the longitudinal parameters for control and stability analysis

From the latter figure, the stabilizing contribution of the horizontal stabilizer is clearly visible. Due to the stabilizing contribution of the horizontal stabilizer, the neutral point of the aircraft is located behind the center of gravity, which defines a longitudinal statically stable aircraft. The magnitude of the stability is defined by the stability margin of the aircraft. The stability margin is defined as the longitudinal distance between the aft center of gravity position and the neutral point, see equation 2.2. When the horizontal stabilizer surface area, for a conventional aircraft, decreases. The neutral point moves towards the center of gravity, decreasing the stability margin of the aircraft. When the neutral point coincides with the center of gravity, the aircraft is called neutrally stable. When the horizontal stabilizer area is further decreased and the neutral point is located in front of the center of gravity, the aircraft is longitudinal statically unstable and possess a negative stability margin.

$$\mathrm{SM} = \frac{x_{\mathrm{np}} - x_{\mathrm{cg}}}{\bar{c}} \tag{2.2}$$

An increase in the stability margin, increases the stability of the aircraft, but this will result in a decrease in controllability. Typical values for the static margin of jet transport aircraft usually are around the order of 5%, however larger values are also known, even ranging up to 15%. The stabilizing surface of any aircraft has to balance the negative pitching moment of the aircraft less tail configuration. This means that from a stability perspective the pitching moment coefficient C_M has to decrease for an increasing angle of attack, α, in order to return to the original state. This criteria can be seen in equation 2.3.

$$\frac{\partial C_M}{\partial \alpha} < 0 \tag{2.3}$$

When equation 2.3 is satisfied, the aircraft can be called longitudinal stable. The contribution of the stabilizing surface to the negative change in pitching moment coefficient with increasing angle of attack is visualized in Figure 2.5. The line B in the latter figure represents the aircraft without stabilizing surface(s). It can be seen that the pitching moment coefficient derivative with respect to the angle of attack is positive. This means that the aircraft will pitch further nose up with increasing angle of attack. This is clearly an unstable configuration, since a return to the original state is impossible.

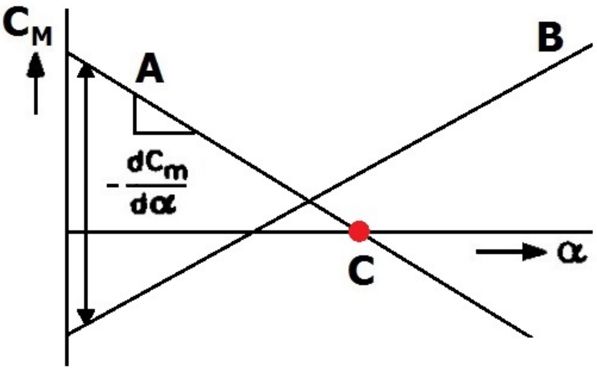

Figure 2.5: Pitching moment contribution of complete aircraft compared to an aircraft without stabilizing surfaces [2].

The contribution of the stabilizing surfaces are included in line A. Line A has a negative pitching moment slope, which satisfies equation 2.3. Therefore any increase or decrease in angle of attack, α, causes the aircraft to return to its original state. In the same figure also a point C is present. Point C denotes the trimmed condition. The total pitching moment coefficient is zero at that location.

2.3.2. DYNAMIC LONGITUDINAL STABILITY

When an aircraft is statically stable, it does not necessarily automatically impose dynamic stability. This implies that dynamic stability needs to be analyzed separately. In the case of longitudinal dynamic stability, two cases can be defined. The long period oscillation, also often referred to as the Phugoid oscillation, and the Short Period (SP) oscillation [14]. During the long period oscillation the airspeed and the pitch angle vary significantly, whereas in the short period oscillation the variation in the airspeed is limited. The short period oscillations can impose limitations on the center of gravity positions as will be seen in more detail in section 2.6.

2.3.3. LONGITUDINAL CONTROL

Whereas the stability of the aircraft is closely related to the aft center of gravity location, the controllability of the aircraft is related to the forward center of gravity location. When the center of gravity moves further aft, towards the neutral point, the controllability of the aircraft increases. One of the important contributions of the stabilizing surface to the aircraft control is the balancing force of the horizontal stabilizing to the pitching moment of the aircraft less tail. The pitching moment of the aircraft less tail is dominated by the pitching moment of the wing, especially with deflections of high-lift devices. In Figure 2.6 three settings are presented, the clean wing configuration, the take-off flap setting and the landing flap setting. In the latter figure it can be seen that for an increasing flap setting the pitching moment coefficient significantly increases. Here it is also very important to note that the center of gravity position plays an significant role in the magnitude of the pitching moment.

The minimum and maximum values for the pitching moment coefficient for all flap settings from Figure 2.6 are displayed in Table 2.1. Also the range between the minimum and maximum values is displayed.

From the latter table it can be concluded that in the case of the clean wing configuration the difference in the pitching moment coefficient between the aft and forward located center of gravity position is 0.27, whereas the difference for the take-off flap setting is 0.43 and for the landing setting even 0.95. This is a very large difference between the most forward and aft located center of gravity position. It can also be concluded that the largest negative pitching moment coefficient which needs to be balanced by the stabilizing surface results from the landing flap setting and the most forward located center of gravity position. This is imposes a limitation on the allowable forward center of gravity posi-

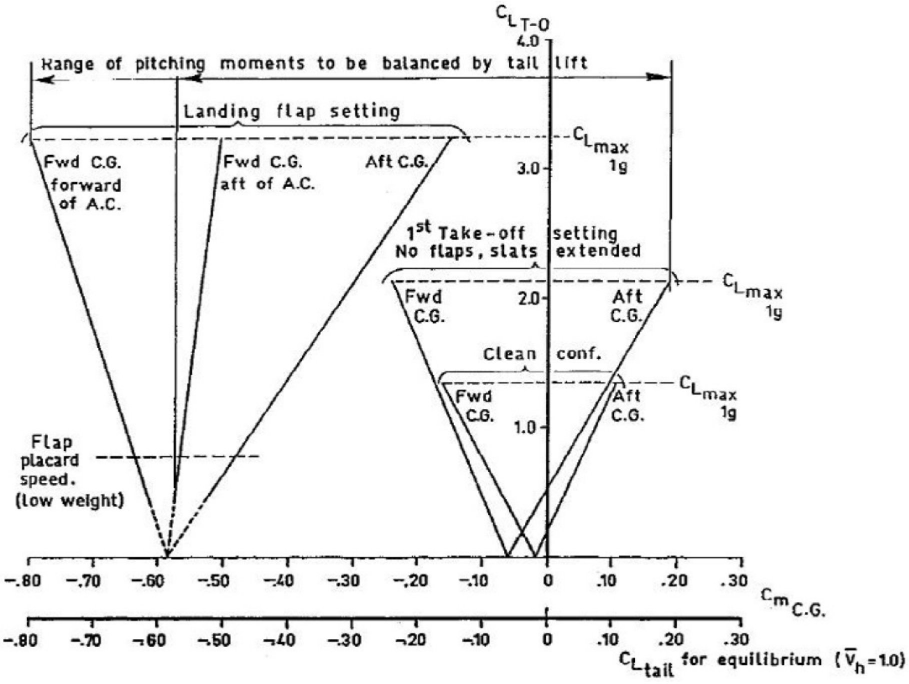

Figure 2.6: Variation of the pitching moment due to increasing flap and slat deflections [3].

Table 2.1: Pitching moment coefficient for different flap settings

Flap Setting	$C_{m_{cg}}$ at aft CG	$C_{m_{cg}}$ at fwd CG	$C_{m_{cg}}$ range
Clean Wing	0.11	-0.16	0.27
Take-off	0.19	-0.24	0.43
Landing	-0.15	-0.80	0.95

tion as will be seen later in section 2.6.

2.4. DOWN- AND UPWASH PREDICTION

When a wing is subjected in a flow field and generates a lifting force, the lift is generated as a result of a downwards deflected flow vector at the trailing-edge of the lifting surface. The angle is called the downwash angle of a lifting surface and effects the effective angle of attack of other downwards located surfaces (i.e. a horizontal stabilizer). For lifting surfaces located in front of the wing, the effective angle of attack is increased as a consequence of the lift generation. The increase in effective angle of attack is called the upwash angle. Both the upwash and downwash angles influence the effective angles of attack of surfaces located upstream and downstream of the main lifting surface, therefore it is important to have an accurate downwash prediction methodology during the preliminary design of the aircraft. The interference effects of two-surface and three-surface aircraft are displayed in Figure 2.7 and Figure 2.8. In the latter figures the influence of an upstream lifting surface on a downstream lifting surface is illustrated. In the case of a conventional aircraft, Figure 2.7, the tip vortices of the wing do not aerodynamically influence the horizontal stabilizer due to the fact that the span of the horizontal stabilizer is much smaller than the wing span. This results in a constant downwash distribution at the location of the horizontal stabilizer.

In the case of a canard aircraft, the wing only influences the canard surface through an increase in effective angle of attack due to the upwash. This can be seen in Figure 2.8(a). However in the latter figure

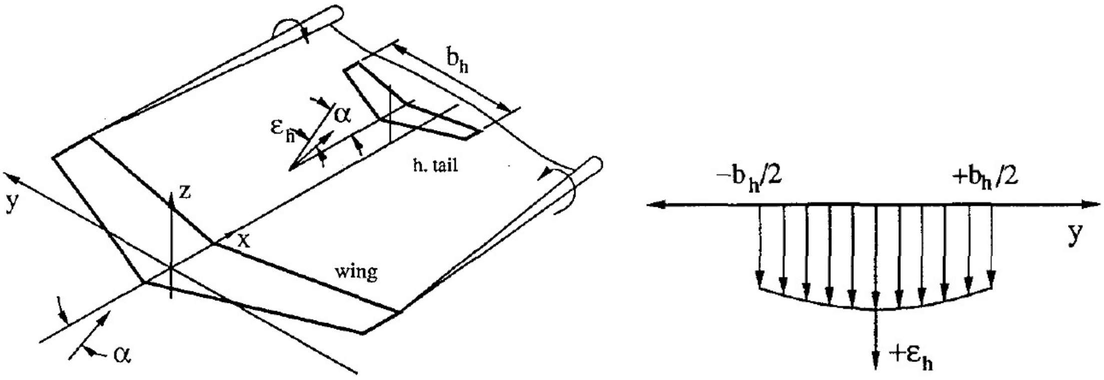

(a) Aircraft configuration (b) Downwash at the tail

Figure 2.7: Downwash at the horizontal stabilizer for a conventional aircraft configuration [4].

it can also be seen that the canard surface aerodynamically influences the main wing. The downwash distribution at the wing is displayed in Figure 2.8(b). The downwash distribution at the wing changes the spanwise lift distribution. In case of a three-surface aircraft, the changed spanwise lift distribution influences the effective angle of attack at the horizontal stabilizer, similarly as on a conventional aircraft configuration. However the changed spanwise lift distribution increases the complexity on the average downwash angle calculation, as opposed to a conventional aircraft , where the main wing is unaltered by an lifting surface further upstream. Two advantages and limitations of two existing methods are discussed next.

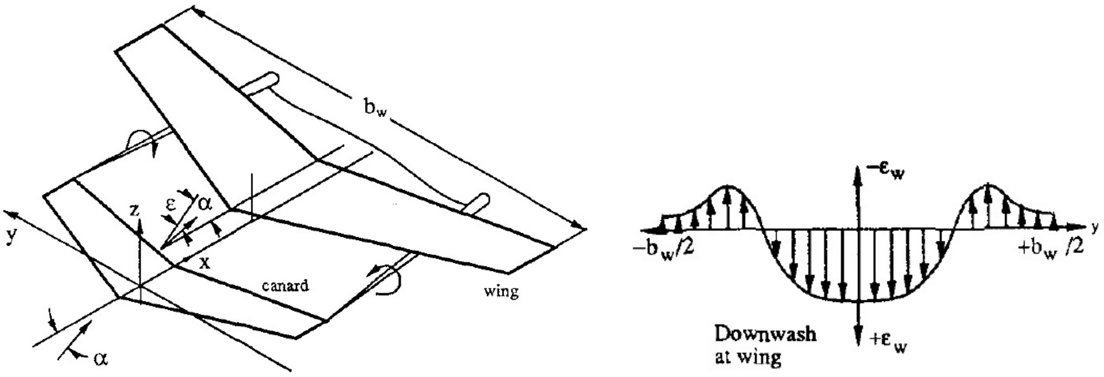

(a) Aircraft configuration (b) Downwash at the wing

Figure 2.8: Downwash at the wing for a canard aircraft configuration[4].

ESDU

The ESDU 97021 method [15] is a downwash prediction method for conventional aircraft, where the horizontal stabilizer is positioned roughly by a distance of half the wing span behind the wing. The 97021 method is able to predict the average downwash angle at the location of the horizontal tail for a t-tail or fuselage mounted stabilizer. The latter method is a graphical method, which is based on extensive wind tunnel data of conventional aircraft. The average downwash angle is calculated in free-air conditions and no ground plane is simulated. However with the extension of ESDU 72023 a correction can be applied to determine the change in average downwash angle at a specific height [16]. The latter method is able to cope with the presence of high-lift devices. The advantages of this method is the ability to determine the average downwash angle for conventional aircraft in ground effect with the presence of high-lift devices. Limitations of the ESDU 97021 and ESDU 72023 methods are the inability to determine the average downwash angle at an arbitrary point in the flow field and the inability to determine the average upwash angle at an arbitrary point in the flow field in front of the wing. From an implementation perspective a disadvantage, but not a limitation, is the digitalization of the graphs. When this method is to be implemented, a total of 57 graphs need to be digitalized. Both the ESDU 97021 out of ground effect and the ESDU 72023 in ground effect method are validated for two aircraft. A t-tail aircraft configuration, the Fokker 100 and a fuselage mounted stabilizer configuration, the Airbus A330. The ESDU 97021 out of ground effect validation is displayed in Figure 2.9.

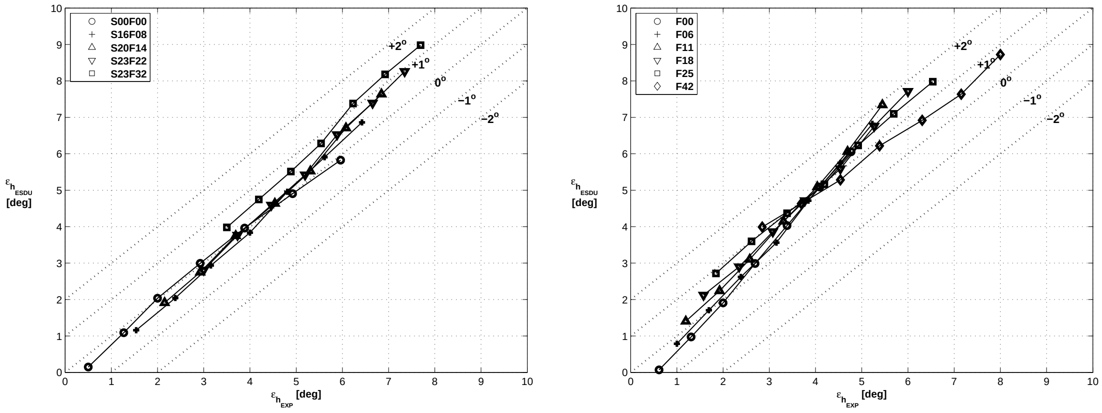

(a) A330

(b) F100

Figure 2.9: ESDU 97021 average downwash angle validation OGE

In Figure 2.9(a) the acronym S16F08 represents the curve with a flap deflection of 8 degrees and a slat deflection of 16 degrees. Each different curve represents a different flap and slat setting. Each curve consists out of 7 data points. Each data point represents a different angle of attack ranging from 0 degrees to 12 degrees with increments of 2 degrees. The experimental data is displayed on the horizontal axis, whereas the obtained average downwash angle form the ESDU method is displayed on the vertical axis. If a curve is displayed on the zero degree deflection curve, the experimental data points coincide with the ESDU data points. From the latter figure it can be seen that the for both the t-tail and the fuselage mounted stabilizer the out of ground effect downwash prediction of the ESDU 97021 method is validated over the entire range of angles of attack and flap and slat settings within an accuracy of $\pm 2^{\circ}$.

The validation of the in ground effect correction method of ESDU 72023 is presented in Figure 2.10(a) and (b). Similar curves are present on the IGE curves as on the OGE curves, although for the Fokker 100 only in ground effect data of the clean wing and the full flap setting was found. It can be seen that the average downwash angle is significantly reduced due to the presence of a ground plane. For the in ground effect analysis the aircraft is positioned on the ground plane. For the Airbus A330 it can be seen that for all flap settings the average downwash angle is slightly under predicted, whereas for higher angles of attack the average downwash angle is slightly over predicted. Similarly as in the OGE case the downwash angles are validated with an accuracy of $\pm 2^{\circ}$. The reduction of the average downwash angle for the Fokker 100 is significantly lower than the reduction in average downwash angle for the Airbus A330. This is due to the fact that the Fokker 100 possess a t-tail configuration where the horizontal stabilizer is positioned much higher above the ground plane, than the fuselage mounted stabilizer. In the case of a fuselage mounted stabilizer and moderate to higher angles of attack, the tailplane is located very close to the ground plane. In the latter case very small increases in downwash angles with angle of attack are obtained. This is clearly visible in Figure 2.10(a), where on the horizontal axis the average downwash angle stagnates on the vertical 2 degrees line. Another limitation of the ESDU method is the inability to simulate the change in spanwise lift on the main lifting surface of the Three-Surface Aircraft (TSA) due the the presence of a canard surface, as discussed earlier in this section. For the ESDU method an unaltered wing scenario is assumed. This disallows the prediction of the average downwash angle for a TSA configuration.

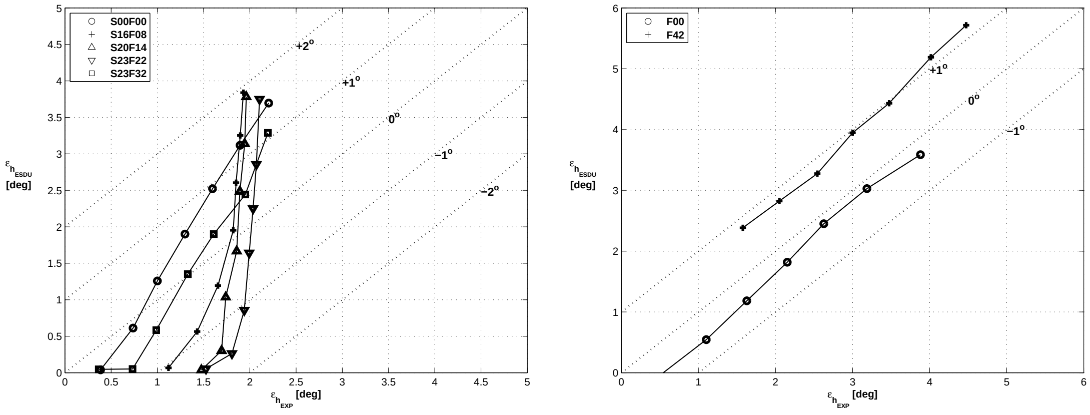

(a) A330

(b) F100

Figure 2.10: ESDU 72023 average downwash angle validation IGE

Slingerland

An analytical method developed by R. Slingerland [17] has an implemented ground effect simulation. The advantage of the Slingerland method over the ESDU 97021 and ESDU 72023 methods is the ability to determine the average downwash angle at an arbitrary point in the flow field behind the wing, whereas the ESDU methods are fixed to a point in the flow field of half the wing span behind the wing. Slingerland method is not based on experimental wind tunnel data, but is an analytical method. This allows for an easier implementation in the sizing methodology. Similarly as displayed in the ESDU method, the analytical Slingerland method is validated for a t-tail aircraft, the Fokker 100 and a fuselage mounted stabilizer, the Airbus A330. The out of ground effect validation is displayed in Figure 2.11(a) and (b). From the latter figure it can be seen that the for both aircraft the Slingerland method is validated within an accuracy of ±2°, showing a slightly under prediction over the entire range of angles of attack and flap and slat settings. Both the ESDU and Slingerland method show a similar accuracy in the prediction of the average downwash angle.

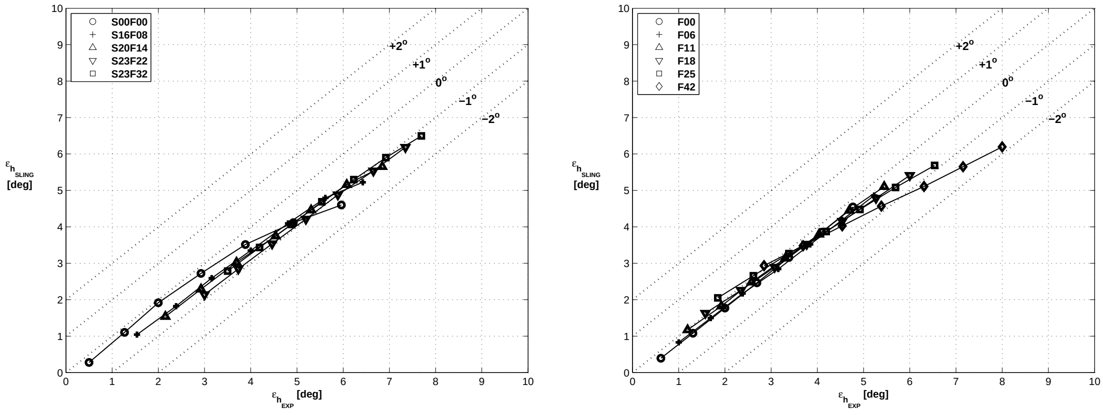

(a) A330

(b) F100

Figure 2.11: Slingerland average downwash angle validation OGE

The in ground effect validation is illustrated in Figure 2.12(a) and (b). Again the in ground effect validation represents zero altitude, where the wheels are just on the ground. The in ground effect analysis of the Slingerland method shows an increased accuracy over the ESDU method. Over the entire range of the data points the Slingerland method shows a slight under prediction and is validated within an accuracy of almost ±1°. Whereas the ESDU method showed a slight over prediction for the t-tail aircraft, the Slingerland method shows a slight under prediction with a maximum error equal in magnitude.

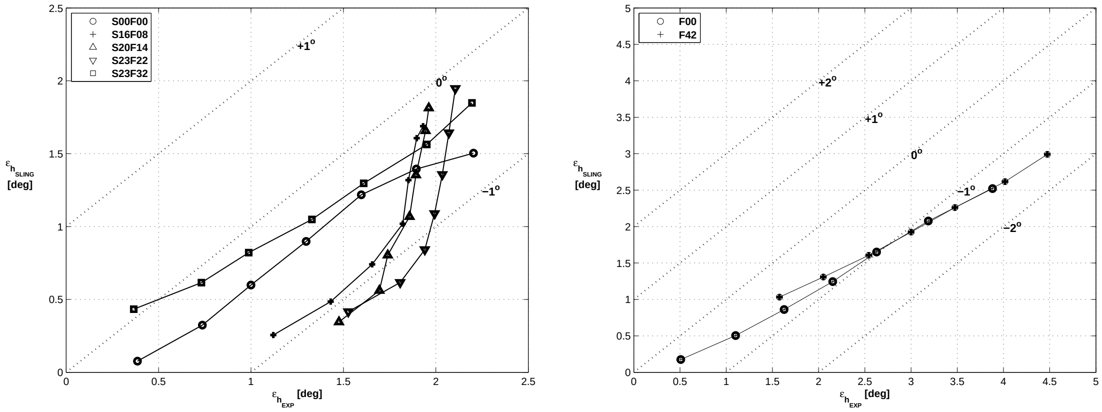

(a) A330

(b) F100

Figure 2.12: Slingerland average downwash angle validation IGE

A limitation to the method is the inability to determine the average upwash angle at an arbitrary point in the flow field in front of the wing. Similarly as for the ESDU method this method does not allow for a simulation of an altered spanwise lift distribution due to the presence of a canard surface for a TSA aircraft. This reduces the accuracy on the average downwash angle calculation at the horizontal stabilizer location for a three-surface aircraft. Both methods are limited in the ability to determine the average upwash angle at an arbitrary point in the flow field and the implementation of adding a third lifting surface in the flow field, which alters the spanwise distribution on the wing. Therefore a new method is needed which is able to cope with these requirements. A developed in and out of ground effect down- and upwash prediction method with the presence of high-lift devices for two- and three-surface aircraft is presented in chapter 3.

2.5. GROUND EFFECT AERODYNAMICS

The changes in aerodynamic characteristics due to the presence of a ground plane on the average downwash angle is briefly discussed in section 2.4. The decrease in the average downwash angle with decreasing altitude due to a ground plane is not the only change in aerodynamic characteristics. Due to the presence of the ground plane the tip vortices of a lifting surface are unable to fully develop. This results in a decreased strength of these tip vortices and therefore a reduction in induced drag C_{D_i}. A second influence in aerodynamic characteristics, is the increase of the lift coefficient for the same angle of attack. This means that for an approaching aircraft (i.e. decreasing altitude, lower than the wing span), when the angle of attack is held fixed, the lift coefficient slowly starts to increase, whereas the drag coefficient starts to decrease. For a pilot this phenomena could be a floating experience, especially very low to the ground, where the increase in lift-to-drag ratio is maximized.

For the take-off phase this situation is obviously reversed, the lift coefficient due to the ground effect starts to decrease, whereas the drag coefficient starts in increase with increasing altitude. In the ground effect region, the stall speed of the aircraft is reduced. This consequence of the reduction in stall speed is that the aircraft must be accelerated further than the in ground effect stall speed during take-off, because when the aircraft enters the out of ground effect region, the stall speed is suddenly increased. For the stabilizing surfaces of an aircraft it is important that the maximum design lift coefficient can be achieved under all flight conditions. A study by Ranzenbach, R on a negative cambered NACA 4412 airfoil used on a modern Formula One car, has shown that the maximum negative lift coefficient could increase from −0.954 out of ground effect to −1.167 in ground effect. This results in an increase of 22.33% solely due to the presence of the ground [18]. The increase in maximum negative lift coefficient could be related to the negative lift contribution of the horizontal stabilizer during the landing and take-off flight phases. The increase in maximum negative lift coefficient seems beneficial for the design of the horizontal stabilizer, because the maximum attainable lift coefficient is only increased. However the effective angle of attack is greatly reduced due to the presence of the ground, significantly decreasing the maximum attainable negative lift coefficient. This is one of the reasons why modern transport aircraft possess an adjustable horizontal stabilizer, where the incidence angle (i.e. effective angle of attack) could be altered for different phases of the flight envelope. The changes in aerodynamic characteristics due to the presence of a ground plane are discussed in this section and the section on down- and upwash prediction. It is important during the preliminary design phase, to have a quick aerodynamic analysis method which is able to predict these changes in aerodynamic coefficients.

2.5.1. REDUCTION IN AVERAGE DOWNWASH ANGLE

The importance of the reduction in the downwash angle In Ground Effect (IGE) with decreasing altitude is displayed in Figure 2.13. Both graphs are created with the developed downwash prediction methodology presented in chapter 3. In the latter figure it can be seen that the average downwash angle is greatly reduced when the aircraft is at an altitude lower than its own wing span. The vertical bar represents the altitude at which the aircraft is at an altitude of its own wing span. If the aircraft further descents, the average downwash angle is greatly reduced for all angles of attack. It is interesting to note that for the full flaps setting the average downwash angle is roughly independent of the angle of attack at zero altitude. This is clearly visible in Figure 3.9(b) where the downwash angles for different angles of attack coincide between the 1.5 and 2 degrees.

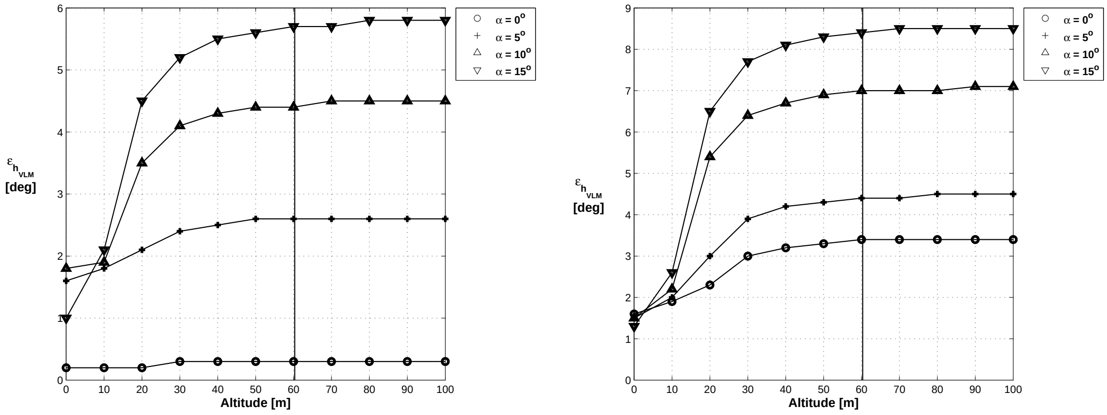

(a) Clean wing (b) Full flaps

Figure 2.13: Reduction of the average downwash angle with altitude for the Airbus A330.

The latter figure illustrates the importance of the reduction in the average downwash angle with decreasing altitude. When the average downwash angle decreases at the horizontal stabilizer, the negative effective angle of attack is also reduced. This is an important design consideration for the sizing of the stabilizing surfaces, as the design constraint states that the maximum design lift coefficient should be attainable in every flight condition. This is further addressed in chapter 4.

2.6. STABILIZING SURFACE SIZING METHODS

In this section sizing methods for the stabilizing surfaces of two-surface and three-surface aircraft configurations are discussed. Currently a volume coefficient sizing method is implemented in the Initiator. The advantages and limitations of the volume coefficient method are discussed briefly in section 2.6.1. A more elaborated sizing method, called the x-plot method, is discussed in section 2.6.2.

2.6.1. VOLUME COEFFICIENTS

Currently the stabilizing surfaces in the Initiator are sized using volume coefficients. The volume coefficient method is a Class I sizing method used in the early stages of the conceptual design phase. With this method it is possible to quickly determine an initial minimum required stabilizing surface area for the horizontal stabilizer, S_h, or of the canard surface, S_c. The volume coefficient method, derived from Roskam, is presented in equation 2.4 [1].

$$S_i = \frac{V_i S \bar{c}}{l_i} \tag{2.4}$$

In the latter equation the subscript i could either represent a c for a canard surface or a h for a horizontal stabilizer. From equation 2.4 it can be seen that the in order to determine the minimum required stabilizing surface area, S_h or S_c, the moment arm, l_h or l_c, the wing surface area, S, mean aerodynamic chord, $\bar{c}$ and the volume coefficient, V_h or V_c, need to be known. The geometric parameters follow from the initial wing design, whereas the volume coefficients are derived from data of similar previously built comparable aircraft. The last statement is also a limitation of this method. The majority of current existing aircraft are conventional two-surface aircraft, where the stabilizing surface is located behind the wing. Not much data is available on canard and three-surface aircraft. This reduces the accuracy of the volume coefficient method. Another limitation of the volume coefficient method is that it is not a requirement based method. The initial sizing based on volume coefficient does not imply that design requirements, as discussed in section 2.1, are satisfied. It is merely a rough approximation method during the conceptual design phase. Therefore the initial sizing method needs to be replaced with a more detailed, requirement based, sizing method.

2.6.2. X-PLOT METHODOLOGY

The x-plot methodology, often also referred to as the scissor plot methodology, is a sizing method for finding the minimum required stabilizing surface area for two-surface and three-surface aircraft configurations. Design constraints impose limits on the forward and aft center of gravity positions. An example of an x-plot diagram is given in 2.14. The latter x-plot is developed with the stabilizing surface sizing methodology, as presented in Chapter 4.

From the latter figure it can be seen that multiple design requirements are implemented in the x-plot. A distinction is made between forward and aft center of gravity limitations. The aft center of gravity limitations are related to the stability of the aircraft, whereas the forward center of gravity limitations are related to the control of the aircraft. This is discussed in the section on stability on control in section 2.3. On the horizontal axis the center of gravity positions are displayed with respect to the Leading-Edge Mean Aerodynamic Chord (LEMAC) of the wing divided by the Mean Aerodynamic Chord (MAC). In Figure 2.14 the horizontal stabilizer area is displayed on the vertical axis. The minimum required area can be read of when the center of gravity range of the aircraft is known. The center of gravity range is determined with the loading diagram, as discussed in 2.3. The required area is defined as the lowest location on the x-plot at which the center of gravity range 'fits' between the forward and aft center of gravity limits. This implies that one dominant forward and one dominant aft center of gravity limit is present. In Figure 2.14 the dominant forward center of gravity limit, is the 'control stall' (requirement 3). The dominant aft center of gravity limit is the 'neutral point stick-fixed' (requirement 2). The advantage of the x-plot method is the ability to apply design requirements on the stabilizing surface sizing. Different design requirements can be imposed or neglected on the x-plot, depending on the desired design requirements. Another advantage of the x-plot methodology is the possibility to size the stabilizing surfaces of all two-surface and three-surface aircraft configurations. For a canard aircraft a similar design strategy as for the conventional aircraft can be set up. Instead of reading of the minimum required horizontal stabilizer area, the minimum required canard surface area can be read of on the vertical axis.

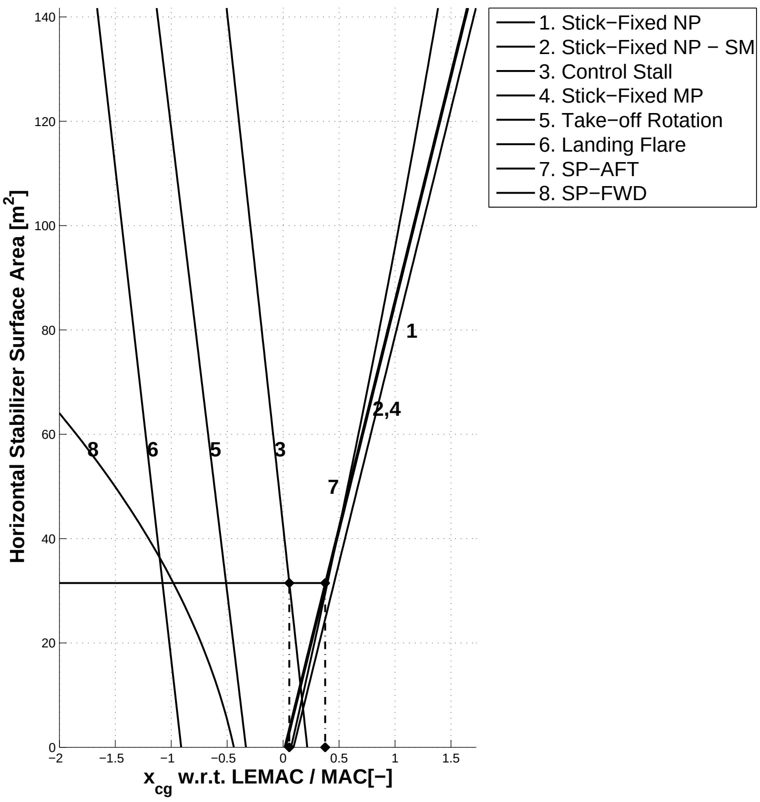

Figure 2.14: Example of a x-plot developed with the stabilizing surface sizing methodology.

With the x-plot methodology it is also possible to determine the minimum required stabilizing surface areas of a three-surface aircraft. Because multiple stabilizing surfaces are present in the latter aircraft configuration, multiple x-plots should be created. An initial canard area to wing area ratio is assumed, this results in a corresponding x-plot to this particular canard to wing area ratio. From the x-plot the minimum horizontal stabilizer area can be determined for the fixed canard area ratio. This design process obviously could be performed the other way around, by fixing a horizontal stabilizer area ratio and determining the canard area ratio. In order to analyze multiple feasible design points, a wide range of initial fixed area ratios could be assumed, this results in an equal amount of corresponding minimum areas for the other stabilizing surface. Because all obtained combinations of canard and horizontal stabilizer area ratios are feasible design points, an extra design constraint should be imposed in order to find the optimum combination of area ratios.

2.7. RELAXED STATIC STABILITY

This thesis assignment focuses on the influence of a reduced stability margin on the overall aircraft performance. Most modern fighter aircraft possess artificial stability during cruise in order to reduce trim drag during supersonic cruise and increase the overall maneuverability of the aircraft. The implementation of relaxed static stability on modern transport aircraft is not as common as it is on modern fighter aircraft. The only known transport aircraft possess a relaxed static stability is the MD-11. The influence on a reduced stability margin on the aircraft performance is clearly visible in the design of the MD-11. The MD-11 was introduced in 1990, and is based on the design of the DC-10. In Table 2.2, aircraft parameters of the DC-10-30 and the MD-11 are highlighted. The DC-10-30 is illustrated in the latter table, because this version of the DC-10 is similar to the MD-11.

Table 2.2: Design differences between the DC-10-30 and the MD-11

Parameter	**DC-10-30**	**MD-11**	**Unit**
Pax (single class)	380	405	[-]
MTOM	265000	285081	[kg]
Wing area, S	367.70	338.90	[m^2]
Tail area, S_h	124.30	85.50	[m^2]
Area ratio, S_h/S	0.338	0.252	[-]

From Table 2.2 the differences between the two aircraft are clearly visible. The Maximum Take-Off Mass (MTOM) of the MD-11 is 7.58 % heavier than the MTOM of the DC-10-30. The wing area of the MD-11 is however 7.83% smaller than the wing area of the DC-10-30. The largest difference lies in the tail area. Although the MD-11 is heavier, the horizontal tail area is 31.21% smaller than the tail area of the DC-10-30. It has to be stated that it is not completely clear what the exact contribution of the decreased stability margin is on the overall aircraft performance in this particular case as this depends on many variables. However the trend in the decreased horizontal tail area is clearly visible in this case. The consequence of a decreased tail mass in theory results in a decrease in required aircraft lift and therefore a smaller wing. Which in turn reduces the overall aircraft mass and thus required fuel. The MTOM mass of the MD-11 is however larger than the MTOM of the DC-10-30, but this is a result of the increase in number of passengers (Pax) and the increase in the corresponding payload and fuel. A size comparison between the DC-10 and the MD-11 is given in Figure 2.15

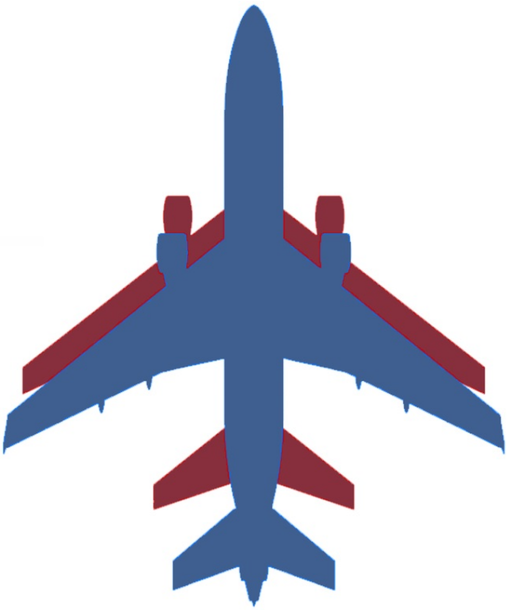

Figure 2.15: Size comparison between the MD-11 and the DC-10.

2.8. ICE ACCRETION

The stabilizing surfaces are designed in such a way that the maximum design lift coefficient could be attained in every flight condition. This includes the changes in aerodynamic characteristics due to the presence of a ground plane as discussed in sections 2.4 and 2.5. So far only optimum flow conditions are addressed, whereas there are situations where the lift coefficient of a lifting surface could be greatly decreased in non-optimal conditions. An example of a non-optimal flow condition is the situation of ice accretion on lifting surfaces. When there is ice present on an aircraft it should be de-iced before take-off in order assure that maximum design lift coefficient could be attained. However, it is possible that during flight, ice is formed on the lifting surfaces of the aircraft, especially in the leading-edge region. Almost all modern jet transport aircraft have an on-board anti-ice system, but due to malfunction of the system or pilot negligence a situation could occur that, for example the maximum negative design lift coefficient of the horizontal stabilizer could not be attained. This is clearly an undesirable situation and should always be avoided. Therefore it is important to know the effects of ice accretion on the aerodynamic characteristics of a lifting surface. From Obert, it follows that there are three main types of ice, namely rime ice, glaze ice and hoar-frost. Hoar-frost is the consequence when water vapour in warm air comes in contact with cold aircraft parts. This occurs mainly during overnight stops [3]. Rime ice and glaze ice are examples of ice accretion which could occur in flight and could significantly reduce the maximum lift coefficient of the lifting surfaces. A study from the Advisory Group for Aerospace Research and Development (AGARD) on the reduction of the maximum negative lift coefficient due to ice accretion on the horizontal stabilizer of the Fokker 28, has shown that with the simulation of ice accretion, the reduction of the maximum negative lift coefficient of the horizontal stabilizer due to ice accretion could be as high as 30% of the initial clean wing maximum lift coefficient [19]. This highlights the importance of ice simulation into the design.

2.9. INITIATOR

As mentioned in the introduction, the stabilizing surface sizing methodology has to be implemented in the Initiator. The Initiator is a preliminary sizing software for the design of conventional and unconventional aircraft configurations, developed at the TU Delft by Langen, T.[6] in 2011. The Initiator is rewritten as a module based sizing software by Elmendorp, R in 2014 [7]. The Initiator is currently written in the Matrix Laboratory (MATLAB). The module based programming allows for programmers to develop different modules, which can be implemented into the Initiator. The Initiator operates with three different types of modules, sizing modules, design modules and analysis modules. The stabilizing surface sizing methodology is a longitudinal stability and control analysis software, with the purpose of sizing the stabilizing surfaces. The created sizing methodology is therefore an analysis module within the Initiator. All modules are operated with dependencies, this allows for an easy integration into the Initiator. The created stabilizing surface sizing methodology is expected to be dependent on the Class II Weight Estimation module, because in the latter module all the required input geometry parameters for the stabilizing surface sizing module are defined. Also in the Class II Weight Estimation module, the loading diagram and the center of gravity range are defined. These are both important input factors for the sizing module.

The Initiator is operated by executing standardized input files for different types of aircraft configurations. The following five aircraft configurations can be executed with the Initiator:

- Conventional aircraft
- Canard aircraft
- Three-Surface aircraft
- Prandtl Aircraft
- Blended-Wing-Body aircraft

The focus of this thesis assignment is on the sizing of the stabilizing surfaces of conventional, canard and three-surface aircraft. The sizing of the stabilizing surfaces of the Prandtl and BWB aircraft are left out of the framework of this thesis assignment, because general design rules do not apply to these configurations. When the methodology is implemented, it is possible to run the design convergence in the Initiator. The design convergence designs the complete aircraft, after which the influence of a certain specified stability margin on the overall aircraft performance can be analyzed.

3

DOWN- AND UPWASH PREDICTION METHODOLOGY

In this section a methodology is presented to predict the average downwash angle at an arbitrary point in the flow field behind a wing or the average upwash angle at an arbitrary point in the flow field in front of the wing with the presence of high lift devices in- or outside the ground effect region. When multiple lifting surfaces are present in a single flow field, interference effects are present. Lifting surfaces placed in the wake of an upstream surface will experience a downwash from that surface. The opposite is also true, lifting surfaces located upstream of another lifting surface further downstream experience an upwash from that surface. This influences the aerodynamic characteristics of both surfaces, this phenomena is known as an interference effect. In this chapter the interference effects between lifting surfaces, in the form of up- and downwash, are explained for conventional and unconventional aircraft configurations. Existing method such as the graphical ESDU method [15],[16] and the analytical Slingerland method [17] are capable of predicting the average downwash angle behind a flapped wing in ground effect. The limitation of the ESDU method is the inability of predicting the average downwash angle at an arbitrary point in the flow field. The ESDU method is based on wind tunnel experiments, where the horizontal stabilizer is located roughly by a distance of half the wing span behind the wing. Another limitation of the ESDU method is the inability of predicting the average upwash angle in front of the wing. The analytically method developed by Slingerland is capable of predicting the average downwash angle at an arbitrary point in the flow field behind a flapped wing in ground effect, however the inability of prediction the average upwash angle is a limitation of this method. Another limitation of both methods is the inability to determine the average downwash angle at an arbitrary point in the flow field behind the wing, when the spanwise lift distribution of the wing is influenced by a canard surface. This is the case on a three-surface aircraft. Therefore a new down- and upwash prediction methodology is needed. In order to make the methodology generic and give the designer a great design flexibility, the methodology should be able to determine the average up- and/or downwash angle at an arbitrary point in the flow field. The developed method is discussed next.

A limitation of the model is the inability to model the fuselage and nacelle contributions. These contributions are therefore left out of the analysis. For the validation of this model, two aircraft are analyzed. The average downwash angle at the horizontal stabilizer location for the Fokker 100, which is an aircraft with a t-tail configuration and the Airbus A330 with a fuselage mounted horizontal stabilizer. The up- and downwash prediction methodology is an integrated part of the stabilizing surface sizing methodology in the Initiator.

3.1. VORTEX LATTICE METHOD (VLM)

A Vortex Lattice Method (VLM) is a numerical computational fluid dynamics program. It finds its root in the lifting line theory of Prandtl. With a VLM model it is possible to simultaneously analyze multiple lifting surfaces in a single flow field, by simulating the surfaces by an infinite number of horseshoe vortices. The VLM is three-dimensional incompressible, inviscid and irrotational representation of the lifting line theory. For higher Mach numbers a compressibility correction is applied by implementing the Prandtl-Glauert compressibility correction. For this purpose the Athena Vortex Lattice (AVL) VLM program is used. [20]. With the AVL program it is possible to analyze generic aircraft geometries and simulate the presence of leading-edge and trailing-edge high-lift devices. A downwash analysis method is present within the AVL program, however the downwash is either calculated directly behind the lifting surface or in the Trefftz plane. It is not possible to directly determine the average downwash angle at an arbitrary point, therefore a new prediction methodology is needed.

3.1.1. OUT OF GROUND EFFECT

When an lifting surface is present in a flow field at an height higher than its own wing span, the ground effects can be neglected. In the latter case, the vortices of the wing are able to fully develop and the downwash distribution is not influenced by the presence of a ground plane, this is visualized in Figure 3.1. In the latter figure the downwash angle, ϵ, directly behind the wing illustrated. At various locations in the flow field behind the wing, different downwash angles are present.

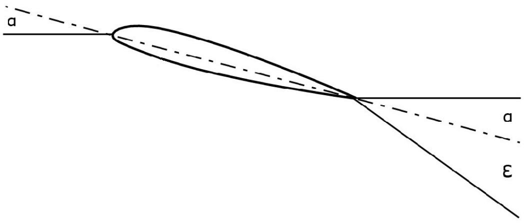

Figure 3.1: Downwash angle of a lifting surface Out of Ground Effect (OGE).

3.1.2. IN GROUND EFFECT

When a lifting surface is present in a flow field at an height lower than its own wing span, the ground effect contribution to the changes in aerodynamic coefficients cannot be neglected. The ground plane simulation within the AVL software is based on the mirroring of the bound vortex below the ground plane. This will induce a velocity distribution at the wing in the opposite direction. A consequence of mirroring the bound vortex distribution is the decrease in the average downwash angle at the horizontal stabilizer location. An example of a wing and horizontal stabilizer in ground effect with a mirroring technique is given in Figure 3.2.

The reduced downwash distribution behind the wing is given in Figure 3.3. In the latter figure a similar airfoil is drawn as in figure 3.1, however in this case a ground plane is present at an height h. The consequence is that the new downwash angle, ϵ, is reduced by $\Delta\epsilon$. The magnitude of the change in downwash angle, $\Delta\epsilon$, is dependent on the height of the lifting surface. For a lower height, h, the magnitude of $\Delta\epsilon$ increases.

3.1.3. SIMULATION OF HIGH-LIFT DEVICES

With a VLM model it is possible to model leading-edge and trailing-edge high-lift devices. As stated earlier, the VLM model is a three-dimensional incompressible, inviscid and irrotational representation of the real model. In this case it is particularly important to address the inviscid case. The flow is assumed to be inviscid, which implies that no viscous effects are taken into account. However in reality viscous effects are present and become significantly more important with larger deflections of high-lift devices. The streamlines around the aft part of a flapped wing do not remain fully attached at the trailing-edge of the flap. In fact the flow angle is smaller than the deflection of the trailing-edge high-lift device due to viscous effects.

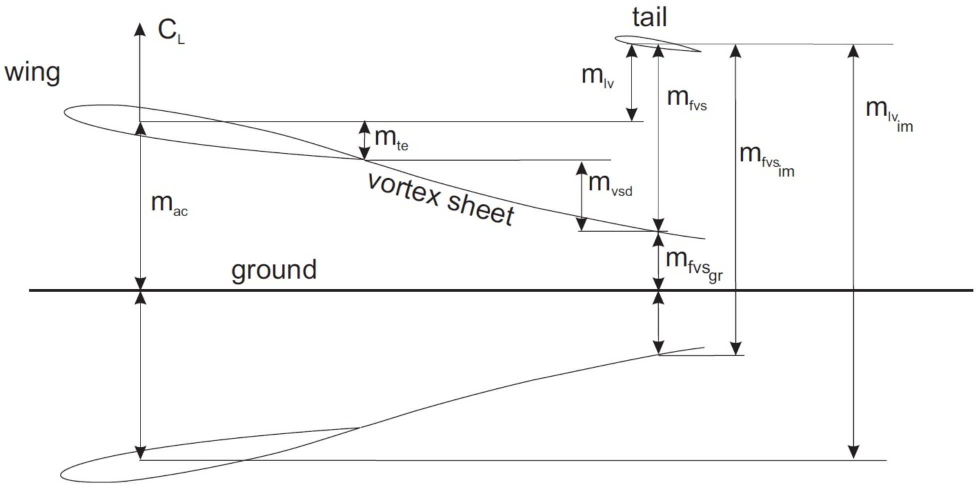

Figure 3.2: Mirroring technique for a wing and tail in ground effect.

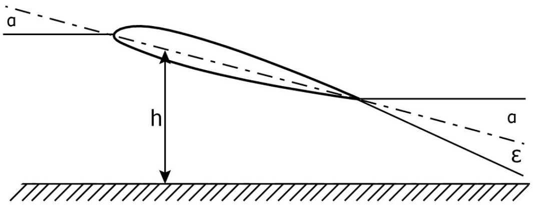

Figure 3.3: Downwash angle of a lifting surface In of Ground Effect (IGE).

In order to account for viscous effects in the vortex lattice method model, the deflection of the geometric flap angle, $\delta_{f_{\text{geo}}}$ is reduced so that the effective flap angle, $\delta_{f_{\text{eff}}}$ is obtained, this is seen in Equation 3.1. The reduction of the flap angle, $\Delta\delta_f$, is obtained graphically with Figure 3.4 [3]. For implementation purposes the latter graph is digitized.

$$\delta_{f_{\text{eff}}} = \delta_{f_{\text{geo}}} - \Delta\delta_f \tag{3.1}$$

The magnitude of the reduction depends on the flap configuration as can be seen in Figure 3.4, where two curves are drawn for two different flap types. The double-slotted flap with vanes and the single-slotted flap. Up to 30^o the effective flap deflection is similar for both flap systems, however from 30^o to 45^o for the single-slotted flap and up to even 55^o for the double-slotted flap with vanes, the reduction in effective flap angle is significantly higher for the single-slotted flap. This highlights the importance of differences in flap systems.

For the validation of the downwash methodology, two aircraft are analyzed with different flap systems and different tail configurations. The Airbus A330 and the Fokker 100, with their real planforms displayed in 3.5 [5]. From the latter figure it can be concluded that the Fokker 100 has no leading-edge high-lift devices and has a double-slotted trailing-edge flap system. The Airbus A330 has a leading-edge slat system and a single-slotted trailing-edge flap system. For the Airbus A330 the single-slotted flap correction curve in Figure 3.4 is used, whereas for the Fokker 100 the double-slotted flap with vane curve is used. The Fokker 100 has a t-tail configuration, whereas the Airbus A330 has a fuselage mounted horizontal stabilizer. The average downwash angle at the location of the horizontal stabilizer for the Fokker 100 is therefore expected to be lower than for the Airbus A330.

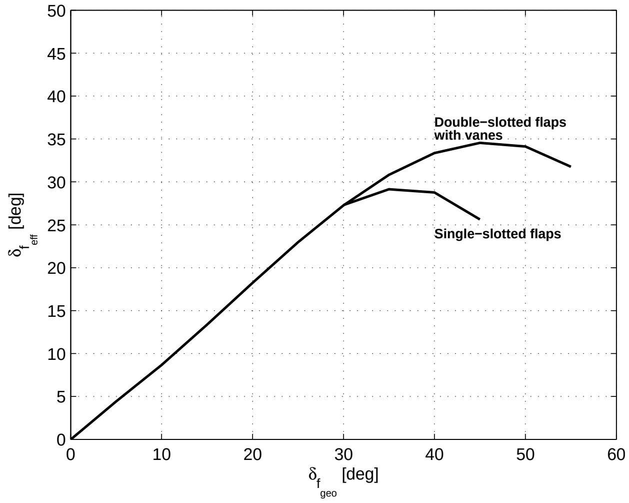

Figure 3.4: Redrawn figure of the reduction of the effective flap angle for single-slotted flaps and double-slotted flaps with vanes [3].

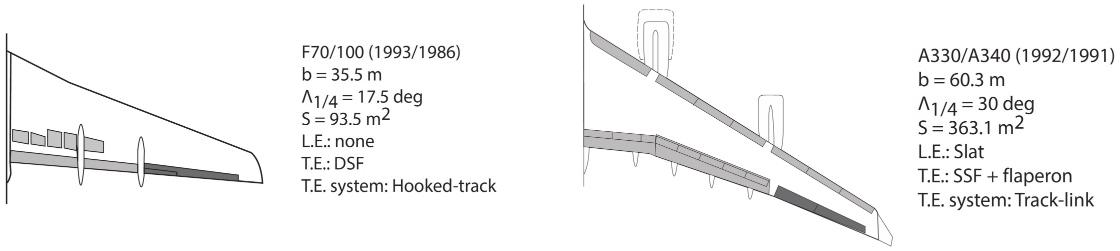

(a) Fokker 100 **(b) Airbus A330**

Figure 3.5: Two-dimensional representation of the wing lay-out with high-lift devices [5].

3.2. DOWNWASH PREDICTION METHODOLOGY

As mentioned earlier, it is not directly possible to determine the average upwash angle at an arbitrary point in the flow field in front of the wing or the average downwash angle at an arbitrary point in the flow field behind a wing with the presence of high-lift devices in- or outside the ground effect region. Therefore a new prediction methodology is developed. The methodology is presented in this section. The average down- and upwash angles are determined by increasing or decreasing the incidence angle of a lifting surface at a location where the down- and/or upwash angle needs to be determined. By changing the incidence angle of the lifting surface, it is possible to reach a zero lift coefficient condition. When the zero lift coefficient is attained, the effective angle of attack of the lifting surface is zero. When the effective angle of attack is zero, the average upwash or downwash angle at that point in the flow field is only a summation of the angle of attack of the aircraft and the incidence angle of the lifting surface, as will be seen later in this section. The goal of the down- and upwash prediction methodology is to attain a zero lift coefficient condition (i.e. zero effective angle of attack) of the surface which needs to be analyzed.

When a lifting surface is located downstream of another lifting surface upstream, it is in the wake and subjected to the downwash distribution of the lifting surface further upstream. This results in a reduced negative effective angle of attack, as displayed in Equation 3.2.

$$\alpha_{h_{\text{eff}}} = \alpha + i_h - \epsilon_h \tag{3.2}$$

In the latter equation it can be seen that the effective angle of attack of a lifting surface further downstream, in this case the horizontal stabilizer, is a summation of the angle of attack of the aircraft, α, the horizontal stabilizer incidence angle, i_h and the negative average downwash angle at the horizontal stabilizer location, ϵ_h.

A similar equation can be set up for the average upwash angle at the location of the canard surface in case of a canard or three-surface aircraft. This is given in Equation 3.3. In the latter equation, the effective angle of attack of a lifting surface further upstream, in this case the canard surface, is a summation of the angle of attack of the aircraft, α, canard incidence angle, i_c and the average upwash angle at the location of the canard surface, ϵ_c.

$$\alpha_{c_{\text{eff}}} = \alpha + i_h + \epsilon_c \tag{3.3}$$

The average up- and downwash angle at an arbitrary point in the flow field can be determined by setting the effective angle of attack to zero. This means that the lift coefficient of that particular surface is zero. By setting the lift coefficient of the horizontal stabilizer, C_{L_h}, to zero (i.e. equal to setting the effective angle of attack of the horizontal stabilizer, $\alpha_{h_{\text{eff}}}$, to zero), the average downwash angle is then only the summation of the aircraft angle of attack and the incidence angle of the horizontal stabilizer, as can be seen in Equation 3.4. Similarly the average upwash angle at the canard surface location can be determined by setting the lift coefficient of the canard surface, C_{L_c}, to zero. In that case the average upwash angle at the canard location follows from Equation 3.5.

$$\epsilon_h = \alpha + i_h \tag{3.4}$$

$$\epsilon_c = -\alpha - i_c \tag{3.5}$$

The average up- and downwash angle can now be determined when the lift coefficient of the stabilizing surface is zero and when the angle of attack and the incidence angle are known. With a VLM it is possible to give multiple lifting surfaces varying incidence angles. By changing the incidence angles of these lifting surfaces it is possible to achieve a zero lift coefficient condition. This process is iteratively and is elaborated next. An UML diagram of the downwash prediction methodology is presented in Section 8.1 of Part II, the part on the code structure, in this thesis report.

The methodology starts by obtaining the wing data. When the methodology is implemented in the Initiator, the wing data is derived from a preliminary sizing estimation of initial input parameters, as discussed in chapter 2. The next step in the process is writing the VLM input file, in this file the wing geometry and horizontal stabilizer geometry are defined. Also the ground plane is defined in this input file. In the input file the Out of Ground Effect (OGE) or an In Ground Effect (IGE) analysis is defined. When IGE is chosen, the height of the ground plane is also defined. When OGE is chosen, no height needs to be specified as no ground plane is present. In the latter case, the analysis is executed in free-air conditions. The deflections of high-lift devices and angle of attack are defined during run AVL.

A detailed description of the downwash prediction methodology code is given in Part II of this thesis report. For clarification a run case example is given next for calculating the average downwash angle at the horizontal stabilizer location. When the wing data is obtained and the VLM run is finalized as described earlier, the lift coefficient of the horizontal stabilizer, C_{L_h}, can be obtained from the output file created by the VLM model. The goal of the methodology is to determine the incidence angle at which the lift coefficient of the horizontal stabilizer is zero.

The pre-defined maximum allowable lift coefficient is set at 0.001 as can be seen in Table 3.1. When the absolute value of the initially calculated lift coefficient of the horizontal stabilizer of canard surface is lower than the maximum allowable lift coefficient, the initial effective angle of attack of the horizontal stabilizer of canard surface is assumed to be zero. When the absolute value of the initial lift coefficient is larger than the allowable maximum lift coefficient, the incidence angle should be adjusted, so that a zero effective angle of attack condition is attained. When the calculated lift coefficient, C_{L_h} or C_{L_c} is positive and larger in magnitude than the maximum allowable lift coefficient, the incidence angle is lowered by one increment. In this case one increment stands for an decrease in incidence angle of 0.1^o. When the calculated lift coefficient,C_{L_h} or C_{L_c}, is negative and larger in magnitude than the maximum allowable lift coefficient, the incidence angle of the incidence angle is increased by the same increment as stated earlier. This is an iterative process and the incidence angles are increased/decreased until the absolute value of the lift coefficient, C_{L_h} or C_{L_c} are lower than the maximum allowable value. In the latter case the effective angle of attack of the horizontal stabilizer or canard surface are assumed to be zero. Because the incidence angle and the angle of attack of the aircraft are both known, the average up- or downwash angle can be determined with Equation 3.4 or Equation 3.5.

3.2.1. ACCURACY OF THE METHODOLOGY

It has to be stated that when the effective angle of attack is assumed to be zero, the lift coefficient of the stabilizing surface is not exactly zero, but has a value which is lower than the maximum allowable lift coefficient. This maximum allowable lift coefficient is explained next. When looking at the fundamental equation for calculating the lift force in Equation 3.6 the lift force is dependent on the maximum allowable lift coefficient.

$$L = C_{L_{h_{\text{max, allowable}}}} \frac{1}{2} \rho V^2 S \tag{3.6}$$

In this particular case, the maximum value for the lift coefficient of the horizontal stabilizer is set to be 0.001. For the sizing of the stabilizing surfaces, the average downwash angle needs to be calculated during high velocity high altitude cruise conditions and for low velocity low altitude landing conditions. Therefore it is interesting to see what the maximum allowable lift force is for these conditions. The maximum lift force at which effective angle of attack of the horizontal stabilizer is assumed to be zero during landing and cruise conditions for the Fokker 100 and the Airbus A330 are displayed in Table 3.1.

Table 3.1: Maximum lift force when the lift coefficient is assumed to be zero.

Parameter	**F100**	**A330**	**Unit**
Max. allowable C_{L_h}	0.001	0.001	[-]
Density, ρ_{landing}	1.225	1.225	[kg/m^3]
Density, ρ_{cruise}	0.413	0.413	[kg/m^3]
Velocity, V_{landing}	92.6	84.9	[m/s]
Velocity, V_{cruise}	227.2	241.9	[m/s]
Wing Area, S	93.5	361.6	[m^2]
Max. allowable lift, L_{landing}	**491**	**1596**	[N]
Max. allowable lift, L_{cruise}	**996**	**4369**	[N]

From the latter table it can be seen that for the Fokker 100 the maximum allowable lift force during cruise conditions is 996N, whereas the maximum allowable lift force for the Airbus A330 is 4369N. When the lift force is below these values during cruise, the effective angle of attack is assumed to be zero. During landing conditions, these values are 491N and 1596N, for the Fokker 100 and Airbus A330 respectively.

3.3. VALIDATION OF THE DOWNWASH PREDICTION

The down- and upwash prediction methodology is implemented and operational in the Initiator. However, for validation purposes the methodology is separated from the Initiator and separate input files are created. The Initiator is a preliminary sizing software, which sizes aircraft based on very elementary initial input parameters, such as the number of passengers, cruise Mach number and aircraft range. These input parameters are derived from actual aircraft and the Initiator designs the aircraft based upon these variables. Because the final aircraft designed in the Initiator is not an exact representation of the actual aircraft, due to difference in wing planform and high-lift device systems for example, it is not suitable for validation purposes. Therefore, the separate input files are developed with the actual aircraft geometry. The developed downwash and upwash prediction methodology is validated for a t-tail aircraft, the Fokker 100 and a conventional fuselage mounted horizontal stabilizer, the Airbus A330. Both aircraft are validated Out of Ground Effect (OGE) and In Ground Effect (IGE) for different flap settings and angles of attack against experimental data. The in ground effect experimental data represents the altitude just prior to lift-off during the ground run. The experimental downwash data is obtained from the analytic downwash prediction method developed by Slingerland [17] and is derived from flight tests.

As mentioned in the introduction part of this chapter the fuselage and nacelle contributions are not part of the analysis model. In the validation model, for the two conventional aircraft configurations, the average downwash angle at the location of the horizontal stabilizer location is only influenced by the wing geometry and the setting of the high-lift devices and the aircraft angle of attack. The modeled wing planform of both aircraft are based on the input files with the actual aircraft geometry. The planform representation of the Fokker 100 and the Airbus A330 are illustrated in Figure 3.6.

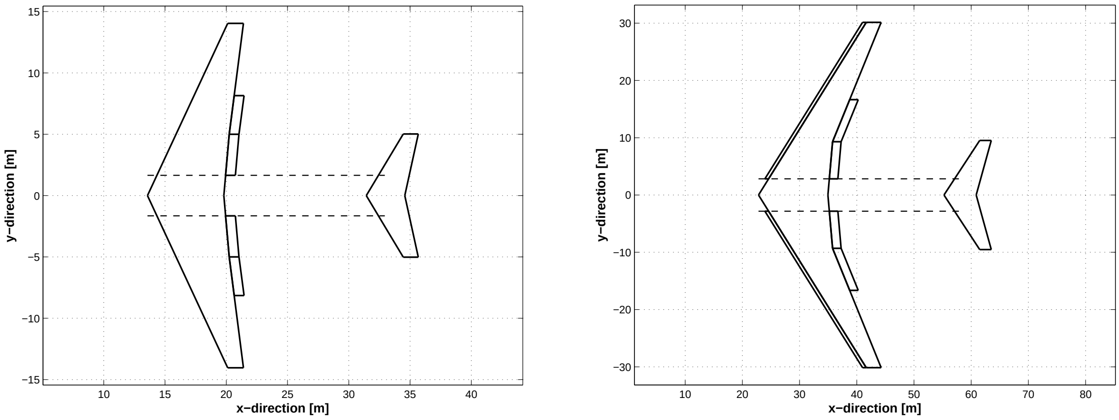

(a) Fokker 100 **(b) Airbus A330**

Figure 3.6: Two-dimensional wing planform representation.

The OGE validation of the Airbus A330 is presented in Figure 3.7. The difference between Figure 3.7(a) and Figure 3.7(b) is the flap deflection correction. In Figure 3.7(b), the flap deflection is corrected to account for viscous effects. It can be seen that the accuracy increases when the flap deflection correction is applied. In both Figure 3.7(a) and Figure 3.7(b) five different curves are present. Each curve represents a different flap and slat setting. For example the curve S16F08 represents the setting where the slat deflection is 16 degrees and the flap deflection is 8 degrees. In Figure 3.7(a) the flap deflection represents the geometric flap deflection, whereas in Figure 3.7(b), the geometric flap deflection is corrected to the effective deflection in order to account for viscous effects. No corrections are applied to deflections of leading-edge high-lift devices. Each of the five curves consist out of 7 data points, where each data point represents a different angle of attack ranging from 0 to 12 degrees with increments of 2 degrees.

In Figure 3.7(a) the accuracy for all data points is within a maximum error of $\pm 1.2^{o}$, whereas the accuracy for all data points in Figure 3.7(b) is within the maximum error margin of $\pm 0.8^{o}$. It can be seen that the average downwash angle increases with increasing flap deflection. The validation of the Fokker 100 is displayed in figures 3.8(a) and 3.8(b). On the Fokker 100 no slats are present, only flap

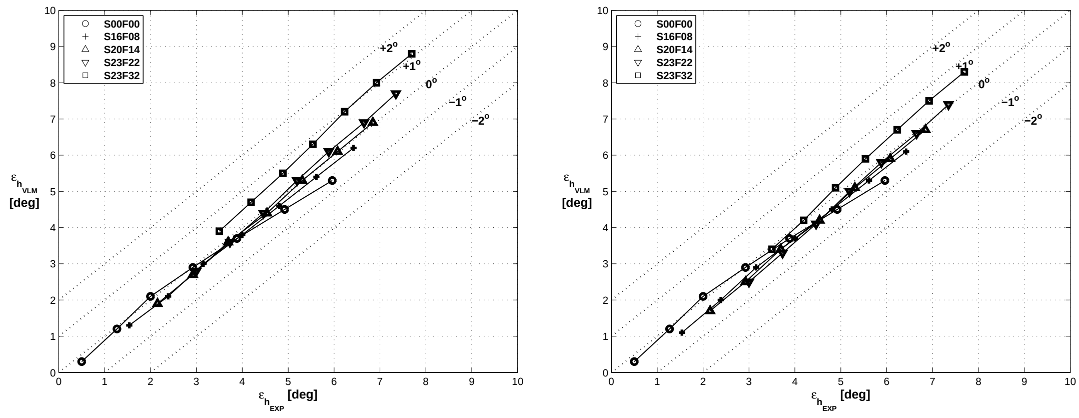

(a) Geometric flap deflection **(b) Effective flap deflection**

Figure 3.7: VLM Validation of the average downwash angle at the horizontal stabilizer of the Airbus A330 Out of Ground Effect (OGE).

deflections are simulated. Similarly as in Figure 3.7 the accuracy increases when the flap deflection correction is applied. The maximum error margin for the effective flap deflection is lower than $\pm 1^{o}$, whereas the maximum error margin for the geometric flap deflection is within $\pm 1.5^{o}$.

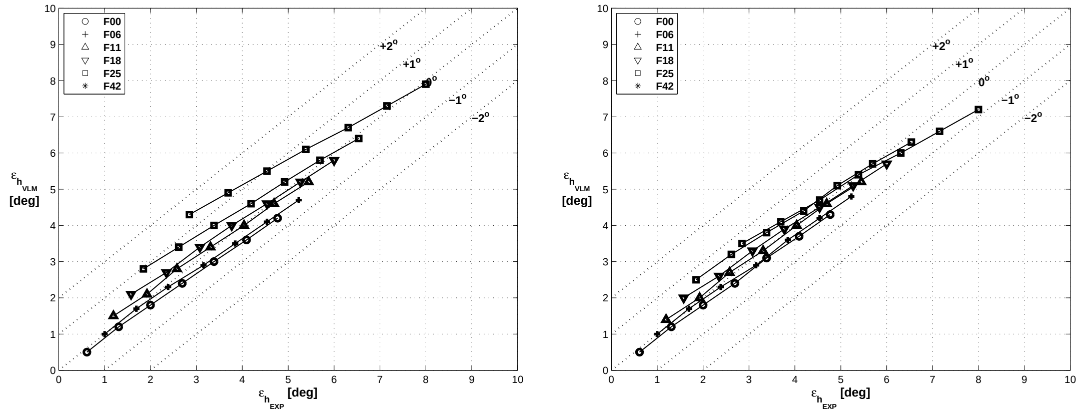

(a) Geometric flap deflection **(b) Effective flap deflection**

Figure 3.8: VLM Validation of the average downwash angle at the horizontal stabilizer of the Fokker 100 Out of Ground Effect (OGE).

The IGE validation of both aircraft are displayed in Figure 3.9. For both aircraft the average downwash angles are validated against experimental data, where the altitude of the aircraft is zero. Similarly as in the OGE validation, the different curves represent different flap settings, whereas the different data points represent different angles of attack. In both figures the geometric flap deflection is corrected to the effecte flap correction in order to account for viscous effects. For the Fokker 100, only data is found for the clean wing and the full flap setting. For both flap settings the maximum error margin was found to be within $\pm 0.75^{o}$ as can be seen in Figure 3.9(a). The validation of the A330 is displayed in Figure 3.9(b). For the A330 data is found for all flap settings in ground effect. The maximum error margin for the A330 is lower than 0.75^{o}, except for the maximum flap deflection setting, which shows an error margin slightly higher than 0.75^{o} for the lower three angles of attack. No experimental data on average upwash angles for canard and three-surface aircraft are found, this leaves the upwash prediction methodology invalidated.

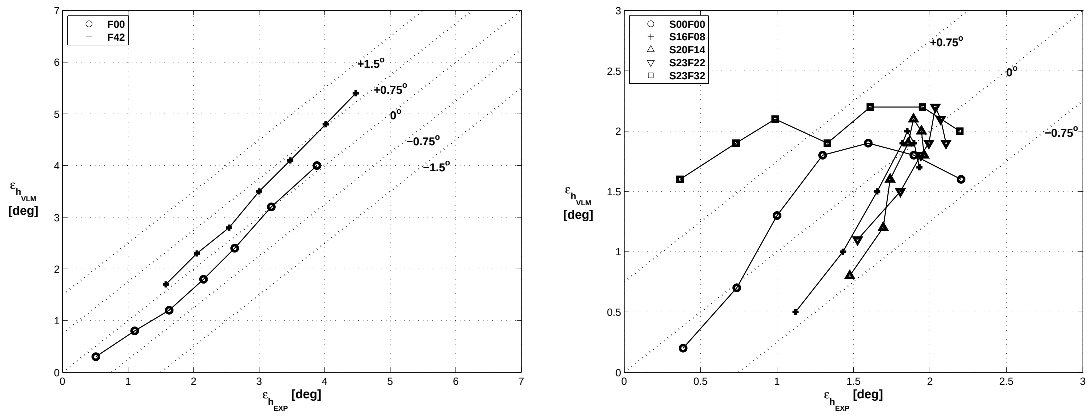

(a) Fokker 100

(b) Airbus A330

Figure 3.9: VLM Validation of the average downwash angle at the horizontal stabilizer of the Fokker 100 and the Airbus A330 In Ground Effect (IGE).

3.4. COMPARISON BETWEEN DOWNWASH PREDICTION METHODS

In this section the comparison is presented between the developed downwash prediction methodology and other earlier mentioned prediction methods, such as the graphical ESDU method and the analytical Slingerland method. The validation of the latter two methods are presented in Chapter 2. The summation of the absolute error is compared for the three methods. This implies that the summation of the absolute errors for all angles of attack and all deflections of high-lift devices for a single aircraft are compared to each other. The out of ground effect comparison is given in Table 3.2.

Table 3.2: Comparison of the three downwash prediction methods, Out of Ground Effect (OGE).

Aircraft	ESDU	Slingerland	VLM
Airbus A330	14.05	27.13	10.04
Fokker 100	35.47	15.49	10.74

From the latter table it can be seen that the summation of the absolute error for all angles of attack and flap deflections of the developed downwash prediction methodology, the VLM method, is lower than the summations of the absolute errors of the ESDU and Slingerland methodologies. In case of the Airbus A330, the summation represents the summation of the absolute error in the prediction of the average downwash angle for 35 data points (five different flap settings and seven different angles of attack). For the A330, this results in an average error, out of ground effect, of 0.40^o for the ESDU method, an average error of 0.78^o for the Slingerland method and an average error of 0.29^o for the developed VLM methodology. In case of the Fokker 100, the summation represents a summation of the absolute error in the prediction of the average downwash angle for 42 data points (six different flap settings and seven different angles of attack). For the F100, this results in an average error, out of ground effect, of 0.84^o for the ESDU method, an average error of 0.37^o for the Slingerland method and an average error of 0.26^o for the developed VLM methodology.

The in ground effect comparison of the average downwash angle for the three prediction methods is given in Table 3.3. From the latter table it can be seen that the summation of the absolute error for all angles of attack and flap deflections of the developed downwash prediction methodology, the developed VLM method, is lower than the summations of the absolute errors of the ESDU and Slingerland methodologies. In case of the Airbus A330, the summation represents the summation of the absolute error in the prediction of the average downwash angle, again for 35 data points. For the A330, this results in an average error, in ground effect, of 0.84^o for the ESDU method, an average error of 0.55^o for the Slingerland method and an average error of 0.34^o for the developed VLM methodology. In case of the Fokker 100, the summation represents a summation of the absolute error in the prediction of the average downwash angle for 14 data points (two different flap settings and seven different angles of attack). For the F100, this results in an average error, in ground effect, of 0.65^o for the ESDU method, an average error of 0.96^o for the Slingerland method and an average error of 0.37^o for the developed VLM methodology.

Table 3.3: Comparison of the three downwash prediction methods, In Ground Effect (IGE).

Aircraft	**ESDU**	**SLINGERLAND**	**VLM**
Airbus A330	29.23	19.90	11.96
Fokker 100	9.14	13.45	5.11

3.5. DOWNWASH PREDICTION FOR UNCONVENTIONAL CONFIGURATIONS

The advantage of the developed down- and upwash prediction module, is the ability to add multiple lifting surfaces to the flow field, which increases the design flexibility. This is especially convenient in the case of a three-surface aircraft configuration. Where current methods are incapable of analyzing the change in spanwise distributions on the wing due to the presence of a canard surface, the VLM module simultaneously analyzes all lifting surfaces. This results in the ability to determine the average downwash angle at the location of the horizontal stabilizer of a three-surface aircraft. The average upwash angle at the canard is much less influenced by the presence of a horizontal stabilizer, than the average downwash angle on the tail by the presence of a canard surface.

4

STABILIZING SURFACE SIZING METHODOLODY

In order to answer the research question and determine the influence of a reduced stability margin on the overall aircraft performance, in terms of a reduced maximum take-off weight for an equal payload, a sizing methodology for the stabilizing surfaces of conventional and unconventional aircraft configurations is developed and implemented in the Initiator. The sizing methodology is presented in this chapter. The core part of the thesis assignment is the development of a sizing methodology for the stabilizing surfaces of two-surface and three-surface aircraft configurations (i.e. sizing methodology of the canard and/or horizontal stabilizer surfaces). Because the sizing of these surfaces is strongly related to the position of the wing, a optimum wing position needs to be determined. The sizing methodology is designed to replace the current stabilizing surface sizing method, implemented in the Initiator. The Initiator is a preliminary aircraft sizing software for the design of conventional and unconventional aircraft configurations. Currently, in the Initiator, the stabilizing surfaces are sized using a Class I volume coefficient method [1]. The sizing based on the Class I volume coefficient method is based on a volume coefficient derived from similar aircraft. This is usually the first step in the design process of the sizing of the canard and horizontal stabilizer and yields in a satisfactory first sizing approximation. However, because the sizing based on the Class I volume coefficient does not automatically satisfy sizing constraints, a more refined sizing method is required. A more refined methodology to size the stabilizing surfaces, which satisfies specified sizing constraints is presented in this chapter. The sizing constraints are discussed in Section 4.1. As mentioned earlier, the sizing methodology needs to be implemented in the Initiator, therefore the default wing positioned needs to be optimized. An optimized wing position is defined as the wing position which results in the lowest required stabilizing surface area. The wing optimization and the sizing methodology for the stabilizing surfaces are presented in Section 4.3.

An important stabilizing surface sizing parameter is the center of gravity range of the aircraft. The center of gravity range is obtained with the use of a loading diagram and is further elaborated in Section 4.2. In the sizing methodology, a vortex lattice method is used to determine the average down- and upwash angles, as presented in Chapter 3. For the calculation of lift coefficients, also a vortex lattice method is used. However, it is found that for the calculation of the pitching moment coefficient and the aerodynamic center, a vortex lattice method is rather inaccurate. The validation of the pitching moment calculation is presented in Section 4.3.7, whereas the comparison of the aerodynamic center calculation is presented in Section 4.3.8. The validation of the developed sizing methodology is presented in Section 4.4. An in ground effect analysis is performed in order to check if the negative design lift coefficient of the horizontal stabilizer can be attained in ground effect. This analysis is discussed in Section 4.5. The implementation of the sizing methodology in the Initiator, is presented in Section 4.6.

4.1. STABILIZING SURFACE SIZING REQUIREMENTS

The presented stabilizing surface sizing methodology in this chapter is derived from the x-plot method as presented by Torenbeek [2]. The x-plot method is a graphical sizing methodology which is based on forward and aft center of gravity limitations. Each center of gravity limitation is related to a sizing constraint, as will be seen in this section. Whereas forward center of gravity limitations are related to the controllability of the aircraft, the aft center of gravity limitations are related to the stability of the aircraft. Therefore a distinction is made between forward and aft center of gravity limitations. For conventional aircraft the following center of gravity limitations are implemented:

1. Stick-fixed neutral points **(aft limit)**
2. Stick-fixed neutral points minus stability margin **(aft limit)**
3. Stick-fixed maneuver points **(aft limit)**
4. Satisfactory short period oscillation characteristics **(aft limit)**
5. Satisfactory short period oscillation characteristics **(fwd limit)**
6. Control capacity required to stall the aircraft **(fwd limit)**
7. Control capacity required for take-off rotation **(fwd limit)**
8. Control capacity required for landing flare-out **(fwd limit)**

From the latter summation it can be seen that eight center of gravity limitations are implemented in the x-plot for a conventional aircraft configuration. The limitations are divided between four aft center of gravity limitations and four forward center of gravity limitations. For unconventional aircraft configurations (i.e. the canard and three-surface aircraft), only number 1,2 and 6 are implemented, due to the inability to apply the other center of gravity limitations to unconventional aircraft configurations. In order determine the minimum required stabilizing surface area using the x-plot method at least one dominant forward limitation and one dominant aft limitation is required, this is further discussed in Section 4.3.

The first sizing constraint, the stick-fixed neutral points aft limit, is the fundamental design constraint related to the static longitudinal stability of the aircraft. It states that when the aircraft is longitudinally trimmed, a disturbance in angle of attack results in a pitching moment which returns the aircraft to an equilibrium. When the stability margin of the aircraft is subtracted from the stick-fixed neutral points the second sizing constraint is obtained. This second sizing constraint, which includes the stability margin, is the core sizing requirement for the research on the influence of a reduced stability margin on the overall aircraft performance in terms of a reduction in maximum take-off mass for an equal payload. The first three sizing constraints are the stability constraints, which are implemented in the x-plot. The third sizing constraint, the stick-fixed maneuver point, represents the aft center of gravity limitation at which the pilot can still pull the column towards him in order to pull the aircraft out of a dive [2].

From the summation it can be seen that there are also two dynamic stability constraints. Constraint four and five represent the forward and aft short period oscillation constraints. The forward short period oscillation constraint is related to a high altitude and high wing loading flight condition. The aft short period oscillation is related to a low speed and low weight flight condition. Both the forward and aft constraints represent satisfactory short period oscillation characteristics. The use of these constraints are further explained in the section on the sizing methodology, Section 4.3.

Besides the three stability stability aft center of gravity constraints and two dynamic stability constraints, there are also three forward center of gravity constraints present, all related to the control of the aircraft. Constraint six, the control capacity required to stall the aircraft, is related to the ability of the stabilizing surface(s) to pitch up the aircraft in order to attain the maximum lift coefficient. The critical design point is the flight condition at which the aircraft is pitched up to the landing angle of attack when the full flap setting is applied and when the center of gravity is positioned in the most adverse location (i.e. most forward location) and the aircraft is subjected to the in ground effect. When the full flap setting is applied, during landing conditions, the wing generates the largest nose-down pitching moment about the aerodynamic center. This needs to be balanced by the stabilizing surface(s). Constraints seven and eight are related to the rotation capacity of the horizontal stabilizer during take-off and the landing flare-out, both are further examined in Section 4.3.

Before the sizing methodology is addressed, the calculation of the center of gravity range is discussed. The center of gravity range is determined with the use of a loading diagram as will be seen in the next section.

4.2. LOADING DIAGRAM

As mentioned earlier, the center of gravity range is an important stabilizing surface sizing parameter for the x-plot methodology. In order to determine the minimum required stabilizing surface area(s), the center of gravity range is required. The minimum required surface area, corresponding to the optimum wing position, is defined as the lowest position on the x-plot at which the center of gravity range can be positioned between the most forward located aft center of gravity constraint and the most aft located forward center of gravity constraint (i.e. the dominant aft and dominant forward constraint). In this section a methodology is presented to determine the center of gravity range of an aircraft for a given wing position. It is important to note that the loading diagram needs to be determined for a given wing position as the initial default wing position in the Initiator needs to be optimized. Therefore a loading diagram is created for the default wing position, a forward wing position and an aft wing position. The default wing position in the Initiator is defined as the position at which the Leading-Edge of the Mean Aerodynamic Chord (LEMAC) is positioned at 45% of the entire fuselage length. The forward wing position is defined at which the LEMAC is positioned at the default wing position minus 5% of the fuselage length, whereas for the aft wing position the LEMAC is positioned at the default wing position plus 5% of the fuselage length. The longitudinal center of gravity position are defined with respect to the LEMAC and are non-dimensionalized by dividing by the Mean Aerodynamic Chord (MAC).

The start of the loading diagram is the Operational Empty Mass (OEM) with a corresponding center of gravity position. The center of gravity position corresponding to the OEM is calculated with a Class II weight estimation methodology. The OEM is independent on the wing position as the total mass is equal for all wing position. However, the corresponding center of gravity position is dependent on the wing position and moves further aft for an aft wing position. Three loading diagrams, developed with the stabilizing surface sizing methodology, for a typical single-aisle transport aircraft are given in Figure 4.1.

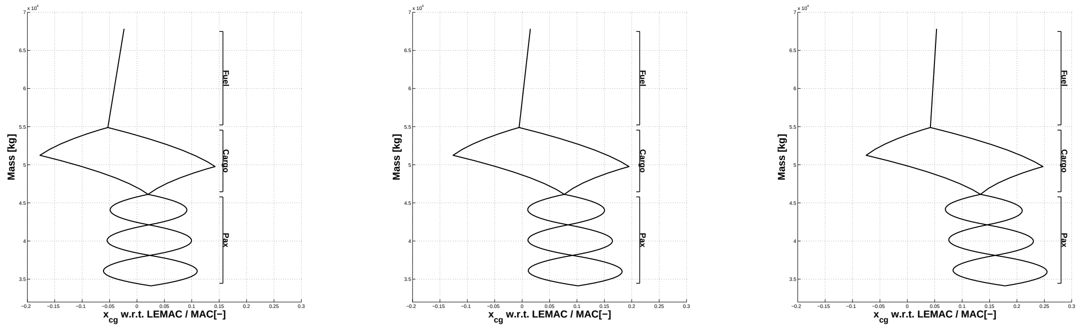

(a) Forward wing position (b) Default wing position (c) Aft wing position

Figure 4.1: Loading diagram for different wing positions for a typical single-aisle transport aircraft.

From the latter figure it is visible that the OEM is equal for all wing positions. It is also visible that the center of gravity position of the empty aircraft with the forward located wing position is located further forward compared to the default wing position. The center of gravity position of the empty aircraft with the aft wing position is located further aft compared to the default wing position. When the center of gravity positions of the OEM corresponding to the three wing positions are known, the aircraft is loaded. The loading process is equal for all wing positions. First the passengers (i.e. Pax) are loaded intro three different travel classes. A distinction is made between economy, business class and first class referring to the three ellipse shaped objects in Figure 4.1. There are two loading scenarios for the passengers, front-to-back loading and back-to-front loading. First the passengers are loaded from the front to the back, after which the passengers are loaded from the front to the back. This results in two extreme loading cases corresponding to the minimum and maximum center of gravity positions related to the passenger loading. After the passenger loading, the cargo is loaded. From Figure 4.1 it can be seen that there is no distinction between the cargo loading. The cargo bay is loaded from the front to the back and the back to the front, resulting in the minimum and maximum center of gravity positions related to the cargo loading. After the cargo loading the aircraft is loaded with fuel. There is only one fuel loading scenario, hence the linear fuel loading bar. Once the passengers, cargo and fuel are loaded, the loading diagram is finalized. When a 2% margin is added to the minimum and maximum center of gravity positions, the most forward and aft located center of gravity locations are determined. The center of gravity range is calculated by subtracting the forward center of gravity position from the aft center of gravity position.

The center of gravity ranges are calculated for each of the three wing positions. By interpolating the center of gravity positions for the wing positions located between the most forward and aft wing positions, a center of gravity ranges diagram is determined. From the center of gravity ranges diagram, the minimum and maximum center of gravity positions can be determined for a given wing position. When the center of gravity ranges diagram is determined, the x-plot is set up, as will be discussed in Section 4.3. The optimum wing position can be determined iteratively by analyzing the center of gravity ranges diagram and the x-plot simultaneously, this method is presented next in the section on sizing methodology.

4.3. SIZING METHODOLOGY

As mentioned in the section on the loading diagram, the optimum wing position is determined iteratively with the center of gravity ranges diagram and the x-plot. In this section, the x-plot method is discussed. When both diagrams are determined, an iterative analysis to find the optimum wing position and the minimum required stabilizing surface area is presented. As mentioned in Section 4.1 on the design requirements, in order to determine a minimum required stabilizing surface area and an optimum wing position, at least one aft center of gravity limit and one forward center of gravity limit needs to be present on the x-plot. When multiple forward and aft center of gravity limitations are present in the x-plot, the dominant forward and dominant aft center of gravity limit determine the minimum required stabilizing surface area. The dominant forward center of gravity limit is defined as the most aft located control limit in the x-plot, whereas the dominant aft center of gravity limit is defined as the most forward located stability limit in the x-plot. This means that in every design case for all aircraft configurations, there is a dominant forward limit and a dominant aft limit.

4.3.1. DOMINANT FORWARD CENTER OF GRAVITY LIMIT

It is found that the dominant forward center of gravity limitation, for all aircraft configurations and allowable stability margins, is the control capacity required to stall the aircraft. This is the requirement that the aircraft should be able to pitch up and reach the maximum angle of attack in landing conditions with full flaps deflected and the center of gravity in the most adverse position (i.e. most forward position). This limit is determined with Equation 4.1 [2].

$$\left(\frac{x_{\text{cg}}}{\bar{c}_w}\right)_{\text{FWD}} = \frac{x_{\text{ac}}}{\bar{c}_w} - \frac{1}{C_{L_{\max}}}\left[C_{L_{h\max}}\frac{l_h S_h}{\bar{c}_w S_w}\frac{V_h}{V_\infty} + C_{L_{c\max}}\frac{l_c S_c}{\bar{c}_w S_w}\frac{V_c}{V_\infty} - C_{m_{\text{ac}}}\right] \tag{4.1}$$

From the latter equation it can be seen that various parameters are required in order to determine the dominant forward center of gravity limit. When this sizing methodology is implemented in the

Initiator, some of these parameters are already determined within earlier modules and are therefore assumed to be input parameters. Only the non-input parameters are briefly discussed in this section.

The non-input parameters for the dominant forward center of gravity limit are discussed next. This first parameter is the aerodynamic center of the tail-less aircraft, x_{ac}, which is further elaborated in Section 4.3.8. The following parameters are the maximum lift coefficients of the horizontal stabilizer, $C_{L_{h}\max}$, and/or the canard, $C_{L_{c}\max}$. At the early stages in the conceptual design process it is difficult to determine an accurate satisfactory magnitude for the maximum lift coefficient of lifting surfaces. Therefore, at this stage it is assumed that the maximum lift coefficient of the horizontal stabilizer and the canard in clean configuration are respectively unity, -1.0 for the horizontal stabilizer and 1.0 for the canard surface. This value is derived from the assumption that high altitude, high velocity transport aircraft possess an adjustable stabilizer with varying incidence angles, which can greatly increase the lifting capabilities of a lifting surface [2]. Due to the fact that ice accretion can significantly reduce the maximum lift coefficient of a stabilizing surface, an ice reduction factor is imposed on the maximum lift coefficient of the stabilizing surfaces. This ice reduction factor is assumed to be 0.73, this is based on an ice accretion study on the reduction of the maximum lift coefficient of the horizontal stabilizer of a Fokker F-28 [21]. This results in a maximum horizontal stabilizer lift coefficient, $C_{L_{h}\max}$ of -0.73 and a maximum canard lift coefficient, $C_{L_{c}\max}$ of 0.73.

The velocity ratio between the free-stream value and the velocity at the stabilizing surfaces are also non-input parameters. The ratio of the free-stream velocity and the velocity at the canard surface, V_c/V_∞, is assumed to be 1. However the ratio of the free-stream velocity and the velocity at the horizontal stabilizer depends on the tail lay-out. For a t-tail this value is 1.0, for a fin-mounted fuselage this value is 0.95, for a fuselage mounted tail, this value is 0.85. The moment arm of the canard, l_c, and horizontal stabilizer, l_h, are also non-input parameters and are re-evaluated for each wing position. The last non-input parameter is the pitching moment coefficient about the aerodynamic center of the aircraft less-tail, this parameter is addressed separately in Section 4.3.7. Then there are also the canard-to-wing,S_c/S, and tail-to-wing,S_h/S, area ratios. These area ratios both simply range from 0 to 1 in order to determine the dominant forward center of gravity limit corresponding to a certain area ratio. The critical design condition for the control capacity required to reach the maximum lift coefficient of the aircraft, is the low speed low altitude landing configuration. This means that the all aerodynamic parameters are calculated at these conditions.

4.3.2. DOMINANT AFT CENTER OF GRAVITY LIMIT

In this section the dominant aft center of gravity limit is discussed. The purpose of this thesis assignment is to research the influence of a reduced stability margin on the aircraft performance in terms of maximum take-off mass for an equal payload. The core of the analysis is the stick-fixed stability curve. The stick-fixed stability curve is determined with Equation 4.2.

$$\left(\frac{x_{\text{cg}}}{\bar{c}_w}\right)_{\text{AFT}} = \frac{x_{\text{ac}}}{\bar{c}_w} + \left[\frac{C_{L_{\alpha_c}}}{C_{L_\alpha}}\left(1+\frac{d\epsilon_c}{d\alpha}\right)\frac{S_c l_c}{S_w \bar{c}_w}\frac{V_c}{V_\infty} + \frac{C_{L_{\alpha_h}}}{C_{L_\alpha}}\left(1-\frac{d\epsilon_h}{d\alpha}\right)\frac{S_h l_h}{S_w \bar{c}_w}\frac{V_h}{V_\infty}\right] - \text{SM} \tag{4.2}$$

From the latter equation it can be seen that the stick-fixed aft center of gravity limitation is related to the stability margin. When the subtraction of the stability margin is eliminated, the stick-fixed neutral points constraint is obtained. When the magnitude of a positive stability margin is reduced or when the stability margin is negative, this aft center of gravity limitation moves further aft, allowing for a smaller stabilizing surface area design. When the stick-fixed stability curve moves further aft it is possible that another aft center of gravity limitations becomes the most forward positioned center of gravity limit. In this analysis this could be the satisfactory short period oscillation characteristics aft center of gravity limit. When this scenario occurs, the dominant aft center of gravity limit will still be the stick-fixed stability curve, because it is possible to operate an aircraft with unfavorable short period oscillation characteristics with a fly-by-wire control system. The reason for implementing the short period oscillation curve in the x-plot is due to the fact that the user of this application requires information for which stability margin the aircraft possesses satisfactory short period oscillation characteristics. This is the reason that these curves are visible in the x-plot. Also it has to be noted that, during the analysis of a reduced stability margin, the assumption is made that the control surfaces are fixed throughout the motion, therefore only stick-fixed analysis are implemented in the x-plot.

The parameters which are determined within this sizing methodology are discussed next. Parameters which are not addressed in this section are input parameters of this sizing module and are already determined within other modules in the Initiator. From Equation 4.2 it can be seen that the aerodynamic center of the aircraft less tail is required. Again this is further elaborated in Section 4.3.8. The downwash gradient, $d\epsilon_h/d\alpha$ and the upwash gradient, $d\epsilon_c/d\alpha$ are determined with the downwash and upwash prediction methodology presented in Chapter 3. The moment arms, velocity ratios and area ratios are determined similarly as described in the paragraph on the dominant forward center of gravity limit. The stability margin, SM, is a parameter which is altered during the analysis in order to research the influence of a reduced stability margin. This leaves only the lift slopes of the stabilizing surfaces, $C_{L_{\alpha_c}}$ and $C_{L_{\alpha_h}}$ and the lift slope of the aircraft less tail. The lift slopes of the stabilizing surfaces are determined with a DATCOM method as presented in Equation 4.3.

$$C_{L_{\alpha_i}} = \frac{2\pi A_i}{2+\sqrt{4+(\frac{A_i\beta}{\eta})^2(1+\frac{\tan^2\Lambda_{c/2}}{\beta^2})}} \tag{4.3}$$

In the latter equation the subscript, i can either represent a c for a canard surface or a h for a horizontal stabilizer surface. The airfoil efficiency coefficient, η is assumed to be constant and 0.95. The Mach number dependent Prandtl compressibility factor is represented by β. The planform parameters (i.e. the aspect ratio, A_i and the half chord sweep angle $\Lambda_{c/2}$) are based on the initial stabilizing surface planform geometry determined with the volume coefficient method. The last parameter which needs to be calculated, for the dominant aft center of gravity limit, is the lift rate coefficient of the aircraft less tail, C_{L_α}. This is calculated using Equation 4.4 [2], where the lift slope of the wing is calculated similarly as the lift slope of the stabilizing surfaces with Equation 4.3.

$$C_{L_\alpha} = C_{L_{\alpha_w}}(1+2.15\frac{b_f}{b}\frac{S_{\text{net}}}{S}+\frac{\pi}{2}\frac{b_f^2}{b}) \tag{4.4}$$

The critical design condition for the stick-fixed stability curve, is the high velocity high altitude cruise configuration, this is due to the forward moving neutral point, which is de-stabilizing factor. This means that the all aerodynamic parameters are calculated at these conditions. Later, in Chapter 5, it will be seen that when the aft center of gravity limitation moves further aft, the minimum required stabilizing surface area is lowered. When the sizing methodology is implemented, the magnitude and sign of the stability margin is changed in order to research the influence of a reduced stability margin on the aircraft performance. The results of the change in stability margin are presented in Chapter 5.

4.3.3. ROTATION CAPACITY

The control capacity required for the take-off rotation and the landing flare-out are rather similar. Both are based on the same equation, but are analyzed in either take-off or landing conditions. For the required rotation capabilities Equation 4.5 is used [2].

$$\left(\frac{x_{\text{cg}}}{\bar{c}_w}\right)_{\text{FWD}} = \left([(\frac{S_h l_h}{S\bar{c}_w} - \frac{C_{L_R}}{C_{L_h}}(\frac{x_g}{\bar{c}_w}-0.25))(\frac{\eta_h\eta_q C_{L_h}}{C_{L_{\text{max}}}})] - \frac{C_{m_{c/4}}}{C_{L_{max}}}\right)\frac{V_R^2}{V_S^2}\frac{\bar{c}_w}{x_g - z_T\sum T/W} \tag{4.5}$$

The latter equation is used for the analysis for both the take-off rotation and the landing flare-out. The parameters which are calculated within the sizing methodology are briefly discussed next. First the stall velocities are addressed, these velocities for the landing and take-off phase are determined by applying Equation 4.6[2]. The stall velocities can directly be calculated, because all parameters visible in Equation 4.6 are already determined within the Initiator.

$$V_S = \sqrt{\frac{W}{S}\frac{2}{\rho}\frac{1}{1.13C_{L_{\max}}}} \tag{4.6}$$

When the stall velocities are calculated, the rotation velocities are determined by multiplying the stall velocities by 1.05. This is the minimum rotation velocity for transport aircraft [2]. The rotation lift coefficients then follow from the lift coefficient calculation with the rotation velocities. This leaves calculations of η_h and η_q. Equation 4.7, for the calculation of η_h is rather straight forward and does not introduce any new variables. However, Equation 4.8 possesses the rotation rate of the aircraft. For take-off rotation and the landing flare-out a rotation rate of 3 deg/s is assumed. This is typical value for modern transport aircraft [2].

$$\eta_h = \frac{x_h - x_g}{l_h}\left(\frac{V_h}{V_R}\right)^2 \tag{4.7}$$

$$\eta_q = 1 + \frac{C_{L_{h\alpha}}}{C_{L_h}}\frac{\dot{\theta}(x_h - x_g)}{V_R} \tag{4.8}$$

Other parameters, in Equation 4.5, such as the summation of the thrust-to-weight ratio, $\sum T/w$, the longitudinal position of the landing gear, x_g, the vertical distance between the thrust line and the center of gravity position, z_T and the maximum lift coefficient $C_{L_{\max}}$ are not further examined as these are input parameters for the stabilizing surface sizing methodology and are already determined within the Initiator.

4.3.4. STICK-FIXED MANEUVER POINTS

The stick-fixed maneuver points are closely related to the stick-fixed neutral points. From Torenbeek it follows that the stick-fixed maneuver points can be approximated by applying Equation 4.9 [2].

$$\left(\frac{x_{\text{cg}}}{\bar{c}_w}\right)_{\text{AFT}} = \frac{x_n}{\bar{c}_w} + 0.55\rho g\frac{S_h l_h^2 C_{L_{h\alpha}}}{W\bar{c}_w} \tag{4.9}$$

Equation 4.9 can directly be determined, because all parameters are already determined within the Initiator.

4.3.5. SATISFACTORY SHORT PERIOD OSCILLATION CHARACTERISTICS

In this section the derivations for the satisfactory short period oscillations curves are presented. The satisfactory shot period oscillation characteristics are related to the stick-fixed maneuver points, described in Section 4.3.4. From Torenbeek it follows that the forward and aft located center of gravity limitations which represent satisfactory short period oscillation characteristics can be approximated by applying Equation 4.10

$$\left(\frac{x_{\text{cg}}}{\bar{c}_w}\right) = -\frac{x_m}{\bar{c}_w} - 0.5\frac{K_Y^2}{\mu_c}\left(\frac{\omega_n}{L_\alpha}\right)C_{L_\alpha} \tag{4.10}$$

In the latter equation the inertia radius of the lateral axis, K_Y, is approximated by applying Equation 4.11, where the moment of inertia is approximated by applying Equation 4.12.

$$K_Y^2 = \frac{I_{yy}g}{W\bar{c}_w^2} \tag{4.11}$$

The moment of inertia is approximated with this estimation method, as presented by Raymer [22], because no reliable moment of inertia calculation method is available in the Initiator at the moment of writing. In Equation 4.12, the nondimensional radii of gyration about the y-axis, R_Y, is assumed to be 0.33 for a four engine wing-mounted aircraft, 0.38 for a two engine wing-mounted aircraft and 0.36 for a fuselage mounted aircraft [22].

$$I_{yy} = \frac{L^2 W R_Y^2}{4g} \tag{4.12}$$

As mentioned earlier, during the summation on the applied center of gravity limitations, it is stated that there are two short period oscillation characteristics. A forward limit and an aft limit. The aft limit is determined by a low speed flight condition with a low aircraft weight, whereas the high altitude high wing loading flight condition represents the forward center of gravity limit [2]. The term ω_n/L_α, in Equation 4.10 determines whether a forward or aft center of gravity limitation is calculated. The latter term is based on a graphical representation of satisfactory handling characteristics of conventional aircraft, as presented by Shomber and Nuttall [23].

4.3.6. WING OPTIMIZATION METHODOLOGY

All stabilizing surface sizing requirements, as presented in Section 4.1, are elaborated in Section 4.3.1 - 4.3.5. These requirements are the basis of the x-plot set-up, as will be seen during the wing optimization strategy for all aircraft configurations. In this section an iterative optimization is presented which results in an optimized wing position and the corresponding minimum required stabilizing surface area(s) for conventional, canard and three-surface aircraft configurations.

For a conventional and a canard aircraft, the optimization strategy is similar. The center of gravity ranges diagram is determined by interpolating the center of gravity ranges for 100 data points between the most aft and most forward located wing position. This results in 100 possible wing locations. For each of these wing positions an x-plot is set-up. This is necessary, because various parameters in the center of gravity limitations equations are dependent on the position of the wing, for example the moment arms of the stabilizing surfaces.

Once the center of gravity ranges diagram and the corresponding x-plots for 100 different wing positions are determined, the optimization process starts. The optimization starts by evaluating the most aft located wing location. The center of gravity range for the first wing position is obtained from the center of gravity ranges diagram. Once this is determined, the x-plot corresponding to the aft located wing position is evaluated. The minimum required stabilizing surface area is calculated by imposing the center of gravity range onto the x-plot and determine which is the lowest possible vertical position at which the center of gravity range can be positioned between the most forward located aft center of gravity limit and the most aft located forward center of gravity limit.

At this stage the minimum required stabilizing surface area is determined for the most aft located wing position. This is however not necessarily the optimum wing position. The optimum wing position is found when the x-coordinates of the center of gravity ranges diagram coincide with the x-coordinates of the x-plot. When the x-coordinates of both the center of gravity ranges diagram and the x-plot for the a given wing position do not coincide, the following wing position is analyzed. This process is iterated until the x-coordinates of the center of gravity ranges diagram and the x-plot coincide. When the latter situation occurs, the optimum wing position is found, corresponding to the minimum required stabilizing surface area. For clarification, an example of an optimized wing position for a typical single-aisle conventional aircraft is given in Figure 4.2.

From Figure 4.2(a), it can be seen that the default wing position, where the LEMAC is positioned at 45.2% of the entire fuselage length, needs to be shifted forward to a position where the LEMAC is positioned at 43.3% of the entire fuselage length. This results in a forward shift of 1.9% of the entire fuselage length, which is equal to an absolute forward shift of 0.79m corresponding to a fuselage length of 41.60m. From Figure 4.2(b) it can be seen that the minimum required horizontal stabilizer surface area corresponding to the optimum wing position is 31.5m^2. In Figure 4.2, it can be seen that the x-coordinates of the optimum wing position in the center of gravity ranges diagram coincide with

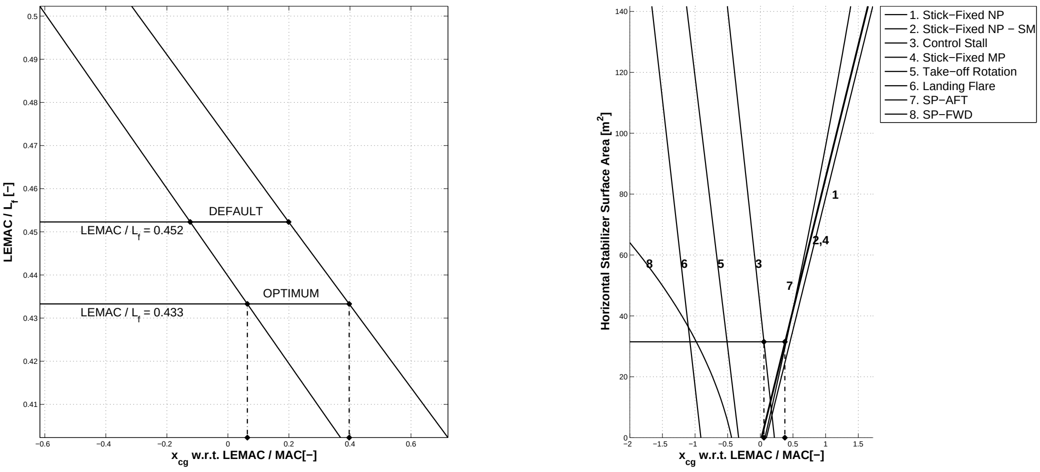

(a) CG Ranges diagram (c) x-Plot

Figure 4.2: Center of gravity ranges diagram and x-plot for a conventional aircraft.

the x-coordinates of the minimum required stabilizing surface area in the x-plot diagram.

The wing optimization methodology for a canard aircraft is similar to the wing optimization methodology for a conventional aircraft. However, for the canard aircraft only the stick-fixed stability curve and the control capacity required to reach the landing lift coefficient curve are present in the x-plot. This is due to the fact that the satisfactory short period oscillation characteristics curves and the rotation capacity curves are based on equations, which are only applicable to conventional aircraft, where the horizontal stabilizer is located behind the wing with a distance of roughly half the wing span. As opposed to the horizontal stabilizer area for a conventional aircraft, the x-plot determines the minimum required canard area for a canard aircraft. An example of a created center of gravity ranges diagram and a x-plot for a typical single-aisle mid-range canard aircraft are illustrated in Figure 4.3.

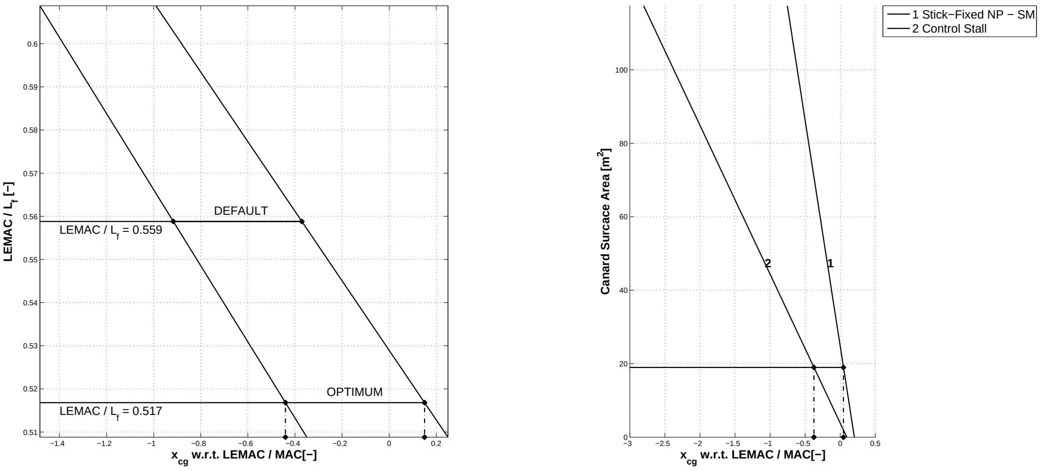

(a) CG Ranges diagram (c) x-Plot

Figure 4.3: Center of gravity ranges diagram and x-plot for a canard aircraft.

From Figure 4.3(a), it can be seen that the optimum wing position is shifted forward compared to the default wing position. The default wing position is defined at which the LEMAC is positioned at 55.9% of the fuselage length, whereas the optimum wing position is defined at which the LEMAC is positioned at 51.7% of the fuselage length. This results in a forward wing shift of 4.2% of the fuselage length. For a corresponding canard fuselage length of 41.53m, this results in an absolute forward shift of 1.74m. From Figure 4.3(b), it can be seen that the minimum required canard area, corresponding to the optimum wing position, is 19.0m^2.

For the three-surface aircraft configuration, the determination of the minimum required stabilizing surfaces is more complex, due to the presence of two stabilizing surfaces (i.e. canard and horizontal stabilizer). In order to reduce the design complexity, a methodology is presented, which determines the minimum required stabilizing surface areas for a fixed wing position. However, there are still infinitely many combinations of canard and horizontal stabilizer areas , for a fixed wing position, which are feasible design points.

For the three-surface aircraft an array of allowable canard-to-wing area ratios are assumed. These values range from 10% - 20% of the wing area with intermediate steps of 1%. This means that there are ten initial allowable canard-to-wing area ratios. By fixing these initial canard-to-wing area ratios, they can be assumed to be a fixed lifting surfaces similarly as for the wing. This allows to apply Equation 4.2 and Equation 4.1 and determine the corresponding minimum required horizontal stabilizer area for each initial canard area with the x-plot methodology.

The x-plot analysis is performed for each of the ten initially assumed canard-to-wing area ratios. This results in an array of corresponding minimum required horizontal stabilizer areas. Each of the ten combinations of corresponding canard-to-wing and tail-to-wing area ratios are feasible design points. Therefore, an extra design constraint is added to the analysis. Each of the feasible design points are analyzed with a vortex lattice method. The extra design constraint implies that the optimum design point, is the aircraft planform geometry which results in the lowest induced drag coefficient during cruise conditions. The results of the VLM analysis are displayed in Figure 4.4(a) where the drag counts are displayed for all feasible planform geometries. It has to be stated that during the VLM drag coefficient analysis only the lifting surfaces are simulated, therefore the drag count of the aircraft is rather low. From Figure 4.4(a) it can be seen that the first aircraft planform results in the lowest drag count. The optimum canard area is thus 10% of the wing area, which results in 11.61m^2 corresponding to a wing area of 116.11m^2 for a single-aisle mid-range three-surface aircraft. The corresponding minimum required horizontal stabilizer area is determine using the x-plot methodology and is displayed in Figure 4.4(b). From the latter figure it is determined that the corresponding horizontal stabilizer area is 21.11m^2, for a single-aisle mid-range three-surface aircraft.

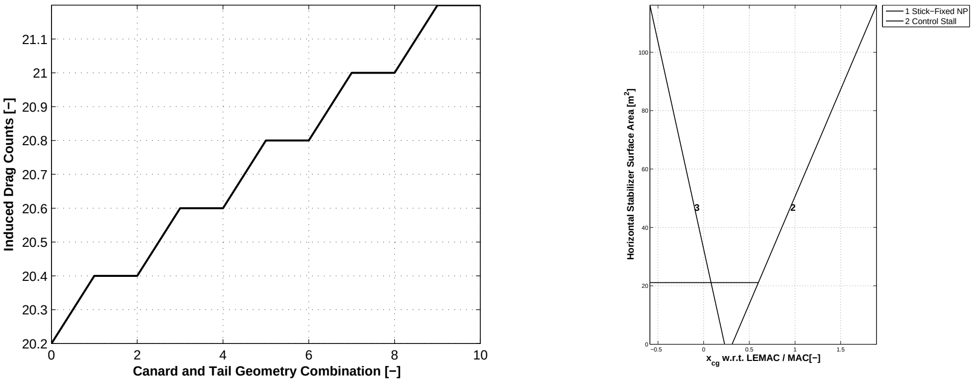

(a) Induced drag counts

(c) x-Plot

Figure 4.4: Center of gravity ranges diagram and x-plot for a three-surface aircraft.

To conclude this section, a methodology is presented to determine the minimum required stabilizing surface areas for conventional, canard and three-surface aircraft. For the conventional and canard aircraft, a wing optimization strategy is presented. However, for the three-surface aircraft only a minimum required canard and horizontal stabilizer calculation is performed. The validation of the sizing methodology against actual aircraft data is presented in Section 4.4.

4.3.7. VALIDATION OF THE PITCHING MOMENT

In this section two methods are presented to determine the tail-off pitching moment coefficient about the aerodynamic center. Both methods are validated against experimental data, based on the validation, a conclusion is drawn which is the most suitable method to calculate the pitching moment coefficient. The pitching moment coefficient is a required parameter in Equation 4.1, for the control leg related to the ability of the aircraft to pitch up to the landing angle of attack with full flaps deflected. During the stabilizing surface sizing methodology, extensive use is made of a Vortex Lattice Method (VLM). In this section it is validated whether the usage of a VLM produces satisfactory results for the pitching moment coefficient calculation. Two different methods are addressed in this section, the earlier mentioned VLM and an analytical method presented by Torenbeek [2]. The analytical Torenbeek method is not further examined in this section. However, a detailed description for clarification is given in Appendix A. Both methods are later validated against experimental data.

For validation purposes, three different aircraft are analyzed. The Fokker 100, the Airbus A300 and the McDonnell Douglas DC-9. The developed planform representations of the three wings for the VLM analysis given in Figure 4.5. The validation of both methods against experimental data are presented in Figure 4.5. In the latter figure the increase in lift coefficient due to flap and slat deflections is given on the horizontal axis. The pitching moment coefficient about the aerodynamic center of the aircraft tail-off is given on the vertical axis. The experimental data is obtained from a paper presented by Obert [24] on pitching moment calculations on tail-off transport aircraft configurations. From Figure 4.5 it can be seen that the pitching moment calculation of the VLM is significantly under predicted for all aircraft and for all values of ΔC_L. The error increases with increasing values of ΔC_L for all aircraft. The analytical Torenbeek shows a good prediction of the tail-off pitching moment coefficient for all values of ΔC_L and for all aircraft configurations. Based on these results, the pitching moment coefficient in Equation 4.1 it calculated with the Torenbeek method. A detailed description on the analytical Torenbeek method is presented in Appendix A.

4.3.8. COMPARISON OF THE AERODYNAMIC CENTER

In this section two methods are presented to determine the aircraft tail-off aerodynamic center. The determination of the aerodynamic center is an important parameter in the x-plot methodology, which is visible in Equation 4.2 and Equation 4.1. Due to the extensive use of a VLM for the calculation of aerodynamic parameters in previous sections, the aerodynamic center could easily be derived from the VLM analysis. However, in this section the calculation of the aerodynamic center with a VLM is compared to a graphical methodology presented by Torenbeek. The latter graphical methodology is based on extensive wind tunnel testing and is assumed to be an accurate prediction methodology. The graphical method by Torenbeek is not further examined in this section. However, for clarification a detailed description is given in Appendix B.

From the graphical method presented by Torenbeek it is found that, three basic planform parameters influence the position of the aerodynamic center. These parameters are the aspect ratio, A, the sweep angle, Λ and the taper ratio, λ. Therefore the calculation of the aerodynamic center with a VLM is compared for variations in these parameters to the Torenbeek method. The comparison of the aerodynamic center calculation between the graphical Torenbeek method and the VLM are illustrated in Figure 4.6. In Figure 4.6(a), the aspect ratio is incrementally increased from 5 to 10, in Figure 4.6(b), the sweep angle is incrementally increased from 20 to 45, whereas in Figure 4.6(c), the taper ratio is incrementally increased from 0.1 to 0.55.

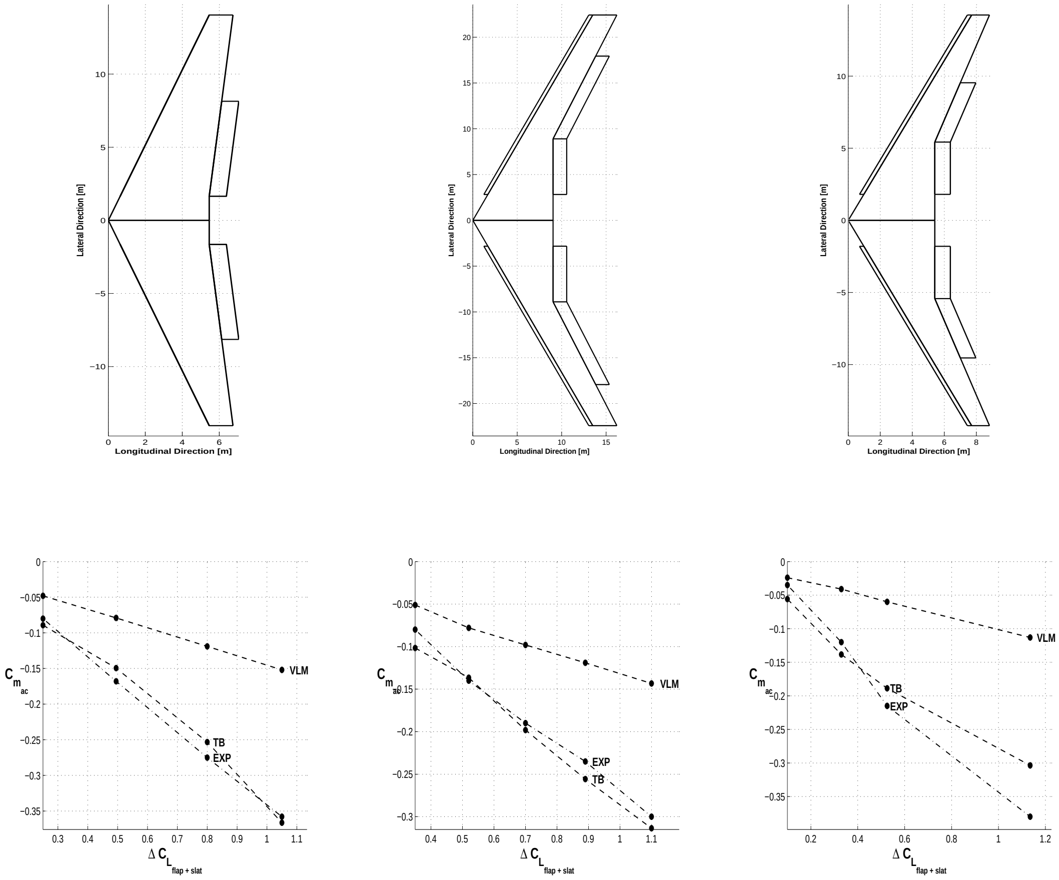

(a) F100 (b) A300 (c) DC-9

Figure 4.5: Validation of the VLM and Torenbeek tail-off pitching moment coefficient calculation.

From Figure 4.6 it can be concluded that the trend in both calculations is similar for all changes in parameters, however the VLM calculation is over predicted compared to the Torenbeek, this is especially true for the change in taper ratio, where the magnitude of the over prediction is largest. The maximum difference for the change A is 14.6%, the maximum difference for the change in Λ is 15.9%, whereas the largest difference for the change in λ is 18.5%. Due to these rather significant differences between the graphical method and the vortex lattice method, it is chosen to digitize the graphical Torenbeek method and implement the latter method into the stabilizing surface sizing methodology. This is further discussed in Appendix B.

4.4. VALIDATION OF THE SIZING METHODOLOGY

The stabilizing surface sizing methodology is implemented in the Initiator as an integral longitudinal stability and control analysis module. The purpose of the Initiator is to design an aircraft based upon fundamental input parameters, such as number of passengers or aircraft range. These input parameters are derived from actual aircraft, such as the B737, F100 and other aircraft. From these input parameters, the aircraft is sized. However, it is found that important stabilizing surface sizing parameters such as the wing area, S, moment arms, l_h and l_c, and center of gravity ranges could differ significantly from the actual values. This makes the implemented tool in the Initiator inapplicable for validation purposes. It is therefore chosen to validate the stabilizing surface sizing methodology outside of the Initiator. Separate input files with the actual aircraft parameters are created for the validation of the sizing methodology. During the validation, a stability margin of 5% is assumed for all

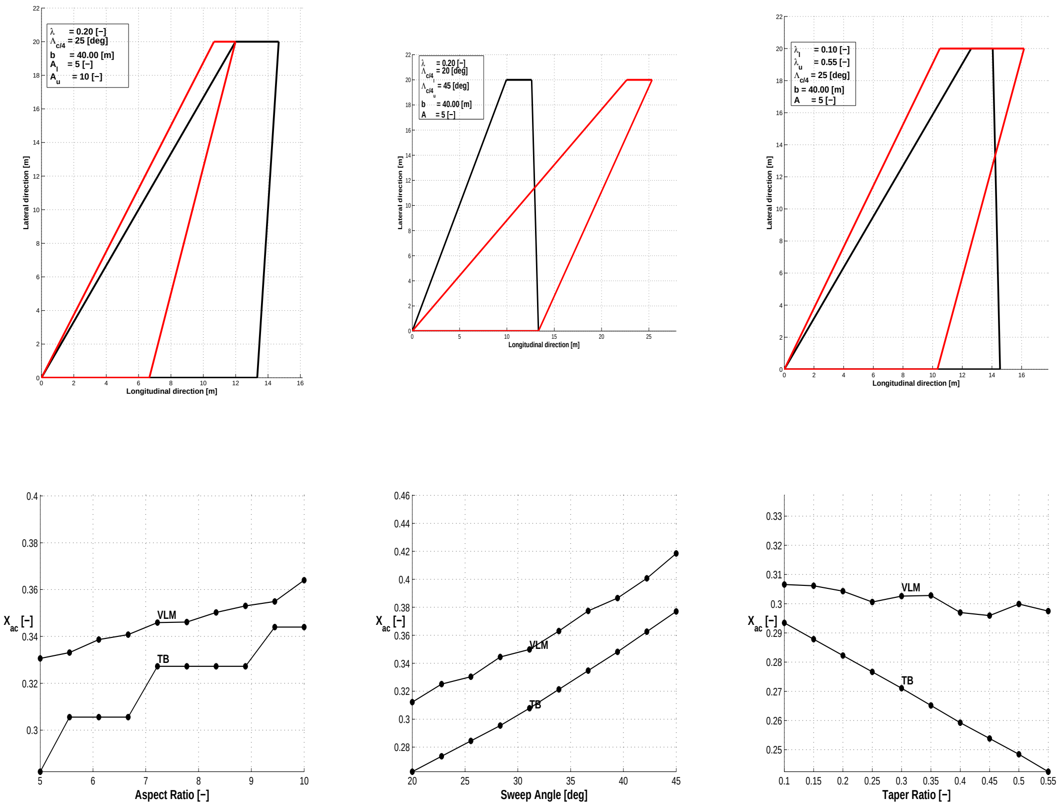

(a) Change in A (b) Change in Λ (c) Change in λ

Figure 4.6: Comparison of the aerodynamic center calculation between the graphical Torenbeek method and the VLM.

aircraft. This is an acceptable assumption for conventional jet transport aircraft [2]. The results of the validation are illustrated in Table 4.1. The center of gravity ranges are derived from actual loading diagrams obtained from Obert [3] and are displayed in the second column of Table 4.1.

Table 4.1: Validation of the stabilizing surface sizing module.

Aircraft	$\mathbf{CG}_{\text{range}}$	$\mathbf{S}_{\mathbf{h}_{\text{actual}}}$	$\mathbf{S}_{\mathbf{h}_{\text{prediction}}}$	$\mathbf{S}_{\mathbf{h}_{\text{error}}}$	$\mathbf{c}_{\mathbf{e}}/\mathbf{c}_{\mathbf{h}_{\text{actual}}}$	$\mathbf{c}_{\mathbf{e}}/\mathbf{c}_{\mathbf{h}_{\text{assumption}}}$	$\mathbf{c}_{\mathbf{e}}/\mathbf{c}_{\mathbf{h}_{\text{error}}}$
B737	0.344	31.31	32.50	3.80%	0.29	0.30	3.45%
F100	0.290	21.72	20.66	-2.10%	0.31	0.30	-3.23%
B767	0.320	77.69	79.32	4.82%	0.30	0.30	0.00%
B727	0.340	34.89	35.25	1.00%	0.32	0.30	-6.25%

From Table 4.1, it can be concluded that the stabilizing surface area sizing module is validated within an error margin of ±5% for all aircraft. The last column in the latter table represents the errors in the actual and assumed elevator chord to tail chord ratios. It has to be stated that the stabilizing surface sizing methodology is only validated for conventional aircraft. It is found that it is rather difficult to obtain actual center of gravity ranges from unconventional aircraft, this leaves the validation of the sizing methodology for canard and three-surface aircraft invalidated.

4.5. GROUND EFFECT ANALYSIS

In this section an in- and outside the ground effect analysis is performed, in order to determine if the assumed maximum design lift coefficient of the horizontal stabilizer, $C_{L_{h_{\max}}}$ can be attained in the ground effect region. In the ground effect region, the average downwash angle at the location of the horizontal stabilizer is significantly reduced, especially for fuselage mounted stabilizers, as was seen in Figure 2.13. Because the average downwash angle at the horizontal stabilizer is significantly reduced, the negative effective angle of attack of the horizontal stabilizer is also reduced. Therefore, a ground effect analysis is performed in order to check whether the maximum negative desgin lift coefficient can be attained in the ground effect region. The maximum negative design lift coefficient, without elevator deflection and including ice accretion, is assumed to be -0.73, as was presented in Section 2.8. During the out of ground effect analysis, the incidence angle of the adjustable horizontal stabilizer is determined, so that the maximum negative design lift coefficient without elevator deflection can be attained. During the in ground effect analysis, the horizontal stabilizer lift coefficient is reduced. Therefore, the corresponding elevator deflection is calculated in order to increase the lifting capabilities of the horizontal stabilizer and attain the maximum negative design lift coefficient, $C_{L_{h_{\max}}}$.

The in ground effect analysis is limited to horizontal stabilizer design of conventional and three-surface aircraft. The canard surface of a canard and three-surface aircraft is much less influenced by the presence of ground plane, because the canard surface is in the upwash of the wing. The control capacity required to pitch the aircraft up to the landing angle of attack, Equation 4.1, is based on the maximum lift coefficient of the horizontal stabilizer with ice accretion and zero elevator deflection. With an adjustable stabilizer it is possible to change the incidence angle of the stabilizer to trim the aircraft for different flight conditions. During the landing flare, when the aircraft is at an altitude lower than its own wing span, the aircraft enters the in ground effect region. The aircraft is a relatively short period in the ground effect region before the touchdown. Therefore it is not possible to change the incidence angle of the horizontal stabilizer when the aircraft is in the ground effect region.

The reduction of the average downwash angle with decreasing altitude reduces the effective negative angle of attack of the horizontal stabilizer, this reduces the lift coefficient. In order to trim the aircraft, in ground effect, the elevator should be deflected. This results in the following landing flare analysis. The aircraft is pitched up to the landing angle of attack and trimmed by decreasing the horizontal stabilizer incidence angle out of ground effect. When the aircraft enters the ground effect region, the aircraft is trimmed by deflecting the elevator up. In the sizing methodology, the required stabilizer setting is calculated out of ground effect corresponding to the horizontal stabilizer design lift coefficient. The elevator deflection to trim the aircraft is then calculated during the in ground effect region. When the required elevator deflection exceeds the maximum allowable elevator deflection, the horizontal stabilizer surface area needs to be increased in order to produce the required balancing lift force. The increase in planform area is determined by the difference in required horizontal stabilizer lift coefficient and the design lift coefficient.

The maximum allowable elevator deflection is defined as a deflection of -15^{o}. The in ground effect simulation is analyzed at an altitude of 2m. Full flap and slat deflections on the wing are simulated. An elevator chord to tail chord ratio of 0.30 is used in the analysis. The results of the landing flare analysis in- and outside the ground effect region are presented in Table 4.2.

Table 4.2: Results of the landing flare trim analysis.

Aircraft	$\mathbf{i_h}$	$\epsilon_{\mathbf{h}_{oge}}$	$\mathbf{C_{L_{h_{oge}}}}$	$\delta_{\mathbf{e}_{oge}}$	$\epsilon_{\mathbf{h}_{ige}}$	$\mathbf{C_{L_{h_{ige}}}}$	$\delta_{\mathbf{e}_{ige}}$
[−]	[deg]	[deg]	[−]	[deg]	[deg]	[−]	[deg]
A320	-10.3	9.9	-0.73	0	2.7	-0.78	-10.4
B737	-8.8	11.6	-0.73	0	4.5	-0.80	-10.5
B767	-10.1	9.8	-0.73	0	2.0	-0.75	-11.2
B777	-9.8	9.9	-0.73	0	1.2	-0.73	-12.1
F100	-9.5	8.5	-0.73	0	5.2	-0.78	-4.1

When the required stabilizer setting is calculated, out of ground effect with zero elevator deflection, corresponding to the design lift coefficient it is found that the required stabilizer setting is very close to the -10^{o} as can be seen in column 2. The out of ground effect results are displayed in column 3-5. When the aircraft enters the ground effect region, the average downwash angle is significantly reduced as can be seen in column 6. In order to trim the aircraft, the elevator needs to be deflected upwards. The in ground effect results are given in column 6-8. In the last column it is observed that the required elevator deflection does not exceed the maximum pre-defined elevator up constraint. This implies that all aircraft can be trimmed in- and outside of the ground effect region, within the design boundaries.

4.6. IMPLEMENTATION OF THE SIZING METHODOLOGY

The goal of the stabilizing surface sizing methodology is to optimize the default wing position and determine the corresponding minimum required stabilizing surface area. The influence of the change in wing position affects the landing gear and the placement of the engines in case of a wing-mounted engine configuration. When wing-mounted engines are present, the engines are subjected to a longitudinal shift, equal to the longitudinal shift of wing. However, for the landing gear this process cannot simply be repeated. When the landing gear is shifted, the design has to be checked whether initial constraints, such as loads on the nose and main gear are not violated. Also the height of the landing gear needs to be re-evaluated in order to determine if the rotation take-off angle of attack can be attained in case of a forward shifted main gear. Therefore it is decided to re-run the landing gear design module within the stabilizing surface sizing methodology with the same design rules as for the initial landing gear design, but for the adjusted wing position. A detailed description on the implementation of the stabilizing surface sizing module in the Initiator is presented in Chapter 8 in Part II of this thesis report.

5

RESULTS AND DISCUSSION

In this chapter the results of the stabilizing surface sizing methodology, as presented in Chapter 4, are discussed. The purpose of this chapter is to analyze and discuss the results of a reduced stability margin on the aircraft performance in terms of a reduction in Maximum Take-Off Mass (MTOM) for an equal payload. Because this thesis assignment focusses on conventional as well as on unconventional aircraft configurations, the results of a typical single-aisle mid-range and double-aisle long-range conventional aircraft, a single-aisle mid-range canard aircraft and a single-aisle mid-range three-surface aircraft are discussed.

The stabilizing surface sizing methodology is validated within an accuracy of 5% when compared to the actual aircraft geometry. This allows for the implementation of an accurate sizing methodology for the stabilizing surfaces in the Initiator. Implementing the sizing methodology in the Initiator implies, that it is added to the design convergence loop. The location where the stabilizing surface sizing module is added is discussed in Part II of this thesis report on the Code Documentation in Chapter 8. The purpose of the design convergence loop is to design the complete aircraft. During the ClassII.V weight estimation analysis and the converges, by re-evaluating the wing loading and the thrust-to-weight ratio. The design convergence loop converges when the difference in MTOM between two iterations in the Class II.V weight estimation loop is lower than a pre-defined tolerance. This tolerance is defined at 5%, this implies that the design convergence is converged when the difference between the initial and the final MTOM of an iteration is lower than 5%. When the design convergence is finished, the MTOM for a specific design point (i.e. a specific stability margin) is determined. By adjusting the magnitude and sign of the stability margin, the MTOM and masses of other major aircraft components can be analyzed for different stability margins. The maximum take-off masses displayed in this chapter are the results of the finished design convergences. The analyzed stability margins range from +10% to -8% for all aircraft configurations. The reduced stability margin, reduces the required stabilizing surface (i.e. tail and/or canard) area, this reduces the mass of the component. The reduction in horizontal stabilizer mass influences other major aircraft components. Therefore, also other major aircraft components, which are influenced by a reduced stability margin are analyzed. Other smaller aircraft components with a near constant mass for all stability margins and which therefore not influence a difference maximum take-off mass are left out of the analysis. The major aircraft components which influence the change in maximum take-off mass are, the engines, wing, fuselage and the stabilizing surfaces. Also the reduction in required fuel mass is displayed.

The influence of a reduced stability margin analysis is performed on conventional and unconventional aircraft configurations. Two different types of conventional aircraft are analyzed. A typical single-aisle mid-range transport aircraft and a typical double-aisle long-range transport aircraft. The mass reduction results of the conventional aircraft are presented in Section 5.1. The unconventional aircraft configurations are a single-aisle mid-range canard aircraft and a single-aisle mid-range three-surface aircraft, the mass reduction results are both discussed in Section 5.2. Due to the reduction in maximum take-off mass, the magnitude of the required fuel is also reduced.

5.1. REDUCED STABILITY MARGIN ON CONVENTIONAL AIRCRAFT

This section presents the results in mass reduction with a decreasing stability margin for conventional aircraft configurations. Two different aircraft are analyzed, a typical single-aisle mid-range transport aircraft and a typical double-aisle long-range transport aircraft. The top-level input requirements, in the Initiator, for the single-aisle aircraft are based on a Airbus A320, with a passenger capacity of 150 and a total payload mass of 20676kg. The double-aisle aircraft is based on a Boeing 777, with a passenger capacity of 394 and a payload mass of 64000kg. The mass reduction results of all the major aircraft components and the maximum take-off mass of the single-aisle aircraft are displayed in Table 5.1.

Table 5.1: Mass reduction of the components of a typical single-aisle mid-range conventional transport aircraft.

SM %	**MTOM** $\cdot 10^3$ [kg]	**Fuel** $\cdot 10^3$ [kg]	**Engine** $\cdot 10^3$ [kg]	**Wing** $\cdot 10^3$ [kg]	**Fuselage** $\cdot 10^3$ [kg]	**Tail** $\cdot 10^3$ [kg]	**S_h** m^2
10	70.60	12.62	5.01	7.35	9.50	663	29.04
8	70.47	12.53	5.00	7.34	9.48	637	27.74
6	70.37	12.50	5.00	7.32	9.46	612	26.39
4	70.07	12.40	4.98	7.27	9.43	585	24.94
2	69.99	12.36	4.98	7.26	9.43	560	23.55
0	69.88	12.33	4.98	7.25	9.41	535	22.20
-2	69.68	12.24	4.96	7.22	9.38	508	20.84
-4	69.66	12.23	4.96	7.21	9.38	508	20.80
-6	69.54	12.19	4.95	7.19	9.36	482	19.48
-8	69.38	12.13	4.93	7.16	9.34	456	18.13
Reduction	**1.73%**	**3.88%**	**1.56%**	**2.57%**	**1.68%**	**31.22%**	**37.57%**

From the latter table it can be seen that the minimum required horizontal stabilizer area for a typical single-aisle mid-range transport aircraft is reduced by 37.57% when the stability margin is reduced from +10% to -8%. The mass of the horizontal stabilizer is reduced slightly less as it is reduced by 31.22% from the +10% datum value to -8%. The influence of the decreased horizontal stabilizer mass on the other major aircraft components is better visualized by displaying the percentage decrease per 2% increments, as is displayed in Figure 5.1.

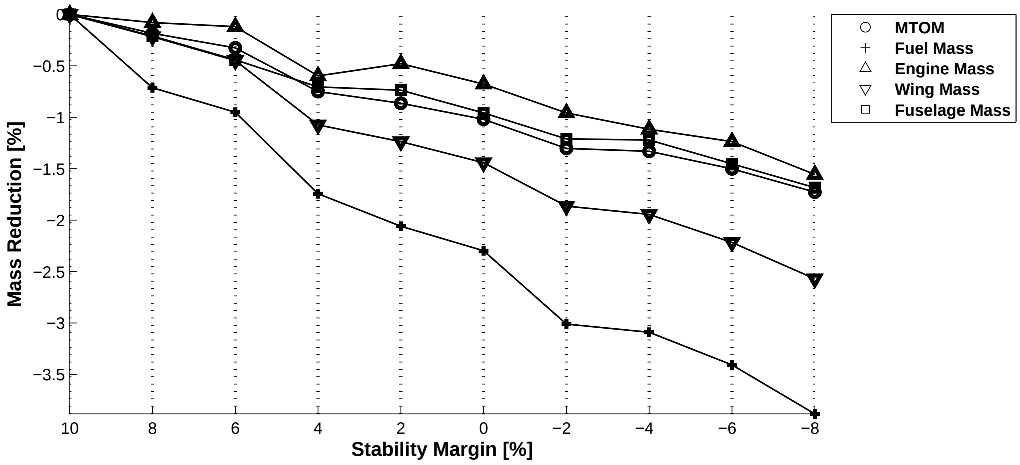

Figure 5.1: Percentage mass reduction of the components of a typical single-aisle mid-range conventional transport aircraft.

From Figure 5.1 it can be seen that the largest percentage mass reduction from the non-stabilizing surface aircraft components, excluding the fuel mass, stems from the wing. The mass of the wing is reduced by 2.57% from a positive stability margin of +10% to a negative stability margin of -8%. The engines possess the smallest percentage mass reduction with a magnitude of 1.56%. The overall largest reduction, excluding the horizontal stabilzier, is derived from the fuel mass, which is reduced by 3.88%. The purpose of this thesis assignment is to research what the influence on a reduced stability margin is on the aircraft performance in terms a reduction in maximum take-off mass for an equal payload. The reduction in maximum take-off mass for a typical single-aisle mid-range transport aircraft with a number of passengers of 150 and a payload of 20676kg, is in the magnitude of 1.73%.

A similar trend in the mass reduction of major aircraft components, as is presented for single-aisle mid-range transport aircraft, is obtained for the double-aisle long-range transport aircraft. The results of the stability analysis for the double-aisle long-range aircraft are displayed in Table 5.2.

Table 5.2: Mass reduction of the components of a typical double-aisle long-range conventional transport aircraft.

SM %	**MTOM** $\cdot 10^3$ [kg]	**Fuel** $\cdot 10^3$ [kg]	**Engine** $\cdot 10^3$ [kg]	**Wing** $\cdot 10^3$ [kg]	**Fuselage** $\cdot 10^3$ [kg]	**Tail** $\cdot 10^3$ [kg]	**S_h** m^2
10	277.09	58.82	18.15	38.67	47.27	3.85	101.00
8	276.65	58.63	18.10	38.59	47.20	3.79	97.99
6	275.47	58.34	18.06	38.51	46.96	3.66	93.17
4	274.56	58.14	18.00	38.35	46.72	3.52	88.52
2	272.84	57.62	17.90	37.97	46.40	3.35	83.38
0	272.22	57.58	17.88	37.90	46.17	3.03	73.60
-2	272.03	57.42	17.85	37.78	45.55	2.85	68.53
-4	270.23	57.25	17.79	37.52	45.45	2.67	63.42
-6	269.16	56.77	17.73	37.37	45.24	2.51	62.37
-8	268.68	56.74	17.73	37.28	45.17	2.35	53.95
Reduction	**3.04%**	**3.54%**	**2.31%**	**3.59%**	**4.44%**	**39.06%**	**46.58%**

From Table 5.2, it can be seen that, similarly as for the single-aisle aircraft, the component which is most affected by the reduced stability margin is, as expected, the horizontal stabilizer. The area of the horizontal stabilizer is decreased by 46.58%, whereas the mass is decreased by 39.06% when the stability margin is reduced from the +10% datum value to a stability margin of -8%. The component which is most influenced by the reduced horizontal stabilizer mass and area is the fuselage. The mass of the fuselage is reduced by 4.44%, whereas the smallest percentage decrease stems from the engines, which are reduced by 2.31%. The incremental percentage decrease for the components which are affected by the horizontal stabilizer are visualized in Figure 5.1.

The reduction in maximum take-off mass for a typical double-aisle long-range transport aircraft with a number of passengers of 394 and a payload of 64000kg, is in the magnitude of 3.08%. The differences between the mass reduction on the single-aisle and double-aisle aircraft are further discussed in Section 5.1.1.

5.1.1. DISCUSSION OF THE MASS REDUCTION ON CONVENTIONAL AIRCRAFT

In the previous section, the results of a reduced stability margin on conventional aircraft are presented. The difference between the result of the single-aisle aircraft and the double-aisle aircraft are discussed in this section. In the previous section, it is obtained that the percentage mass reduction of the aircraft components from the double-aisle aircraft are larger than for the single-aisle aircraft. This in turn is a result due to the larger percentage mass reduction of the horizontal stabilizer of the double-aisle aircraft, which is reduced by 39.06% for the double-aisle aircraft and 31.22% for the single-aisle aircraft. The larger percentage reduction in horizontal stabilizer mass for the double-aisle aircraft is a result of the differences in wing shift between the maximum positive and maximum negative stability

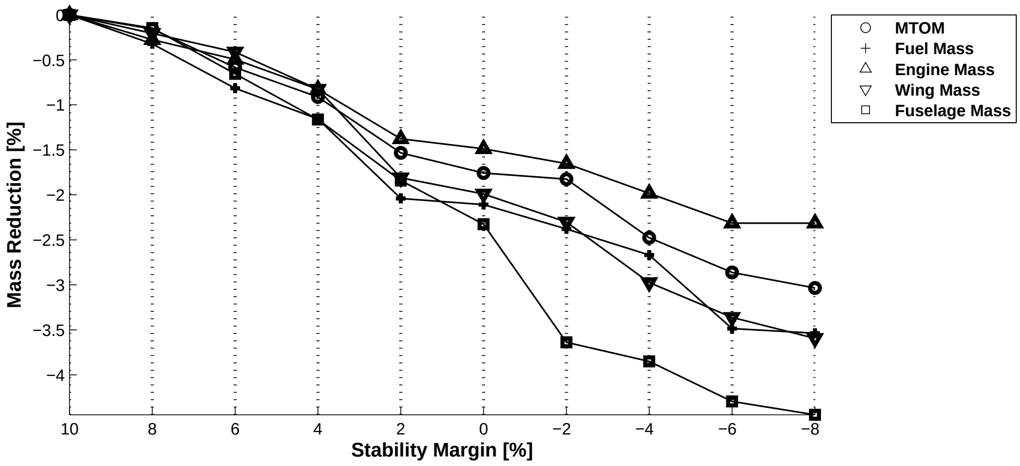

Figure 5.2: Percentage mass reduction of the components of a typical double-aisle long-range conventional transport aircraft.

margin for the two aircraft. In the case of the single-aisle aircraft the wing is shifted rearward when the stability margin is reduced from +10% to -8%, this results in a 0.5% reduction of the horizontal stabilizer moment arm. In case of the double-aisle aircraft the wing is shifted forward when the stability margin is reduced from +10% to -8%, this results in a 0.81% increase in horizontal stabilizer moment arm. This is the main reason for the larger percentage reduction in horizontal stabilizer mass for the double-aisle long-range aircraft.

A second, however less influential, reason is the shift in aerodynamic centres of the aircraft-less-tail combination between the two aircraft. The aerodynamic center, calculated at take-off conditions, of the aircraft-less-tail combination of the double-aisle aircraft is shifted slightly forward when the stability margin is reduced. This results in a small forward shift of the control capacity required at stall leg in the x-plot, which allows for a smaller minimum required horizontal stabilizer area. In case of the single-aisle aircraft, the aerodynamic center, again calculated at take-off conditions, is shifted slightly aft. This in turn results in a small aft shift of the control capacity required at stall leg in the x-plot and thus a larger minimum required horizontal stabilizer area. The combination of the increase in horizontal stabilizer moment arm and the forward shift of the control capacity required at stall leg in the x-plot, results in a larger percentage mass reduction of the horizontal stabilizer mass for the double-aisle long-range aircraft.

The larger percentage horizontal stabilizer mass reduction of the double-aisle aircraft is the reason for the larger percentage mass reduction of the other aircraft components. All mass components of the double-aisle aircraft possess a larger percentage reduction than the single-aisle aircraft. However, the percentage reduction in required fuel mass is larger for the single-aisle aircraft. For both aircraft the lift-to-drag ratio,L/D, is increased when the stability margin is reduced from +10% to -8%. The initial and final L/D ratios are displayed in Table 5.3. The initial L/D ratio corresponds to the +10% stability margin datum value, whereas the final L/D ratio corresponds to -8% stability margin. The lift-to-drag ratios are calculated at cruise conditions.

Table 5.3: L/D ratios during cruise conditions of the single-aisle mid-range aircraft and the double-aisle long-range aircraft.

Aircraft	L/D_{initial}	L/D_{final}	Increase
Single-aisle mid-range	16.6	17.1	3.01%
Double-aisle long-range	13.3	13.5	1.50%

From the latter table it can be seen that the increase in lift-to-drag ratio for the single-aisle aircraft is larger than for the double-aisle aircraft. This is the reason for the larger percentage fuel mass reduction on the single-aisle aircraft. The increase in L/D ratios for both aircraft are a results of a reduced drag coefficient during cruise conditions. The lift coefficient at cruise conditions is not affected by a reduction in stability margin.

The reductions in aircraft size and wing shift, for a decreasing stability margin, for both the single-aisle aircraft and the double-aisle aircraft are illustrated in Figure 5.3. In both cases, the smaller aircraft represents the aircraft with a stability margin of -8%.

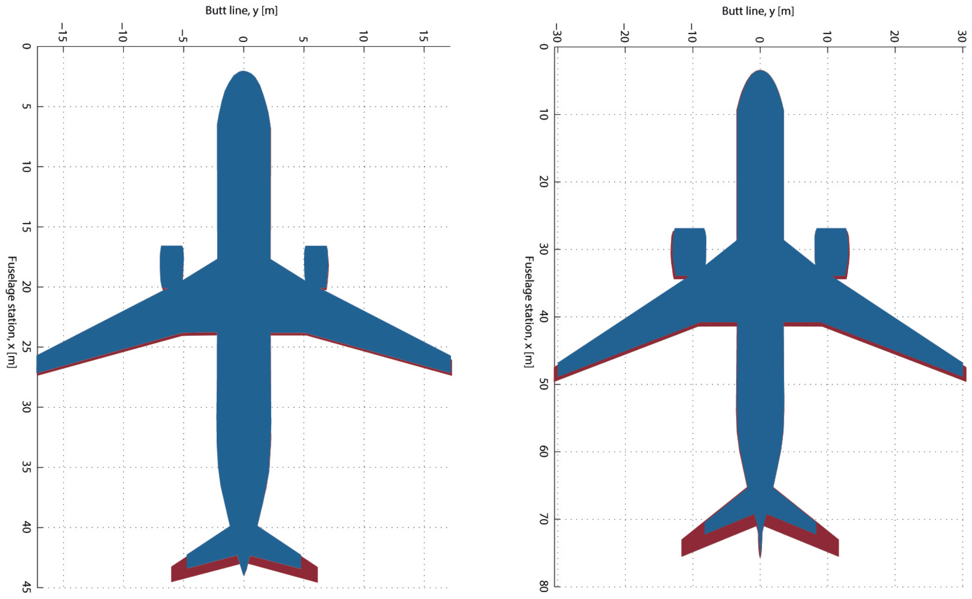

(a) single-aisle mid-range

(c) double-aisle long-range

Figure 5.3: Reduced aircraft size with decreasing stability margin on conventional aircraft configurations

5.2. Reduced stability margin on unconventional aircraft

The stabilizing surface sizing methodology is designed to cope with unconventional aircraft configurations. The unconventional configurations are the canard and the three-surface aircraft configurations. The influence of a reduced stability margin on both unconventional aircraft configurations are presented and discussed in this section. First the canard aircraft is discussed in Section 5.2.1, the results on three-surface aircraft are presented in Section 5.2.2.

5.2.1. Canard aircraft

In this section the results of a reduced stability margin on a canard aircraft are presented and discussed. The top-level input requirements, in the Initiator, for the canard aircraft are based on a Airbus A320, with a passenger capacity of 150 and a total payload mass of 20536kg. Similarly as the analysis on the conventional aircraft, the stability margin is reduced from a positive 10% datum value to a final negative 8% value. As opposed to the conventional aircraft, for the canard aircraft it is expected that the largest mass reduction on a single component stems from the stabilizing canard surface. The mass reduction of similar major aircraft components, as for the conventional aircraft, are displayed in Table 5.4.

From Table 5.4 it can be seen that the canard surface area is reduced by 28.99% when the stability margin is reduced from +10% to -8%, this results in a canard mass reduction of 22.94%. The largest mass reduction on other components of the canard aircraft stems from the wing. The wing mass is reduced by 2.08%. The engine possesses the smallest mass reduction, it is reduced by 0.62%. The reduction in the maximum take-off mass is however rather limited. The maximum take-off mass, for an equal payload of 20536kg, is reduced by 0.15%. This is due to the fact that the percentage reduction on the canard surface is smaller than for example the percentage horizontal stabilizer mass reduction on the conventional aircraft. The required fuel mass is reduced by 2.40%.

Table 5.4: Mass reduction of the components of a canard aircraft.

SM	**MTOM**	**Fuel**	**Engine**	**Wing**	**Fuselage**	**Canard**	**S_c**
%	$\cdot 10^3$ [kg]	$\cdot 10^3$ [kg]	$\cdot 10^3$ [kg]	$\cdot 10^3$ [kg]	$\cdot 10^3$ [kg]	$\cdot 10^3$ [kg]	m^2
10	62.12	8.35	4.17	8.51	6.14	763	35.05
8	62.11	8.34	4.17	8.48	6.10	744	33.95
6	62.10	8.32	4.17	8.47	6.08	725	32.81
4	62.10	8.30	4.16	8.45	6.08	706	31.63
2	62.10	8.25	4.16	8.44	6.07	687	30.51
0	62.08	8.24	4.16	8.42	6.06	667	29.35
-2	62.07	8.23	4.15	8.40	6.05	647	28.19
-4	62.06	8.19	4.15	8.38	6.03	626	27.06
-6	62.05	8.18	4.14	8.36	6.02	606	25.91
-8	62.03	8.15	4.14	8.35	6.01	588	24.89
Reduction	**0.15%**	**2.40%**	**0.62%**	**2.08%**	**1.95%**	**22.94%**	**28.99%**

Similarly as for the conventional aircraft, the incremental percentage reduction of the aircraft components which are influenced by the decrease in the stabilizing surface mass are displayed in Figure 5.4. From the latter figure it is visible that the mass reduction of the engine and the maximum take-off mass are less influenced by the reduced stability margin than the wing, fuselage and canard surface.

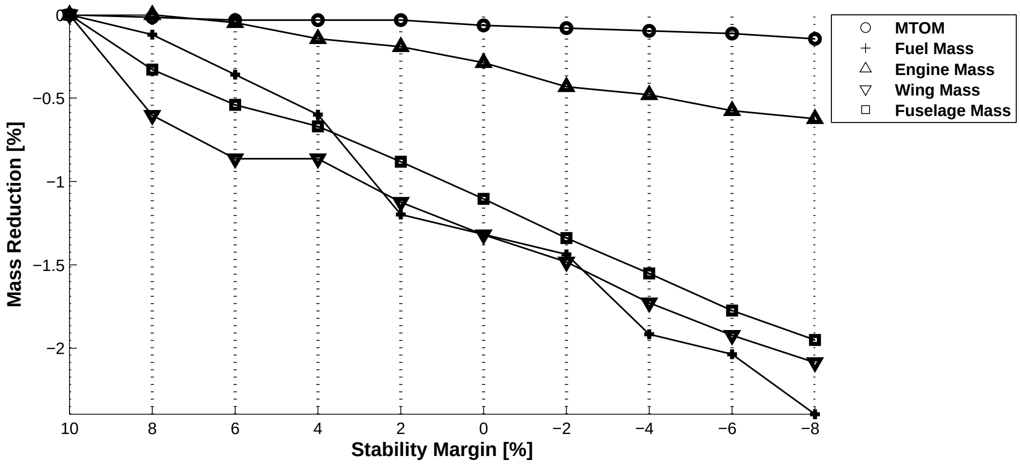

Figure 5.4: Percentage mass reduction of the components of a canard.

The reduction in aircraft size and wing shift, for a decreasing stability margin, for the canard aircraft is illustrated in Figure 5.5. The smaller aircraft represents the aircraft with a stability margin of -8%.

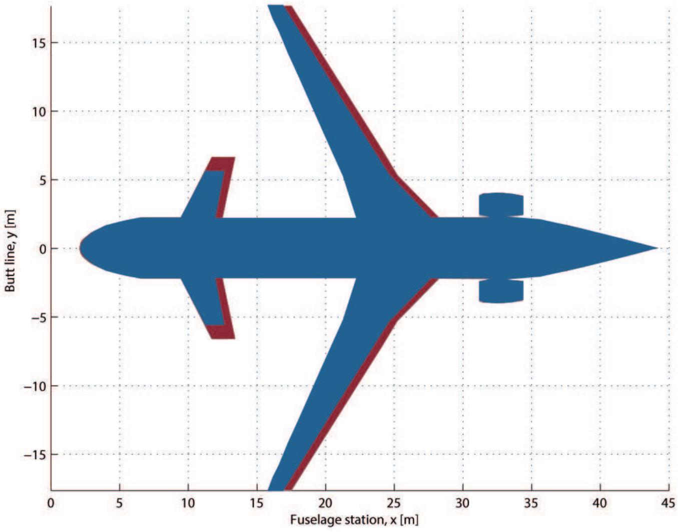

Figure 5.5: Reduced aircraft size with decreasing stability margin on a canard aircraft configuration

5.2.2. THREE-SURFACE AIRCRAFT

In this section the results of the reduced stability margin on the aircraft components of a three-surface aircraft are presented. The top-level input requirements, in the Initiator, for the three-surface aircraft are based on a Airbus A320, with a passenger capacity of 150 and a total payload mass of 20536kg. The mass reduction results on the major aircraft components, due to a reduced stability margin of +10% to a value of -8% are presented in Table 5.5.

Table 5.5: Mass reduction of the components of a three-surface aircraft.

SM %	**MTOM** $\cdot 10^3$ [kg]	**Fuel** $\cdot 10^3$ [kg]	**Engine** $\cdot 10^3$ [kg]	**Wing** $\cdot 10^3$ [kg]	**Fuselage** $\cdot 10^3$ [kg]	**Canard** $\cdot 10^3$ [kg]	$\mathbf{S_c}$ m^2	**Tail** $\cdot 10^3$ [kg]	$\mathbf{S_h}$ m^2
10	71.21	11.05	5.63	9.58	9.21	438	18.50	608	23.58
8	71.07	10.97	5.59	9.57	9.19	440	18.56	587	22.41
6	71.06	10.96	5.57	9.57	9.17	441	18.61	564	21.22
4	71.03	10.94	5.53	9.57	9.17	441	18.61	540	19.98
2	70.91	10.88	5.50	9.56	9.15	442	18.63	515	18.75
0	70.84	10.85	5.46	9.56	9.13	442	18.64	490	17.51
-2	70.83	10.83	5.46	9.56	9.12	443	18.65	464	16.27
-4	70.72	10.78	5.42	9.55	9.10	443	18.67	464	16.27
-6	70.71	10.77	5.42	9.55	9.08	444	18.69	438	15.05
-8	70.54	10.75	5.41	9.54	9.05	444	18.69	410	13.79
Red.	**0.94%**	**2.71%**	**3.78%**	**1.67%**	**0.30%**	**1.37%**	**-1.03%**	**32.57%**	**41.52%**

From the latter table it can be concluded that the largest percentage mass reduction stems from the horizontal stabilizer, which is reduced by 32.57%. The mass of the canard is however slightly increased, which is visible from the negative reduction of 1.03%. This is a result of the design methodology. During the sizing of the stabilizing surfaces of a three-surface aircraft, for a single stability margin design point, multiple feasible combinations of canard-to-wing and tail-to-wing ratios are found. An extra design constraint is added to determine the optimum feasible point. All feasible combinations are analyzed during cruise conditions and the combination which yields the lowest induced drag coefficient, is assumed to be the optimum design point. In turns out that optimum canard surface area, as can be seen in Figure 4.4(a), is the area which possess the lowest allowable canard-to-wing area ratio for all stability margins and is therefore not reduced.

The large reduction in horizontal stabilizer mass is therefore the reason for the reduction in mass on the other major aircraft components. The largest percentage reduction in mass, excluding the non-stabilizing surfaces, stems from the engines, which are reduced by 3.78%. The smallest percentage mass reduction stems from the fuselage, which is reduced by 0.30%.

The maximum take-off mass of the three-surface aircraft is reduced by 0.94% when the stability margin is reduced from +10% to -8% for an equal payload of 20536kg. The incremental percentage reduction of the non-stabilizing surface components is better visualized in Figure 5.6.

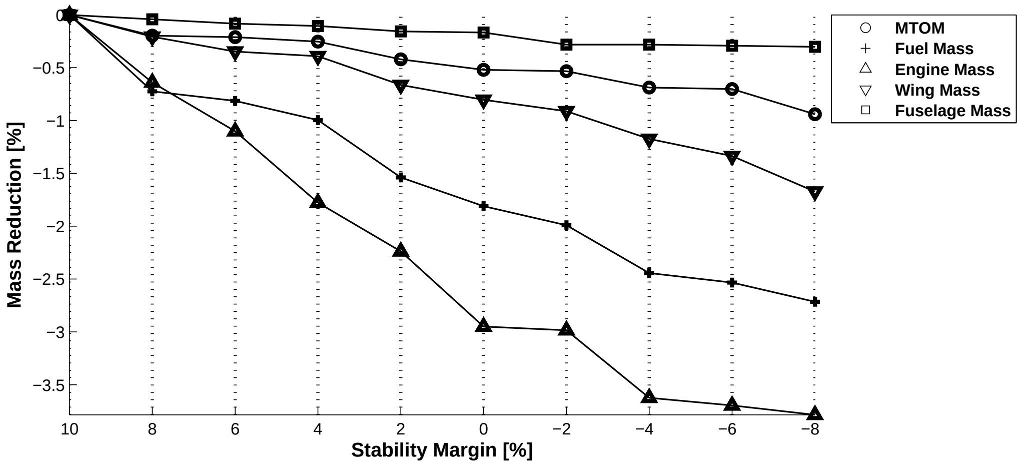

Figure 5.6: Percentage mass reduction of the components of a three-surface aircraft.

The reduction in aircraft size and wing shift, for a decreasing stability margin, for the three-surface aircraft is illustrated in Figure 5.7. The smaller aircraft represents the aircraft with a stability margin of -8%.

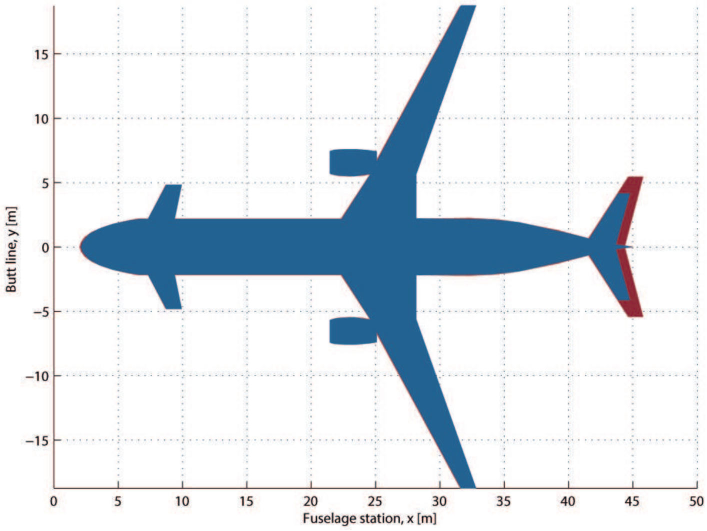

Figure 5.7: Reduced aircraft size with decreasing stability margin on a three-surface aicraft.

6

CONCLUSION AND RECOMMENDATIONS

This chapter contents the conclusion and recommendations regarding the thesis research. The conclusion is given in Section 6.1, whereas the recommendations are given in Section 6.2.

6.1. CONCLUSION

The purpose of this thesis assignment is to answer the research question, which is defined as:

"What is the influence of a decreased static longitudinal stability on the overall aircraft performance in terms of maximum take-off mass?"

The objective of the thesis assignment is to develop a longitudinal stability and control analysis methodology for conventional and unconventional aircraft configurations. Unconventional aircraft configurations are defined as canard and three-surface aircraft. The core of the stability and control methodology is to develop and implement a stabilizing surface sizing module in the Initiator.

The objective is achieved by developing a stabilizing surface (i.e. canard and horizontal stabilizer) sizing methodology for conventional, canard and three-surface aircraft in the Initiator, which replaces the currently implemented volume coefficient method. The stabilizing surface sizing methodology is developed, in such a manner that the stability margin is a user input parameter. This implies that the user can directly determine the influence of a certain stability margin on the design of the stabilizing surfaces. Also the influence of a decreased stabilizing surface sizing area on other aircraft components is determined.

An integral part of the stabilizing surface sizing methodology is to develop an accurate down- and upwash prediction method. Importantly the method needs to be able to determine the average downwash angle at an arbitrary point in the flow field behind a wing with the presence of high-lift devices in- and outside the ground effect region. Also the average upwash angle should be determined at an arbitrary point in the flow field in front of a wing with the presence of high-lift devices in and outside the ground effect region. The developed down- and upwash prediction methodology is validated against experimental data for two conventional aircraft, which include a fuselage-mounted horizontal stabilizer and a t-tail configuration. Both aircraft are validated against experimental data for different settings of high-lift devices in- and outside the ground effect region within a maximum error of $\pm 1^{\circ}$. The developed downwash prediction methodology, showed an increased accuracy in the prediction of the average downwash angle compared to other existing methods. No experimental data was found on average upwash angles on canard aircraft, which leaves the average upwash calculation on the canard surface of canard and three-surface aircraft configurations invalidated.

The stabilizing surface sizing methodology is validated for four different conventional aircraft. The minimum required horizontal stabilizer area is predicted within an accuracy of ±5% against the actual aircraft geometry. No actual values of allowable center of gravity ranges on canard and three-surface aircraft were found, which leaves the prediction of the minimum required canard area for a canard aircraft and the prediction of the minimum required canard and horizontal stabilizer area for a three-surface aircraft invalidated.

The implementation of the stabilizing surface sizing methodology, in the Initiator, allows for a rapid design of all other major aircraft components. This allows the user to research the influence a reduced stability margin on the overall aircraft performance in terms of maximum take-off mass with an equal payload. When the stability margin is reduced from a rather large positive value of 10% to a rather large negative 8% the reduction in maximum take-off mass for a typical single-aisle conventional mid-range aircraft is 1.73%, whereas the reduction in maximum take-off mass for a typical double-aisle conventional long-range aircraft is 3.04%. The larger reduction for the double-aisle long-range aircraft is a result of the larger decrease in minimum required horizontal stabilizer area. This in turn is a result of the larger increase in horizontal stabilizer moment arm of the long-range aircraft compared to the mid-range aircraft. The reduction in maximum take-off mass for a single-aisle canard aircraft is 0.15%. This is a rather small reduction compared to the conventional aircraft, which is a result due to the smaller decrease in minimum required canard area. This in turn is a result due to the small available design space in the x-plot compared to the available space in the x-plot of a horizontal stabilizer. The maximum take-off mass for a single-aisle three-surface aircraft is decreased by 0.94%.

When the stability margin is reduced, from +10% to -8%, during the analysis of a reduced stability margin on conventional aircraft, as presented in Chapter 5 the horizontal stabilizer areas are reduced by 37.57% and 46.58% for respectively a single-aisle mid-range aircraft and a double-aisle long-range aircraft. These results show a similarity between the reduced stability margin of the MD-11 compared to its predecessor, the DC-10. The horizontal stabilizer area of the MD-11 is reduced by 31.21% compared to the DC-10.

6.2. RECOMMENDATAIONS

In this section, several recommendations are presented regarding the longitudinal stability and control analysis methodology.

- During the stabilizing surface sizing methodology, the control forces are neglected in the x-plot. The purpose of the Initiator is to design high-speed high-altitude transport aircraft which operate with an irreversible flight control system. However, for future applications it might be desirable to design smaller aircraft with reversible control systems. In the latter case it is advised to implement control forces in the longitudinal stability and control analysis.

- Currently in the calculation, on the satisfactory short period oscillation characteristics, a rough approximation method is used for the moment of inertia calculation. When in the future a reliable moment of inertia prediction module is developed, it is advised to replace the current approximation method.

- When it is desirable to increase the accuracy of the down- and upwash prediction methodology at the cost of computational time, it could be achieved by decreasing the maximum allowable iteration difference and the incremental incidence angle steps.

- Currently the consequences of a reduced stability margin on the control system of the aircraft are neglected. In order to operate an aircraft with a negative stability, a fly-by-wire system is required for a safe operation. By adding a control system analysis, the maximum allowable negative stability margin could be determined.

II

CODE DOCUMENTATION

7

INTRODUCTION

In this section the documentation of the code is presented. The development and the implementation of the longitudinal stability and control analysis, with the purpose of sizing the stabilizing surfaces of conventional and unconventional aircraft is discussed in this part of the report. The name of the stabilizing surface sizing module, in the Initiator, is *StabilizingSurfaceSizing*. An integral part of the stabilizing surface sizing methodology is a newly developed methodology to predict the average down- and upwash angles at arbitrary points in the flow field. Both methods are further explained in Chapter 8. The background of the code is presented in this chapter, in Section 7.1.

7.1. BACKGROUND

The background of the stabilizing surface sizing methodology is presented in this section. The goal of the developed module, is to determine the minimum required stabilizing surface area(s) corresponding to an optimized wing position. The module needs to be able to cope with a large number of different conventional aircraft, as well as unconventional aircraft. Unconventional aircraft are defined as canard and three-surface aircraft.

When the minimum required stabilizing surface area(s) and the optimized wing position are determined, the user is able to adjust the stability margin of the aircraft as a user input value. Due to the adjustment of the stability margin, the user can directly determine what the influence of a reduced stability margin is on the minimum required stabilizing surface area(s) as well as on other major aircraft components and thus the overall performance of the aircraft.

The *StabilizingSurfaceSizing* module is implemented in the conceptual aircraft sizing tool, called the Initiator. Therefore, the sizing module cannot be operated as a stand-alone application, because it requires a large number of input parameters from the *Class2WeightEstimation* module. The output of the *StabilizingSurfaceSizing* module is an optimized wing position corresponding to the minimum required stabilizing surface area(s) and a re-designed landing gear, when the default wing position is shifted to the optimum position.

The implementation of the sizing module in the Initiator, allows the user to run the *DesignConvergence* module. During the design convergence, the complete aircraft is designed. During each iteration of the *Class25WeightEstimation*, the wing loading and the thrust-to-weight ratio are re-evaluated. This implies that also the *StabilizingSurfaceSizing* is re-evaluated. When the *DesignConvergence* module converges on the maximum take-off mass, the influence of a certain specified stability margin on other aircraft components can be determined. This allows the user to research the influence various stability margins on the aircraft performance in terms of maximum take-off mass for an equal payload.

8

PROGRAM STRUCTURE

The outline and structure of the code is presented in this chapter. The developed longitudinal stability and control analysis, the *StabilizingSurfaceSizing* module, is divided into two parts. The down- and upwash prediction module is an integral part of the overall stabilizing surface sizing module, however both methods are treated separately. First the down- and upwash prediction module is discussed in Section 8.1, whereas the stabilizing surface sizing module is discussed in Section 8.2.

8.1. DOWNWASH MODULE

The downwash module is an integral part of the overall stabilizing surface sizing module. The downwash module is developed to determine the average downwash angle at an arbitrary point in the flow field behind a wing with the presence of high-lift devices in- and outside of the ground effect region. Also the average upwash angle can be determined at an arbitrary point in the flow field in front of the wing with the presence of high-lift devices in- and outside the ground effect region. The methodology is developed with a Vortex Lattice Method (VLM) module, this allows for the analysis of multiple lifting surfaces in a single flow field. Due to this methodology it is also possible to determine the average downwash angle at the horizontal stabilizer in case of a three-surface aircraft. The placement of the down- and upwash prediction methodology is discussed in Section 8.2. The goal of the down- and upwash prediction methodology, is to adjust the incidence angle, of the to be analyzed stabilizing surface, so that the lift coefficient of the latter surface is zero. Then when the angle of attack is a known input parameter and the incidence angle is determined at which the lift coefficient is zero, the effective angle of attack is zero and Equation 8.1 changes to Equation 8.2 in case of a horizontal stabilizer and the average downwash angle is determined.

$$\alpha_{h_{\text{eff}}} = \alpha + i_h - \epsilon_h \tag{8.1}$$

$$\epsilon_h = \alpha + i_h \tag{8.2}$$

In case of canard surface, Equation 8.3 changes to 8.4 and the average upwash angle is determined.

$$\alpha_{c_{\text{eff}}} = \alpha + i_h + \epsilon_c \tag{8.3}$$

$$\epsilon_c = -\alpha - i_c \tag{8.4}$$

The activity diagram of the prediction of the average downwash angle at the location of the horizontal stabilizer is given in Figure 8.1. Obtaining the wing planform geometry and the placement of the high-lift devices is the first step in the process. The wing and high-lift devices geometry is written into an AVL input file. In the latter input file, the wing, high-lift device and stabilizing surface(s) geometries are specified. A more detailed description of the AVL input file is given in Section 8.1.1.

Once the input file is created, a **.key** file is written, which contains the run case parameters. Such as the angle of attack and the magnitudes of high-lift device deflections. After the creation of the **.key** file, AVL is ran. An output file is created from which the initial horizontal stabilizer lift coefficient, C_{L_h}, is obtained. A pre-defined maximum allowable value for lift coefficient is set at 0.001. This implies that when the absolute lift coefficient of the horizontal stabilizer is lower than the pre-defined maximum allowable value, the lift coefficient is assumed to be zero.

When the initial absolute value of C_{L_h} is lower than the maximum allowable value, the effective angle of attack is already zero and the average downwash angle is calculated with Equation 8.2, however when the initial absolute value is larger than the maximum allowable value, the incidence angle needs to be adjusted. In case of moderate to large angles of attack the lift coefficient of the horizontal stabilizer tends to be positive, therefore in the latter case the incidence angle needs to be decreased in order to reach a zero effective angle of attack of the horizontal stabilizer. In case of smaller angles of attack, the lift coefficient at the horizontal stabilizer tens to be negative, due to the downwash distribution of the wing. Therefore, the incidence angle needs to be increased in order to reach a zero effective angle of attack. This process is iterated until the absolute value of the lift coefficient is lower than the pre-defined maximum allowable value of C_{L_h}. The incremental step in the adjustment of the incidence angles is 0.5^o. The calculation process is similar for the average upwash angle calculation in case of a canard aircraft and the average downwash angle at the horizontal stabilizer in case of a three-surface aircraft.

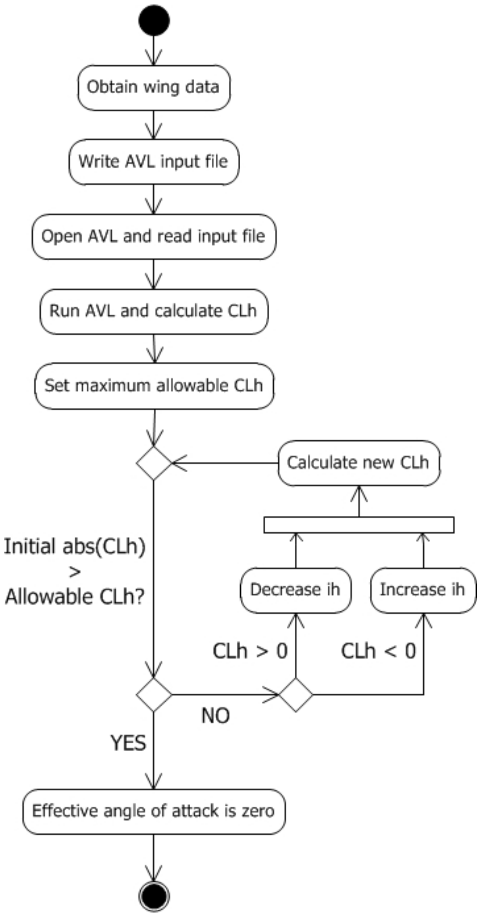
Obtain wing data
Write AVL input file
Open AVL and read input file
Run AVL and calculate CLh
Set maximum allowable CLh
Calculate new CLh
Initial abs(CLh) > Allowable CLh?
Decrease ih
Increase ih
CLh > 0
CLh < 0
NO
YES
Effective angle of attack is zero

Figure 8.1: Activity diagram of the developed downwash prediction methodology.

8.1.1. AVL INPUT FILE

In this section a detailed description is given for the AVL input file. Once the wing, high-lift device and stabilizing surface(s) geometries are obtained from the input parameters. These geometries are rewritten into an AVL input file. An example of an AVL input file for an Airbus A320 is given in 8.2.

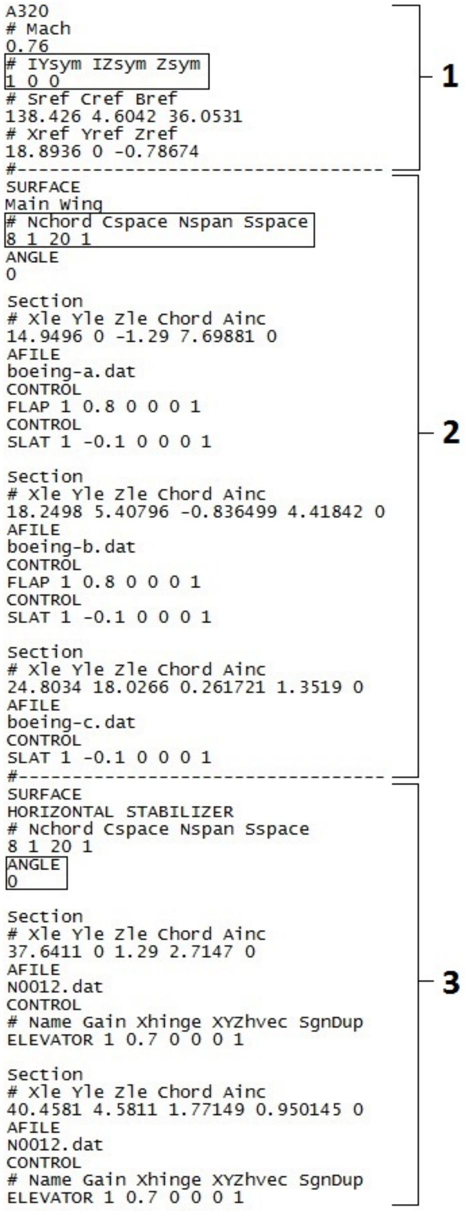

```
A320
# Mach
0.76
# IYsym IZsym Zsym
1 0 0
# Sref Cref Bref
138.426 4.6042 36.0531
# Xref Yref Zref
18.8936 0 -0.78674
#-----------------------------------
SURFACE
Main Wing
# Nchord Cspace Nspan Sspace
8 1 20 1
ANGLE
0

Section
# Xle Yle Zle Chord Ainc
14.9496 0 -1.29 7.69881 0
AFILE
boeing-a.dat
CONTROL
FLAP 1 0.8 0 0 0 1
CONTROL
SLAT 1 -0.1 0 0 0 1

Section
# Xle Yle Zle Chord Ainc
18.2498 5.40796 -0.836499 4.41842 0
AFILE
boeing-b.dat
CONTROL
FLAP 1 0.8 0 0 0 1
CONTROL
SLAT 1 -0.1 0 0 0 1

Section
# Xle Yle Zle Chord Ainc
24.8034 18.0266 0.261721 1.3519 0
AFILE
boeing-c.dat
CONTROL
SLAT 1 -0.1 0 0 0 1
#-----------------------------------
SURFACE
HORIZONTAL STABILIZER
# Nchord Cspace Nspan Sspace
8 1 20 1
ANGLE
0

Section
# Xle Yle Zle Chord Ainc
37.6411 0 1.29 2.7147 0
AFILE
N0012.dat
CONTROL
# Name Gain Xhinge XYZhvec SgnDup
ELEVATOR 1 0.7 0 0 0 1

Section
# Xle Yle Zle Chord Ainc
40.4581 4.5811 1.77149 0.950145 0
AFILE
N0012.dat
CONTROL
# Name Gain Xhinge XYZhvec SgnDup
ELEVATOR 1 0.7 0 0 0 1
```

Figure 8.2: Example of an AVL input file of an conventional aircraft.

In the latter figure it can be seen that the input file is divided in three parts. The first part is related to the overall run case parameters. In this section, the Mach number, the reference parameters such as wing area, mean aerodynamic chord and the wing span are defined. Also the position of the center of gravity is defined. The rectangular block in the first part of the input file is related to the mirroring of the wing and the altitude of the aircraft. When the variable **IYsym** is 1, only half of the aircraft is specified about the axis of symmetry, as can be seen in Figures 8.3-8.5. The parameter, **IZsym**, is an important parameter for the downwash prediction methodology. If the latter variable is zero, no ground plane is present in the flow field. However, when **IZsym** is equal to one, a ground plane is present in the flow field and the aircraft is analyzed in ground effect. The height of the plane is specified with the variable **Zsym**.

The second part of the input file is related to the wing of the aircraft. In the latter part, the wing and high-lift devices geometries are specified. Also the wing airfoils are defined in the second part. The rectangular block in the second part is related to the panelling of the wing. The parameter,**Nchord**, represents the number of chordwise panels, which in this case is 8. The parameter, **Nspan**, represents the number of spanwise panels, which in this case is 20. The parameters, **Cspace** and **Sspace** represent the spacing of the panels. Both are in this case chosen to be one, which represents a cosine spacing of the panels. The panelling of a conventional, canard and three-surface aircraft are illustrated in Figures 8.3-8.5. It can be seen that the spacing of the chordwise panels is smaller near the leading-edge and trailing-edge, whereas the spacing of the spanwise panels is smaller near the root and tip of the wing.

The third part of the input file example is related to the horizontal stabilizer. In the latter part, the horizontal stabilizer and elevator geometries are specified. Also the horizontal stabilizer airfoils are specified in the third part. The last important parameter addressed in this section is the rectangular block in the third part of the input file. The parameter, **Angle**, in the rectangular block is related to the incidence angle of the horizontal stabilizer. During the prediction of the average downwash angle at the horizontal stabilizer, as presented in Section 8.1, the parameter, **Angle**, is changed to adjust the incidence of the horizontal stabilizer and to determine the incidence angle at which the lift coefficient of the horizontal stabilizer, C_{L_h} is zero.

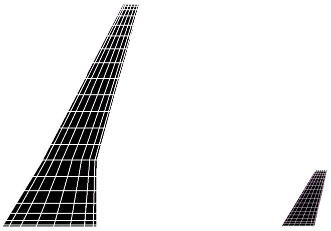

Figure 8.3: Example of the chord- and spanwise panel distribution of the lifting surfaces of a conventional aircraft, used in the down- and upwash prediction methodology.

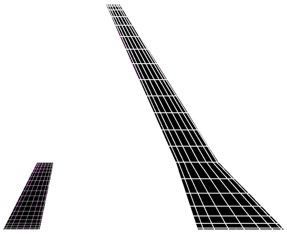

Figure 8.4: Example of the chord- and spanwise panel distribution of the lifting surfaces of a canard aircraft, used in the down- and upwash prediction methodology.

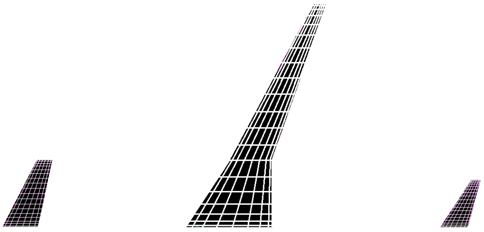

Figure 8.5: Example of the chord- and spanwise panel distribution of the lifting surfaces of a three-surface aircraft, used in the down- and upwash prediction methodology.

8.2. STABILIZING SURFACE SIZING MODULE

As mentioned in the previous section, the down- and upwash prediction methodology is an integral part of the stabilizing surface sizing methodology. In this section the sizing methodology is further elaborated. The purpose of the sizing methodology is to determine the optimized wing position corresponding to the minimum required stabilizing surface(s). The activity diagram of the stabilizing surface sizing methodology is given in Figure 8.6. From the latter figure it can be seen that the results of the *ClassIIWeightEstimation* module are the input parameters for the *StabilizingSurfaceSizing* module. Once the results of the *ClassIIWeightEstimation* module are obtained, the down- and upwash prediction methodology is addressed. This module is explained in detail in Section 8.1.

After the down- and upwash prediction methodology, the loading diagram of the aircraft is determined for three different wing positions. First the default position, then an extreme forward wing position and an extreme aft wing position. The forward wing position is defined as the default wing position minus 5% of the entire fuselage length, whereas the aft wing position is defined as the default wing position plus 5% of the entire fuselage length. From the loading diagrams of the three wing positions, the corresponding center of gravity ranges are determined. These center of gravity ranges form the basis of the center of gravity ranges diagram. In order to set-up the center of gravity ranges diagram, the center of gravity ranges for the wing positions between the most aft and forward located wing positions are interpolated for 100 wing positions. This results in the center of gravity ranges diagram. The most forward located wing position is located 5% of the entire fuselage length forward of the default wing position and the most aft located wing position is located 5% of the entire fuselage length behind the default wing position. This results in a total wing position range of 10% of the entire fuselage length. The 100 possible wing positions, result in an incremental wing position step of 0.1% of the entire fuselage length.

Once the center of gravity ranges diagram is set-up, all wing position dependent and wing position independent variables are calculated, which are required in order to set-up the x-plots. All required parameters are addressed in Section 4.3 and are not further elaborated in this section. At this stage a loading diagram is set-up for 100 wing positions, where each wing position is related to one x-plot. A different x-plot is created for a certain wing position, as certain variables, required in the x-plot analysis, are dependent on the wing positions, such as the moment arms of the stabilizing surfaces, l_c and l_h.

The start of the wing optimization strategy starts with the most aft located wing position. The center or gravity range for the aft located wing position is obtained from the loading diagram. Then for this center of gravity position, the minimum required stabilizing surface area is determined from the corresponding x-plot. A minimum required area is obtained when the center of gravity range intersects with the most forward located aft center of gravity limit and the most aft located forward center of gravity limit, as described in Section 4.3. This results in two x-coordinates in the x-plot. These x-coordinates are compared to the x-coordinates of the center of gravity ranges diagram for the aft located wing position. When the x-coordinates of the x-plot and the center of gravity ranges diagram coincide, the optimum wing position is found. However, when these coordinates do not coincide, which is likely for the extreme aft located wing position, a new wing position is assumed and the process is repeated. The new wing position is the aft located wing position, minus the incremental wing position step of 0.1%. The latter process is repeated until the x-coordinates coincide and the optimum wing position is found. Simultaneously the minimum required stabilizing surface area is obtained.

When the minimum required stabilizing surface area is obtained, the planform of the horizontal stabilizer or canard is re-designed. For the re-design of the planform, the initial aspect ratio, A, sweep angle, Λ and taper ratio, λ are held fixed. Therefore, the new span, root and tip chords can be determined.

After the redesign, an in ground effect analysis is performed for the horizontal stabilizer on a conventional or three-surface aircraft. The reduction of the average downwash angle with altitude, due to the presence of a ground plane, can significantly reduce the negative effective angle of attack of the horizontal stabilizer. This reduces the magnitude of the negative lift coefficient, C_{L_h}. This check is performed in order to analyse if the maximum design lift coefficient of the horizontal stabilizer can be attained in- and outside the ground effect region. When the aircraft is outside of the ground effect region, where the pilot can adjust the incidence angle of the adjustable stabilizer during the landing approach, the incidence angle is determined at which the maximum design lift coefficient can be attained with zero elevator deflection. When the aircraft is inside of the ground effect region, where the pilot does not have sufficient time to adjust the incidence angle of the horizontal stabilizer during the landing approach, the elevator should be deflected in order to attain the maximum design lift coefficient inside the ground effect region. At this stage, the horizontal stabilizer is adjusted for the out of ground effect incidence angle and the elevator deflection is calculated in order to attain the maximum design lift coefficient in ground effect. When a larger elevator up deflection is required than the predefined maximum allowable value, which is set at -15^{o}, the maximum design lift coefficient cannot be attained in ground effect. This results in the second loop in the stabilizing surface sizing methodology as displayed in Figure 8.6. In order to reach the required lift force to trim the aircraft in ground effect, the area of the horizontal stabilizer, S_h is increased. The increase is determined from the difference between the maximum design lift coefficient and the lift coefficient corresponding to the in ground effect lift coefficient with max elevator up.

After the in ground effect analysis, the landing gear is re-designed for the optimized wing position, the re-design is based on the same design rules as the initial landing gear design within the *ClassIIWeight-Estimation* module. The design strategy for the landing gear is repeated in the *StabilizingSurfaceSizing* module. The re-design determines if the loads on the nose and main gear are violated. Also length of the landing gear is re-designed so that the take-off angle of attack can be attained without the fuselage nose cone touching the ground. When the landing gear is redesigned, the design of the stabilizing surface sizing methodology is completed. The result is an optimized wing position, the corresponding minimum required stabilizing surface(s) and a re-designed landing gear. The last step in Figure 8.6 is to overwrite the wing position, stabilizing surface planforms and landing gear parameters in the Initiator.

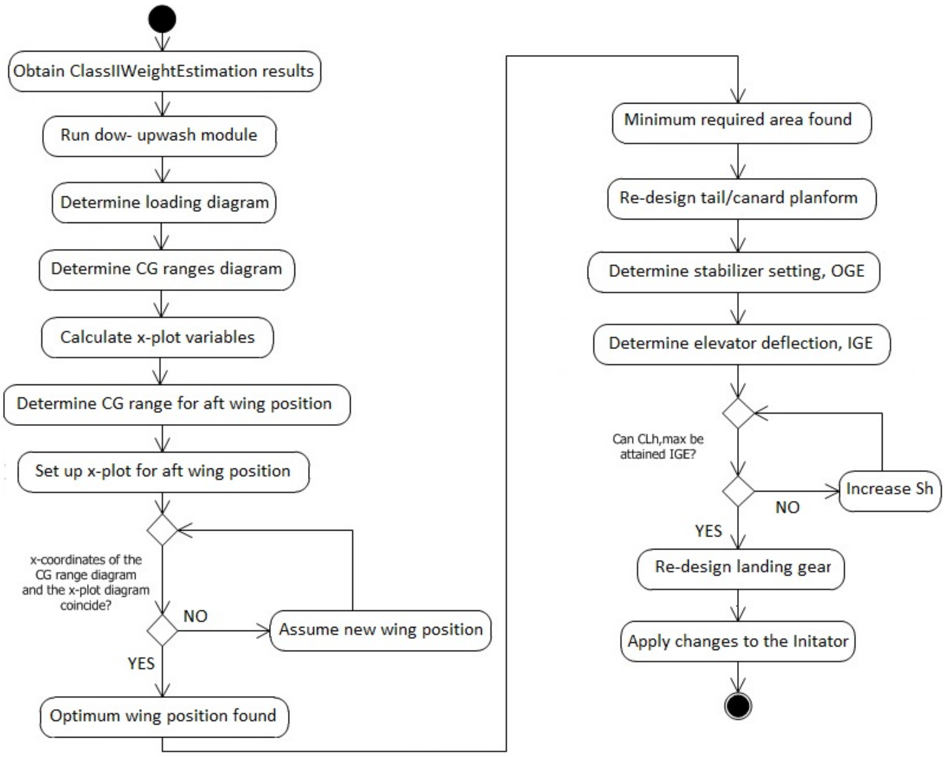
Obtain ClassIIWeightEstimation results
Run dow- upwash module
Determine loading diagram
Determine CG ranges diagram
Calculate x-plot variables
Determine CG range for aft wing position
Set up x-plot for aft wing position
x-coordinates of the CG range diagram and the x-plot diagram coincide?
NO
Assume new wing position
YES
Optimum wing position found
Minimum required area found
Re-design tail/canard planform
Determine stabilizer setting, OGE
Determine elevator deflection, IGE
Can CLh,max be attained IGE?
NO
Increase Sh
YES
Re-design landing gear
Apply changes to the Initator

Figure 8.6: Activity diagram of the developed stabilizing surface sizing methodology.

8.3. DESIGN CONVERGENCE

In this section the implementation of the stabilizing surface sizing methodology in the Initiator is further elaborated. The Initiator is divided in separate modules, which are related to each other through dependencies. If one module A is dependent on module B and the user of the Initiator wants to run module A, the Initiator automatically first runs module B, because module A is dependent on module B. Therefore, the implementation of the stabilizing surface sizing module is related to the dependency of the module on other modules. The implementation of the developed module, allows for addressing the design convergence. The purpose of the design convergence is to run all developed modules and design the complete aircraft. The activity diagram of the design convergence is illustrated in Figure 8.7.

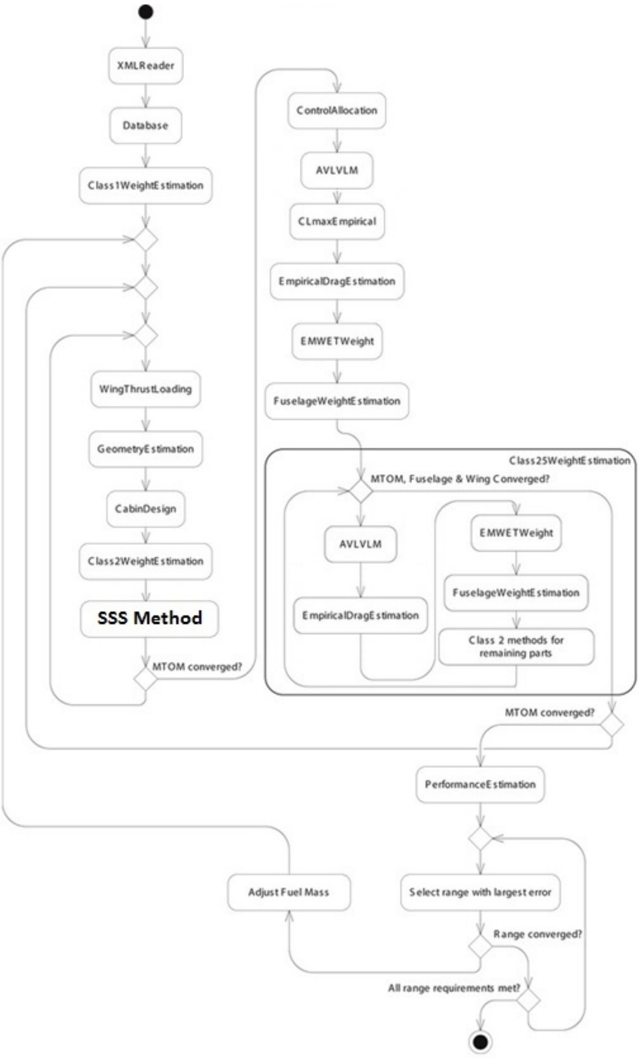
XMLReader
Database
Class1WeightEstimation
WingThrustLoading
GeometryEstimation
CabinDesign
Class2WeightEstimation
SSS Method
MTOM converged?
ControlAllocation
AVLVLM
CLmaxEmpirical
EmpiricalDragEstimation
EMWETWeight
FuselageWeightEstimation
Class25WeightEstimation
MTOM, Fuselage & Wing Converged?
AVLVLM
EmpiricalDragEstimation
EMWETWeight
FuselageWeightEstimation
Class 2 methods for remaining parts
MTOM converged?
PerformanceEstimation
Adjust Fuel Mass
Select range with largest error
Range converged?
All range requirements met?

Figure 8.7: Activity diagram of the Initiator design convergence with the implemented *StabilizingSurfaceSizing* module.

In the latter figure, the module *SSS method* represents the *StabilizingSurfaceSizing* module. The input for the *StabilizingSurfaceSizing* are the results of the *ClassIIWeightEstmiation* module, therefore the *StabilizingSurfaceSizing* module is made dependent on the *ClassIIWeightEstmiation* module, this is illustrated in Figure 8.7, where the module *SSSMethod* represents the stabilizing surface sizing module.

BIBLIOGRAPHY

[1] J. Roskam, *Airplane Design: Layout design of cockpit, fuselage, wing and empennage : cutaways and inboard profiles* (DARcorporation, 1989).

[2] E. Torenbeek, *Synthesis of Subsonic Airplane Design: An Introduction to the Preliminary Design of Subsonic General Aviation and Transport Aircraft, with Emphasis on Layout, Aerodynamic Design, Propulsion and Performance* (Springer, 1982).

[3] E. Obert, *Aerodynamic Design of Transport Aircraft* (Ios Press, 2009).

[4] D. Levy, *Prediction of average downwash gradient for canard configurations,* in *Aerospace Sciences Meetings* (American Institute of Aeronautics and Astronautics, 1992).

[5] D. Zaccai, *Design Framework for Trailing-Edge High-Lift Systems a Knowledge Based Engineering Application*, Master's thesis, Delft University of Technology (2014).

[6] T. Langen, *Development of a conceptual design tool for conventional and boxwing aircraft*, Master's thesis, Delft University of Technology (2011).

[7] R. Elmendorp, *Synthesis of Novel Aircraft Concepts for Future Air Travel*, Msc. thesis, Delft University of Technology (2014).

[8] E. A. S. A. (EASA), *Certification specification for large aeroplanes cs-25,* **Amendment 3** (2007).

[9] E. Kendall, *The aerodynamics of three-surface airplanes,* in *Aircraft Design and Operations Meetings* (American Institute of Aeronautics and Astronautics, 1984).

[10] G. Butler, *An analytical study of the induced drag of canard-wing-tail aircraft configurations with various levels of static stability,* Aeronautical Journal (1983).

[11] E. Kendall, *Performance trades of two-surface and three-surface configurations,* in *General Aviation Technology Conference* (American Institute of Aeronautics and Astronautics, 1984).

[12] E. Kendall, *The minimum induced drag, longitudinal trim and static longitudinal stability of two-surface and three-surface airplanes,* in *Fluid Dynamics and Co-located Conferences* (American Institute of Aeronautics and Astronautics, 1984).

[13] K. Rokhsaz and B. Selberg, *Comparison of vortex lattice and prandtl-munk results for optimized three-surface aircraft,* in *Aircraft Design and Technology Meeting* (American Institute of Aeronautics and Astronautics, 1986).

[14] Unpublished, *Ae3202 flight dynamics lecture notes,* Delft University of Technology (2011).

[15] ESDU, *Effect of trailing-edge flap deployment on anverage downwash at the tailplane at low speeds,* (1997).

[16] ESDU, *Low-speed longitudinal aerodynamic characteristics of aircraft in ground effect,* (1972).

[17] R. Slingerland, *Prediction of a Tail Downwash, Ground Effect and Minimum Unstick Speed of Jet Transport Aircraft*, Phd. thesis, Delft University of Technology (2005).

[18] R. Ranzenbach and J. Barlow, *Two dimensional elliptic bluff body in ground effect - wind tunnel and road conditions,* in *Fluid Dynamics and Co-located Conferences* (American Institute of Aeronautics and Astronautics, 1996).

[19] A. G. for Aerospace Research and Development, *Effect of simulated ice roughness, CP-160*, Tech. Rep.

[20] Y. H. Drela, M., *Athena vortex lattice user manual,* MIT Aero & Astro (2013).

[21] E. Obert, *Low-speed stability and control characteristics of transport aircraft with particular reference to taliplane design,* (1974).

[22] D. Raymer, *AIAA Education Series* (Amer Inst of Aeronautics &, 2013).

[23] H. Shomber and E. Nuttall, *Longitudinal handling qualities criteria: an evaluation,* (American Institute of Aeronautics and Astronautics, 1967).

[24] E. Obert, *An analysis of the low-speed zero-lift pitching moment, aerodynamic centre position and downwash characteristics of tail-off transport aircraft configurations,* (1991).

A

Appendix A

In this section a detailed description is presented on the digitized calculation of the aircraft tail-off pitching moment coefficient about the aerodynamic center, based on the graphical method presented by Torenbeek [2]. This aerodynamic parameter is required in Equation 4.1. The pitching moment coefficient about the aerodynamic center of the aircraft tail-off is a contribution of the clean wing pitching moment, a flap deflection contribution, a fuselage contribution and a engine nacelle contribution. The total contribution is given in Equation A.1.

$$C_{m_{\text{ac}}} = C_{m_{\text{ac}_w}} + \Delta_f C_{m_{\text{ac}}} + \Delta_{\text{fus}} C_{m_{\text{ac}}} + \Delta_{\text{nac}} C_{m_{\text{ac}}} \tag{A.1}$$

The first term on the right-hand-side of Equation A.1 represents the pitching moment of the clean wing, which is approximated with Equation A.2.

$$C_{m_{\text{ac}_w}} = C_{m_{0,\text{airfoil}}}\left(\frac{A\cos^2\Lambda}{A+2\cos\Lambda}\right) \tag{A.2}$$

From Equation A.2 it can be seen that for calculation the pitching moment coefficient of the clean wing, the airfoil pitching moment coefficient, $C_{m_{0,\text{airfoil}}}$, the aspect ratio, A and the sweep angle, Λ are required. The wing airfoil, the wing aspect ratio and wing sweep angle are all input parameter of the sizing methodology. With the two-dimensional flow analysis software, XFOIL, the pitching moment coefficient of the two-dimensional aircraft is calculated.

The third term on the right-hand-side of Equation A.1, is the fuselage contribution to the pitching moment about the aerodynamic center. The fuselage contribution is approximated with Equation A.3

$$\Delta_{\text{fus}} C_{m_{\text{ac}}} = -1.8\left(1-\frac{2.5 b_f}{l_f}\right)\frac{\pi b_f h_f l_f}{4S\bar{c}}\frac{C_{L_0}}{C_{L_{\alpha_{wf}}}} \tag{A.3}$$

The geometric parameters in Equation A.3 are the width of the fuselage, b_f, the length of the fuselage, l_f, the height of the fuselage, h_f, the wing area, S and the mean aerodynamic chord, $\bar{c}$. All these parameters are input parameters of the stabilizing surface sizing methodology and do not need to be determined within the sizing module. Other parameters such as the lift coefficient of the flapped wing at zero angle of attack, C_{L_0} is determined with a vortex lattice method. The lift slope of the wing-fuselage combination is determined by applying a correction to the lift slope of the wing. The lift slope of the wing-fuselage combination is determined with Equation A.4, whereas the lift slope of the wing is determined with a DATCOM method, given in Equation A.5.

$$C_{L_{\alpha_{wf}}} = C_{L_{\alpha_w}}\left(1+2.15\frac{b_f}{b}\right)\frac{S_{\text{net}}}{S} + \frac{\pi}{2}\frac{b_f^2}{S} \tag{A.4}$$

$$C_{L_{\alpha_w}} = \frac{2\pi A_w}{1+\sqrt{4+\left(\frac{A_w\beta}{\eta}\right)^2\left(1+\frac{\tan^2\Lambda_{c/2}}{\beta^2}\right)}} \tag{A.5}$$

The lift slope of the wing, $C_{L_{\alpha_w}}$, and the lift slope of the wing-fuselage combination, $C_{L_{\alpha_{wf}}}$ are easily determined, based on the geometric parameters of the wing and the fuselage. The Prandtl compressibility correction factor, β is a function of the Mach number, which is a known input parameter of the sizing methodology. The airfoil efficiency coefficient eta, η is assumed to be constant scalar with a magnitude of 0.95.

The third term on the right-hand-side of Equation A.1 depends on the engine placement. For fuselage-mounted engines and full flap deflection a constant of +0.2 is assumed, whereas for wing-mounted engines and full flap deflections a constant of -0.05 is assumed.

The second term on the right-hand-side of Equation A.1 deserves the most attention as the change pitching moment due to flap deflections generally is the largest contribution. In order to generically determine the change in pitching moment coefficient due to flap deflections, the graphical method needs to be digitized. This is discussed in the last part of this Appenxix. The change in pitching moment coefficient due the a certain flap deflection is determined with Equation A.6, where the contribution of the sweep angle is calculated with Equation A.7.

$$\Delta_f C_{m_{c/4}} = \mu_2\left\{-\mu_1\Delta C_{l_{\max}}\frac{c'}{c}-\left[C_L+\Delta C_{l_{\max}}\left(1-\frac{S_{wf}}{S}\right)\right]\frac{1}{8}\frac{c'}{c}\left(\frac{c'}{c}-1\right)\right\}+C \tag{A.6}$$

$$C = 0.7\frac{A}{1+2/A}\mu_3\Delta C_{l_{\max}}\tan\Lambda_{1/4} \tag{A.7}$$

From Equation A.6 it can be seen that with the latter equation, the change in pitching moment coefficient due to a certain flap extension is calculated about the quarter chord. With Equation A.8, the coefficient about the quarter chord is converted to a pitching moment coefficient about the aerodynamic center. The calculation of the aerodynamic center is further examined in Appendix B.

$$C_{m_{\text{ac}}} = C_{m_{c/4}} - C_L\left(0.25-\frac{x_{\text{ac}}}{\bar{c}}\right) \tag{A.8}$$

The parameters of Equation A.6 are discussed next. The increase in lift coefficient $\Delta C_{l_{\max}}$, represents the two-dimensional increase in lift coefficient generated by the flaps. This parameter is calculated with the two-dimensional flow analysis software, XFOIL. The lift coefficient, C_L represents the three-dimensional wing lift coefficient with flaps deployed. This coefficient is determined with a vortex lattice method. The wing area, S, the aspect ratio, A, the ratio between the flapped wing area and the reference wing area, S_{wf} and the quarter chord sweep angle, $\Lambda_{c/4}$ are geometric input parameters and do not need to be determined within the stabilizing surface sizing methodology. However, the remaining parameters need to be determined graphically. First the parameters, μ_1, μ_2 and μ_3 are addressed.

The parameter μ_1 represent the influence of an increased camber due to a specific flap deflection. Therefore μ_1 is a function of the flap deflection, which is visualized in Figure A.1. In Figure A.1(a) the actual figure as presented by Torenbeek is presented, whereas in Figure A.1(b) the digitized figure is illustrated which is required for the generic calculation of the pitching moment.

The parameter μ_2 accounts for the transformation of the two-dimensional calculation to a three-dimensional calculation. μ_2 is a function of the flap span to wing span ratio, b_f/b and the taper ratio, λ. Both the actual figure and the digitized figure are illustrated in Figure A.2.

The parameter μ_3 accounts for the effect of the sweep angle on the change in pitching moment coefficient. In Figure A.3, the actual and the digitized figure for the calculation of μ_3 are presented. From the latter figure it is visible that the parameter μ_3 is dependent on the flap span to wing span ratio,

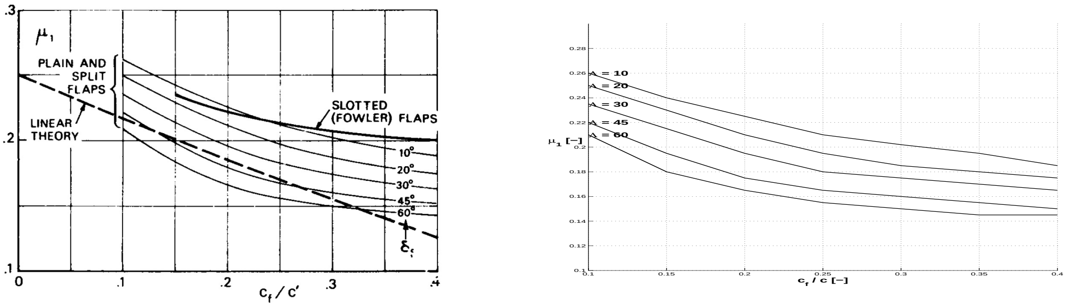

(a) Actual figure

(b) Digitized figure

Figure A.1: Actual figure, as presented by Torenbeek, and the digitized figure developed for the stabilizing surface sizing methodology of parameter μ_2[2].

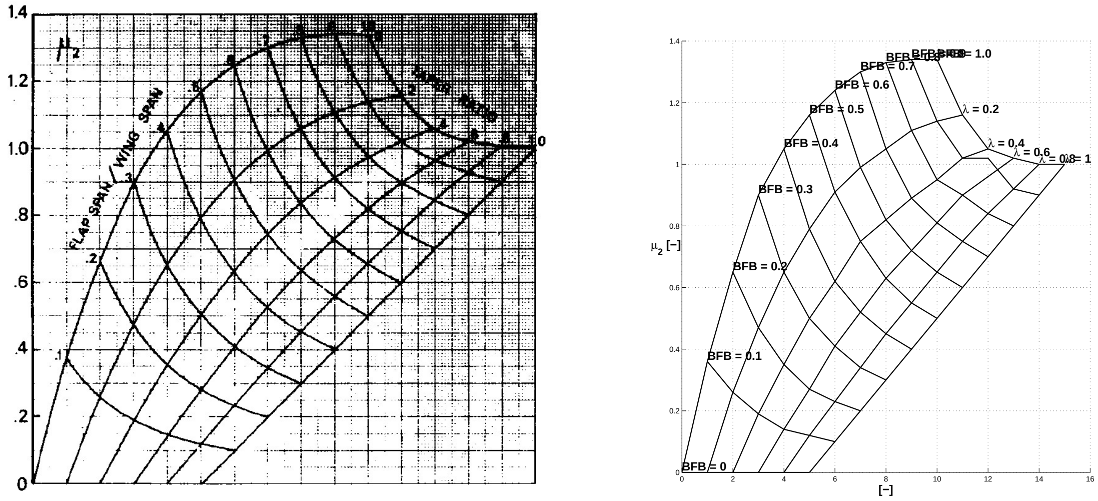

(a) Actual figure

(b) Digitized figure

Figure A.2: Actual figure, as presented by Torenbeek, and the digitized figure developed for the stabilizing surface sizing methodology of parameter μ_2[2].

b_f/b and the taper ratio, λ.

Finally, the ratio between the unflapped wing chord and the flapped wing chord, $\frac{c'}{c}$ is discussed. The chord of the flapped wing is determined with Equation A.9, where the difference between the flapped chord and the unflapped chord, ΔC is determined with the figure presented in Figure A.4.

$$c' = c + \Delta c \tag{A.9}$$

All figures presented in this Appendix are digitized as functions in MATLAB. The implies that the dependency of the parameters, such as taper ratio, flap to wing span ratio, flap deflection are programmed as input parameters. The output parameters of the functions are μ_1, μ_2, μ_3 and $\frac{\Delta c}{c_f}$. An example on the automated calculation of parameter μ_2 is given next.

The parameter μ_2 is dependent on the flap span to wing span ratio and the taper ratio. Both these variables are input parameters of the developed function in MATLAB. The visualization of the calculation is presented in Figure A.5. In the latter example a flap span to wing span ratio of 0.65 and a taper ratio of 0.25 are assumed. First, it is determined in which skewed square the design point is located. This is visualized in Figure A.5(b) by four red dots. Finally the offset of the design point between the upper and lower points is determined. For example the taper ratio of 0.25 is located between the ta-

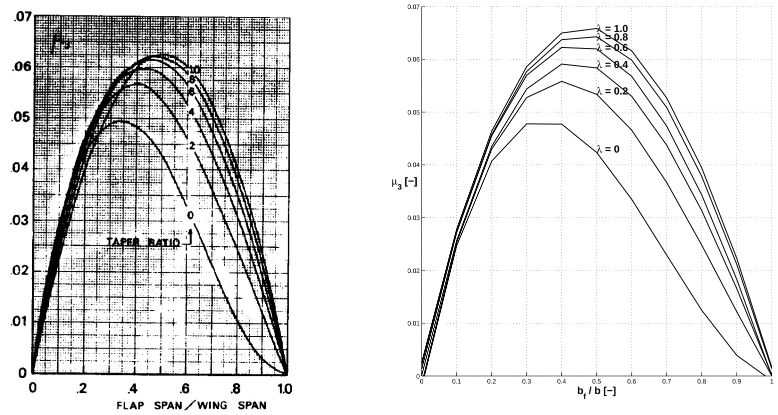

(a) Actual figure (b) Digitized figure

Figure A.3: Actual figure, as presented by Torenbeek, and the digitized figure developed for the stabilizing surface sizing methodology of parameter μ_3[2].

per ratio of 0.2 and the taper ratio of 0.4. The percentage location of the design point between the upper and lower taper ratio bounds is determined. A similar procedure for the flap span to wing span ratio is executed. In this particular case the flap span to wing span ratio of 0.65 is located exactly between the upper and lower bounds of 0.6 and 0.7. Once the design point is determined in the digitized figure, the corresponding x- and y-coordinates are determined, where the y-coordinate results in the corresponding value for μ_2. From the actual figure a value of 0.96 for μ_2 is obtained, whereas from the digitized figure a value of 0.97 for μ_2 is obtained. This results in an over prediction of 1.04%. Similar results are obtained for other input values and other digitized figures.

A similar strategy is used for the calculation of the parameters μ_1, μ_3 and $\frac{\Delta c}{c_f}$. All required parameters for the calculation of the pitching moment coefficient about the aerodynamic center are addressed in this Appendix, except for the calculation of the aerodynamic center. This parameter is further examined in Appendix B.

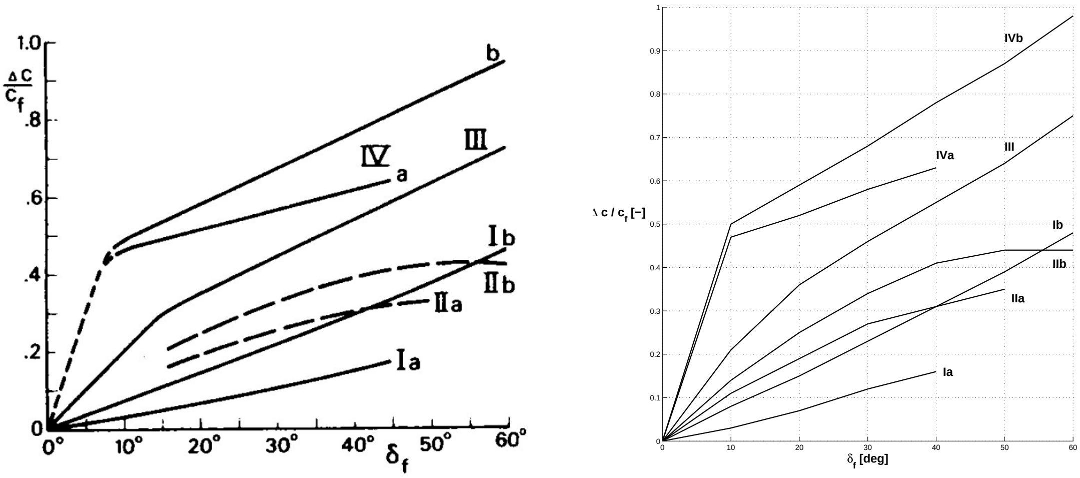

(a) Actual figure

(b) Digitized figure

Figure A.4: Actual figure, as presented by Torenbeek, and the digitized figure developed for the stabilizing surface sizing methodology of parameter $\frac{\Delta c}{c_f}$ [2].

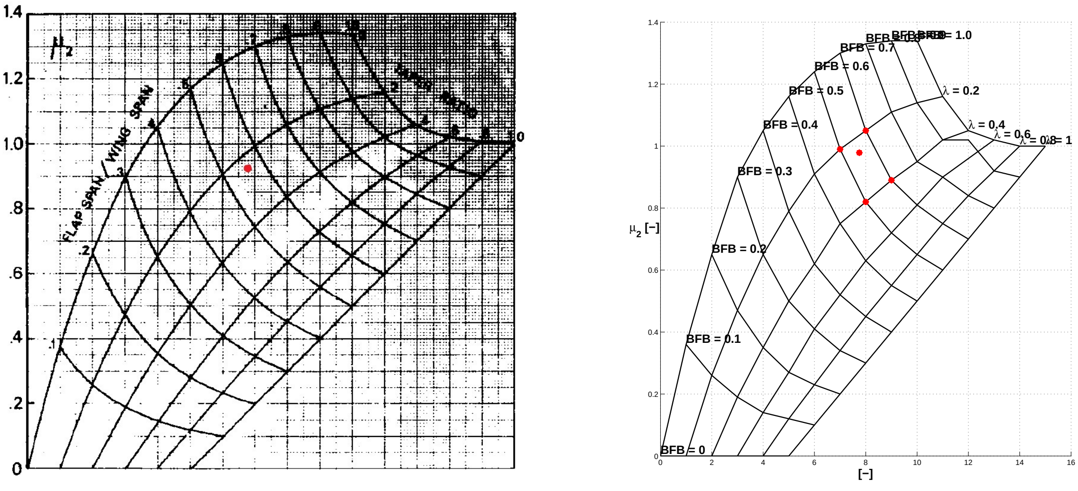

(a) Actual figure

(b) Digitized figure

Figure A.5: Comparison of the graphical calculation of parameter μ_2 and the ditigized calculation of the latter parameter.

B

Appendix B

In this section a detailed description is presented on the digitized calculation of the aircraft tail-off aerodynamic center, based on the graphical method presented by Torenbeek [2]. The aerodynamic center of the aircraft tail-off combination is a summation of the aerodynamic center of the wing-fuselage combination, the nacelle contribution and the thrust contribution. The total summation is given in Equation B.1

$$\frac{x_{\text{ac}}}{c} = \left(\frac{x_{\text{ac}}}{c}\right)_{wf} + \left(\frac{x_{\text{ac}}}{c}\right)_{\text{nac}} + \left(\frac{x_{\text{ac}}}{c}\right)_{t} \tag{B.1}$$

The first term on the right-hand-side of Equation B.1, represents the aerodynamic center of the wing-fuselage combination. This term is determined by applying two fuselage correction factors to the aerodynamic center of the wing. The aerodynamic center of the wing-fuselage combination is determined with Equation B.2.

$$\left(\frac{x_{\text{ac}}}{c}\right)_{wf} = \left(\frac{x_{\text{ac}}}{c}\right)_{w} - \left(\frac{1.8}{C_{L_{\alpha_{wf}}}}\frac{b_f h_f l_{fn}}{S\bar{c}}\right) + \left(\frac{0.273}{1+\lambda}\frac{b_f c_g(b-b_f)}{\bar{c}^2(b+2.15b_f}\tan\Lambda_{c/4}\right) \tag{B.2}$$

The first term on the right-hand-side (RHS) of Equation B.2 represents the aerodynamic center of the wing, which is discussed later in this Appendix. The second term on the (RHS) of Equation B.2 represents correction factor related to the forward shift of the aerodynamic center due to presence of the fuselage in front and aft of the wing. The second term on the RHS of equation B.2 represents the correction factor related to the lift loss in the wing-fuselage intersection due to lift carry-over. The geometric parameters in Equation B.2, such as the fuselage width, b_f, fuselage height, h_f, length of the fuselage in front of the wing, l_{fn}, wing area, S, mean aerodynamic chord, $\bar{c}$, wing span, b, taper ratio, λ, the mean geometric chord, c_g and sweep angle, $\Lambda_{c/4}$ are input parameters for the stabilizing surface sizing methodology and are not further examined in this Appendix. The lift slope of the wing-fuselage combination is calculated as described in Appendix A with Equation A.4. This only leaves the aerodynamic center of the wing in Equation B.3.

The aerodynamic center of the wing is determined through digitized carpet plots. The actual carpet plots are visualized in Figure B.1, whereas the digitized carpet plots are illustrated in Figure B.2.

The carpet plot is divided into five separate smaller carpet plots. The term βA determines which carpet plot should be addressed. The parameter β is the Prandtl compressibility factor which depends on the Mach number. The Mach number and the aspect ratio, A are both input parameters of the sizing module. Therefore the term βA can directly be determined. The carpet plots are divided into five different values for βA, these values are; 2, 4, 6, 8 and 10. All are visible in Figure B.1 and Figure B.2. Five different functions are developed in MATLAB for the five different carpet plots. A single carpet plot depends on the taper ratio, λ and the Mach number corrected sweep angle Λ_β. The Mach number

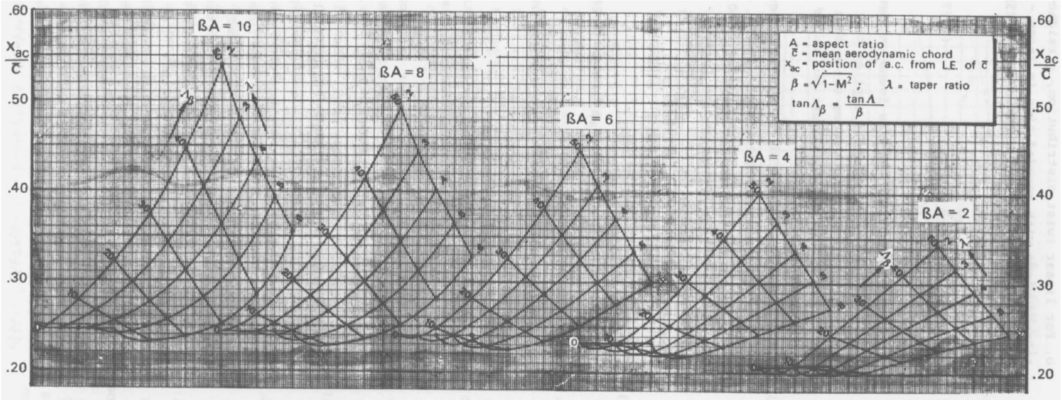

Figure B.1: Actual representation of the carpet plots [2].

corrected sweep angle, Λ_β is determined with Equation B.4.

$$\left(\frac{x_{\text{ac}}}{c}\right)_{wf} = \left(\frac{x_{\text{ac}}}{c}\right)_{w} - \left(\frac{1.8}{C_{L_{\alpha_{wf}}}}\frac{b_f h_f l_{fn}}{S\bar{c}}\right) + \left(\frac{0.273}{1+\lambda}\frac{b_f c_g(b-b_f)}{\bar{c}^2(b+2.15b_f}\tan\Lambda_{c/4}\right) \tag{B.3}$$

$$\Lambda_\beta = \tan^{-1}\left(\frac{\tan\Lambda}{\beta}\right) \tag{B.4}$$

Once the Mach number corrected sweep angle, Λ_β, the taper ratio, λ and the term βB are known, the aerodynamic center is calculated. The similar calculation strategy as for the calculation of μ_2 in Appendix A is used. For a given sweep angle, the upper and lower bounds are determined. For example, when Λ_β is 25$^{\text{o}}$, the upper bound is 30$^{\text{o}}$ and the lower bound is 20$^{\text{o}}$. The percentage location between the lower and upper sweep angle bounds is determined. This process is repeated for the taper ratio. For a given input taper ratio of 0.25, the upper taper ratio bound is 0.3 and the lower taper ratio bound is 0.2. Again the percentage location of the design point between the upper and lower bound is determined. This results in a calculation of the corresponding x- and y-coordinates of the design points. The y-coordinate results in the non-dimensionalized aerodynamic center of the wing. The second term on the RHS of Equation B.1 is determined with Equation B.5.

$$\left(\frac{x_{\text{ac}}}{c}\right)_{\text{nac}} = \sum k_n \frac{b_n^2 l_n}{S\bar{c}C_{L_{\alpha_{wf}}}} \tag{B.5}$$

In the latter equation, the parameter k_n depends on the placement of the engines. When the engines are placed in front the LEMAC, a value of -4 is assumed for k_n. When the engines are placed behind the LEMAC a value of -2.5 is assumed for k_n. The parameter b_n is the width of the nacelle, whereas the parameter l_n is the distance of the nacelle in front of the wing. In case of rear fuselage-mounted engines, l_n is negative. The lift slope of the wing fuselage combination is already addressed in this Appendix. All geometric parameters are input parameters of the stabilizing surface sizing methodology and can directly be implemented in the aerodynamic center calculation. The last term on the RHS of Equation B.1 represents the shift in aerodynamic center due to thrust. The latter term is approximated with Equation B.6.

$$\left(\frac{x_{\text{ac}}}{c}\right)_{t} = -\sum_{1}^{n} \frac{T}{W}\frac{z_T}{\bar{c}} \tag{B.6}$$

In the latter equation, the thrust, T, the aircraft weight, W, the moment arm of the thrust vector relative to the center of gravity, z_T and the mean aerodynamic chord, $\bar{c}$ are input parameters for the stabilizing surface sizing methodology and can also directly be implemented in the calculation of the aerodynamic center.

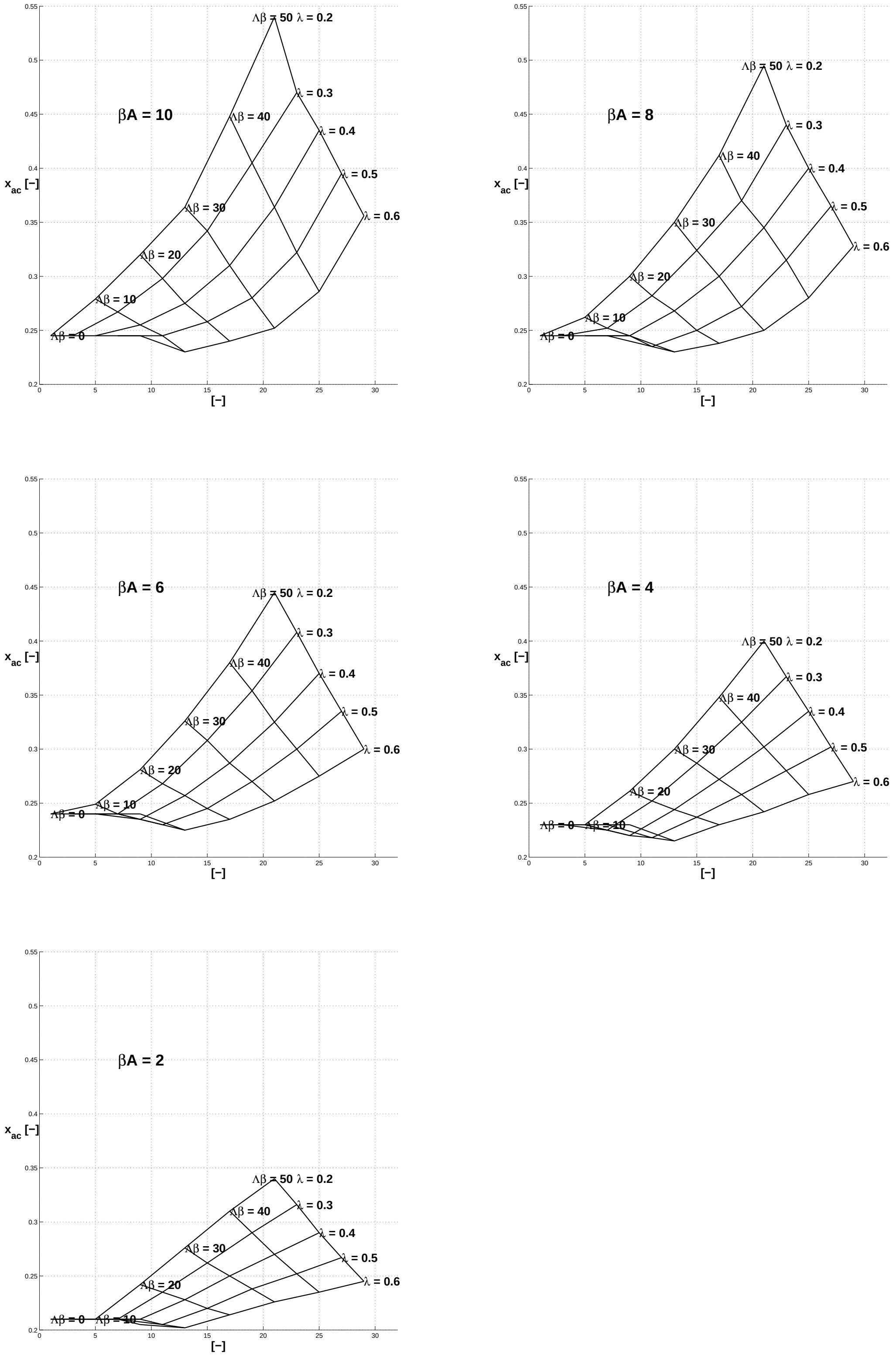

Figure B.2: Digitization of the carpet plots.